LIGA-MICROMACHINED TIGHT MICROWAVE COUPLERS

A Thesis Submitted to the College of
Graduate Studies and Research
in Partial Fulfillment of the Requirements
for the Degree of Master of Science
in the Department of Electrical Engineering
University of Saskatchewan
Saskatoon

by

Anton Kachayev

Fall 2003

PERMISSION TO USE

In presenting this thesis in partial fulfillment of the requirements for a Postgraduate degree from the University of Saskatchewan, I agree that the Libraries of this University may make it freely available for inspection. I further agree that permission for copying of this thesis in any manner, in whole or in part, for scholarly purposes may be granted by the professor or professors who supervised my thesis work or, in their absence, by the Head of the Department or the Dean of the College in which my thesis work was done. It is understood that any copying or publication or use of this thesis or parts thereof for financial gain shall not be allowed without my written permission. It is also understood that due recognition shall be given to me and to the University of Saskatchewan in any scholarly use which may be made of any material in my thesis.

Requests for permission to copy or to make other use of material in this thesis in whole or part should be addressed to:

Head of the Department of Electrical Engineering,
College of Engineering
University of Saskatchewan
Saskatoon, Canada
S7N 5A9

ABSTRACT

There are a significant number of microwave applications, including active antenna arrays, wireless communication systems, navigational applications, etc., where improvement of such qualities as manufacturing costs, size, weight, power consumption, etc. is still on the agenda of today's RF design. In order to meet these requirements, new technologies must be actively involved in fabrication of RF components with improved characteristics. One of such fabrication technologies is called LIGA, used before primarily in fluidics, photonics, bioengineering, and micromechanics, and only recently receiving growing attention in RF component fabrication.

One of the RF components suffering limitations in performance due to limitations in fabrication capabilities is the compact single metal layer (SML) coupled-line 3-dB coupler, also called "hybrid", required in some applications thanks to its ability to divide power equally and electrically isolate the output from the input. In today's practical edge-coupled SML coupler designs, the level of coupling is limited by the capabilities of the photolithographic process to print the coupled lines close enough for tight coupling and it is usually no tighter that 8 dB.

A promising way to overcome this limitation is increasing the area of metallic interface of the coupled lines, thus increasing the mutual capacitance of the lines, and inherently the coupling between them. This should be preferably done with keeping the coupler compact with respect to the footprint area, which is attained by making taller conductors, i.e. employing the third dimension. In contrast with previously used RF component fabrication processes, LIGA is the technology that allows the designer to explore the third dimension and build tall conductors while being also able to use small features. When the two-dimensional edge-coupled SML couplers are extended into the three-dimensional structures, they rather become ***the side-coupled SML couplers***.

Tall-conductor coupled lines have been characterized in this work to reveal their dependence on their geometry and a 3-dB SML coupler with tall conductors has been developed and fabricated using LIGA at the Institute for Microstructure Technology (IMT), Karlsruhe, Germany. The simulation and measurement results demonstrate the potentially

superior performance of LIGA couplers, and the promising capabilities of LIGA for fabrication of RF microstructures.

ACKNOWLEDGEMENTS

I would like to acknowledge my genuine gratitude to my supervising professor, Dr. David M. Klymyshyn, who has bent every effort to facilitate implementation of this research and has given an invaluable support throughout the course of the work on this project and preparation of this present thesis.

I am deeply obliged to the Institute for Microstructure Technology (IMT) of Karlsruhe, Germany and its personnel, especially Sven Achenbach and Volker Saile, who made fabrication of the couplers and, therefore, the whole project possible.

I am also truly grateful to Telecommunications Research Laboratories (TRLabs) Saskatoon and its personnel for providing me with financial assistance, for accordance of a privilege to use its facilities, and rendering assistance in all matters regarding my research.

DEDICATION

To my beloved parents, Lydia and Alexander Kachayev, who taught me “To strive, to seek, to find, and not to yield”.

Table Of Contents

List of Tables

List of Figures

List of Abbreviations

CPW – Coplanar Waveguide

DXRL – Deep X-Ray Lithography

FEM – Finite Element Method

HVAR – High Vertical Aspect Ratio

LIGA – Roentgen-Lithography Galvanik Abformung (*German for* "X-ray Lithography Electrodeposition Moulding")

MEMS – Micro-Electro-Mechanical Systems

MMIC – Monolithic Microwave Integrated Circuits

PMMA – Poly-Methyl-Methacrylate

RF – Radio Frequency

RIE – Reactive Ion Etching

SEM – Scanning Electron Microscopy

SML – Single Metal Layer

TEM – Transverse ElectroMagnetic

TRL – Thru-Reflect-Line

TRM – Transmit/Receive Module

VNA – Vector Network Analyzer

Chapter 1
INTRODUCTION

1.1 Coupled Structures

As frequency of an electrical signal becomes greater, the corresponding wavelength becomes commensurable with the dimensions of the signal-carrying lines. As this happens, geometrical parameters of the signal-carrying lines may no longer be neglected when designing electronic circuits, for potentials and currents are no longer constant along the length of the lines and per-unit-length line parameters, viz. resistance, inductance, conductance, and capacitance significantly affect propagation of the signal along the line. Thus, the problem of designing the lines acquires another domain, spatial, in addition to the time domain. The signal-carrying lines used in microwave circuits are usually referred to as transmission lines, as any other line employed to convey energy, e.g. transmission lines in electrical power engineering, where the problem of the line design also has to account for variation of potentials and currents along the length of the line and per-unit-length parameters, but due to immense lengths of the lines rather than high operating frequency.

Transmission lines employed in microwave circuits typically have two main missions: (1) transfer of electromagnetic energy between circuit elements, and (2) serving as waveguiding media for creation of separate circuit elements such as couplers, filters, baluns (balanced-to-unbalanced transformers), etc.

When two or more unshielded transmission lines supporting propagation of time-varying electromagnetic fields are placed in close proximity, see Fig. 1.1, they demonstrate electromagnetic coupling between each other due to excitation of the electromotive forces in the line affected by the time-varying fields of the other line, which gives rise to additional per-unit-length parameters, viz. mutual capacitance, which describes interaction between the lines in terms of voltages, and mutual inductance, which describes interaction between the lines in terms of currents. Such structures are called parallel edge-coupled structures, if

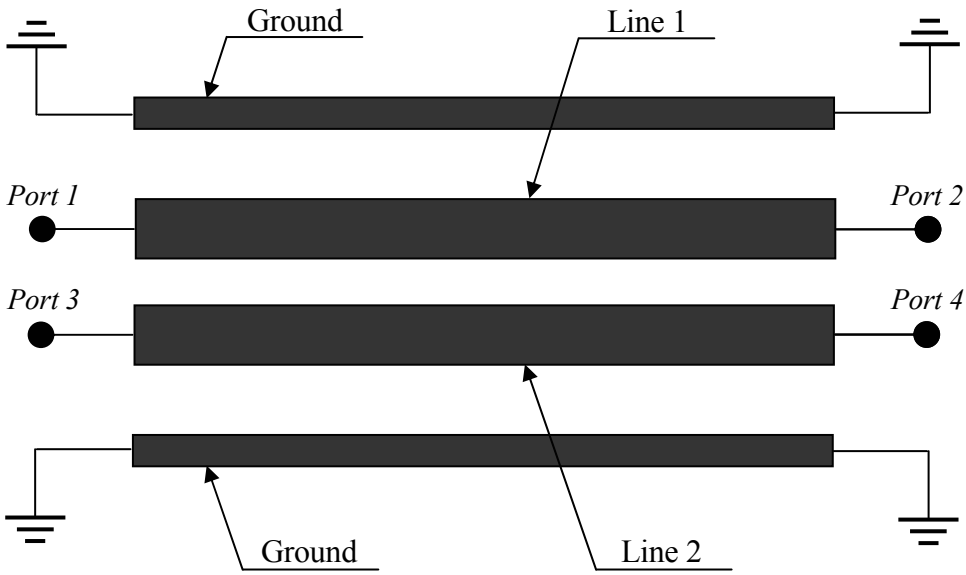

Figure 1.1 A general representation of coupled lines

the lines lie in a common plane, or broadside-coupled structures, if the lines are placed one above the other. A graphical representation of these in a stripline waveguiding medium is given in Fig. 1.2 (a stripline waveguide consists of a signal conductor placed between two ground planes as shown in the figure). The distance to which the lines should be brought together in order for appreciable electromagnetic coupling to appear is defined relative to the distance between the signal lines and the lines, serving as electric potential reference, referred to as grounds. Generally, the distance between the signal lines should not be much greater than the distance between the lines and the ground in order not to confine electromagnetic fields only around the signal lines.

Electromagnetic coupling between transmission lines may be classified as either desirable or parasitic. Desirable coupling is created intentionally in the structures that operationally depend on interaction of the electromagnetic fields supported by the lines. Such structures include couplers, filters, and baluns. Parasitic coupling, also referred to as crosstalk, is an unwanted effect observed in closely spaced interconnecting traces or lumped elements that operate on either high frequencies or pulses with sharp edges. High levels of parasitic coupling may significantly deteriorate electrical performance of the circuits; therefore para-

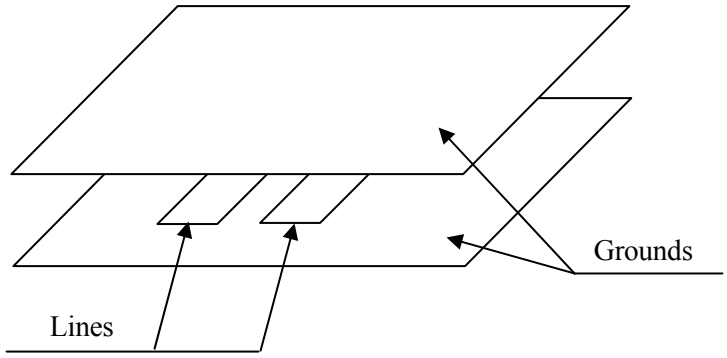

(a)

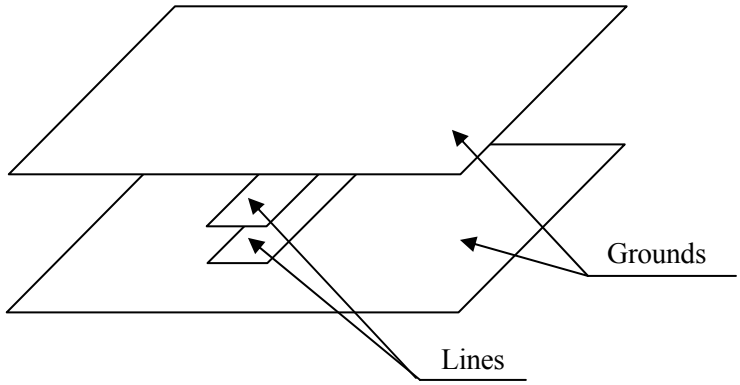

(b)

Figure 1.2 Representation of edge-coupled (a) and broadside-coupled (b) structures in stripline waveguiding medium

sitic coupling should be accounted for when designing circuits with high density of arrangement of elements and additional measures should be taken to decrease the influence of crosstalk.

1.2 The Need for Compact Tight Couplers

Couplers have been used extensively in a wide variety of microwave applications, including power division/combining and signal sampling. The majority of couplers provide coupling levels within the 8 – 40-dB range [1]. However, several applications require greater levels of coupling, up to 3-dB, which corresponds to division of incoming power into two

equal halves. One such application is the active antenna array, where usage of compact components is critical.

An active antenna array is a combination of transmit/receive modules (TRM), each performing the functions of final amplification for transmitted signals, preliminary amplification for received signals, and control of the phase and amplitude of these signals to electronically steer the antenna beam [2]. In order for an active antenna array to operate properly within the whole frequency and spatial range, the spacing between the TRMs should be no greater than half-wavelength at the highest operating frequency [2]. For instance, an active antenna array operating in free space at 30 GHz must have TRMs spaced no further than 5 mm from each other. This gives appreciation of how compact, yet complex enough each TRM should be to meet the aforementioned functional requirements. Moreover, TRMs must be of low cost in order for active antenna arrays to be economically feasible since virtually thousands of TRMs are required for high gain active antenna arrays. This requires increased levels of circuit integration to make fabrication less expensive.

Notwithstanding being faced with this multitude of engineering and economical problems, each TRM's power amplifier is required to output high power, which is a contradictory requirement for solid-state active devices, being the backbone of monolithic microwave integrated circuits (MMIC), to be of small size and feature a high output power at high operating frequency [3]. Hence, summation of output power from a number of power amplifiers is a must for high overall transmit output power of each TRM.

Power combining networks consist of a number of branches with power amplifiers, each fed from a common signal source through a power divider that divides the input signal between the branches. Amplified signals from the output of each branch power amplifier are combined into a common output signal with the help of a power combiner. Power-combining networks of this type are called corporate networks [4]. An example of such a network is given in Figure 1.3. Here, the output power of the network is twice the output power of each branch. In addition to the advantage of power combining, this network provides redundancy: if one of the branch amplifiers fails, the whole network remains operational, though with half the normal output power.

Both power dividers and power combiners in the corporate power-combining networks are the same microwave devices, viz. 3-dB directional couplers, and are four-port reciprocal

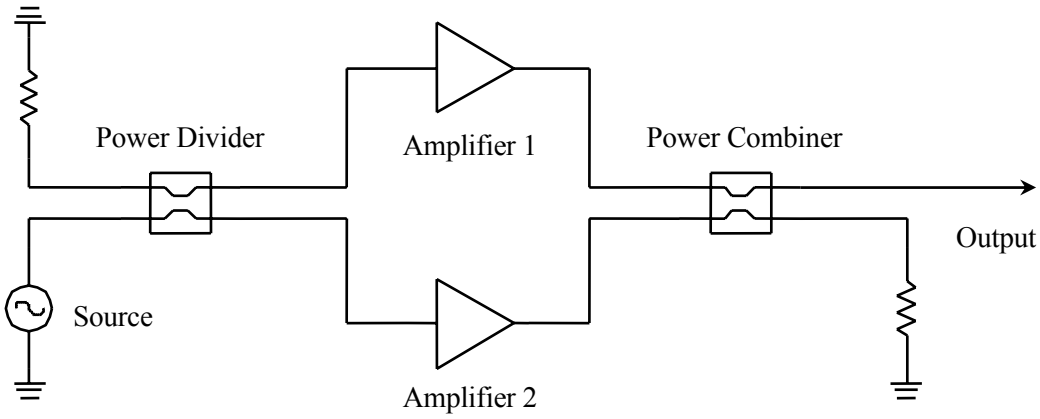

Figure 1.3 Power-combining corporate network employing couplers

devices, which means that any port can serve as the input port and the remaining ports will serve as relevant output ports.

The most popular couplers are the SML edge-coupled couplers owing to their simplicity and optimum area utilization. They are often implemented in the planar waveguiding media, which are the waveguides of choice in the prevailing majority of small-scale microwave circuits. However, the SML edge-coupled couplers are unable to attain the 3-dB level of coupling due to prohibitively narrow gaps between the signal traces required for as tight a level of coupling as 3 dB, which compromises the very possibility of fabrication of such couplers. Therefore, microwave designers having conventional circuit fabrication technologies at their disposal have to resort to other, more complex coupler configurations such as multi-dielectric layer broadside-coupled striplines (see Fig. 1.4a), which greatly increases production complexity, especially in MMIC's; multi-line couplers such as the Lange coupler (see Fig. 1.4b), which are not optimum from the area utilization point of view and require wire jumpers, which add parasitic inductances; or branch-line couplers (see Fig. 1.4c), which are neither compact in area, nor wide in frequency bandwidth [2].

As it will be shown further in the thesis, increasing the level of coupling with retaining feasibility of the coupled-line structures may be attained by following one or both of the following methods: (1) enlarging the area of metal interface in the field interaction volume of the coupled structure, or (2) applying dielectric materials with high relative permittivity.

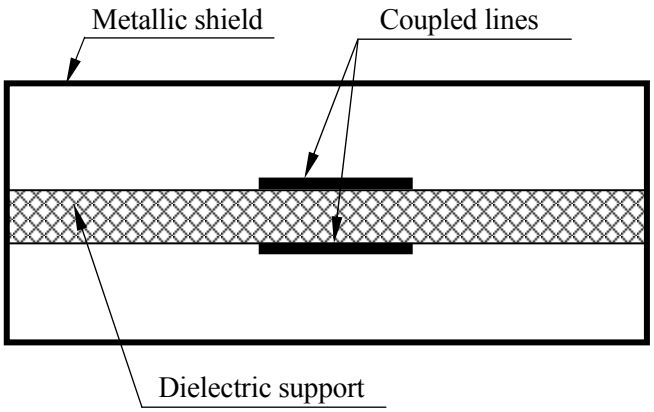

(a)

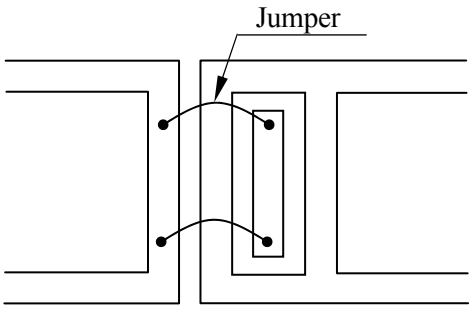

(b)

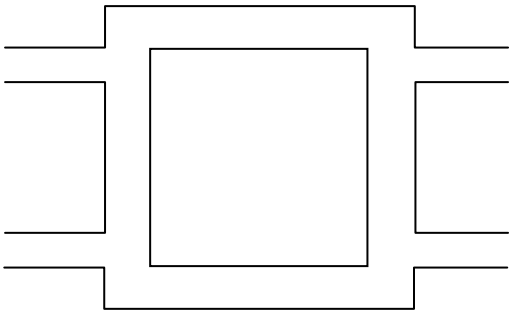

(c)

Figure 1.4 Popular types of tight couplers:
a) Broadside stripline coupler (cross-sectional view)
b) Lange coupler (top view)
c) Branch-line coupler (top view)

Following the latter approach might significantly deteriorate high-frequency performance of microwave devices fabricated using dielectric materials with high relative permittivity. Therefore, following the first approach could be considered more beneficial to obtain simple 3-dB couplers.

In MMICs, or small-scale circuit environment, optimum enlargement of metal interface area with respect to chip area utilization may be achieved by exploring the third, traditionally unused, dimension, viz. the height of metal structures serving as signal lines. The fabrication technology that allows production of small-scale tall metallic structures combined with the precision and aptitude for large-scale fabrication of integrated circuits is the deep X-ray lithography (DXRL) and its spin-off techniques such as LIGA (DXRL with replication).

1.3 Deep X-Ray Lithography and LIGA

Recently, application of deep X-ray lithography (DXRL) to RF structures has received increased attention. The ability to fabricate tall freestanding structures or, alternatively, deep cavities of arbitrary lateral shapes with high precision offers advantages in the fabrication of both dynamically operating RF MEMS, such as switches and tuneable components, as well as statically operating RF microstructures, such as couplers, inductors, transformers, filters, etc.

DXRL traces its history back to 1975, when Romankiw et al of IBM combined X-ray lithography and electrodeposition for the first time [5]. It allowed fabrication of metal structures with high vertical aspect ratios (ratio of the maximum structure height to the minimum horizontal feature size as shown in Figure 1.5), but the requirement for X-ray expo-

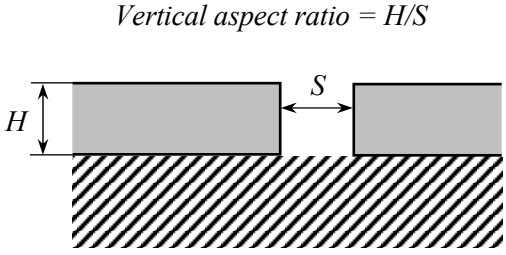

Figure 1.5 Definition of vertical aspect ratio

sure related procedures in the technique made it relatively expensive and not economically viable for large-scale production. The cost of potential large-scale fabrication was reduced by introduction of the metal deposition and moulding procedures following lithography by Ehrfeld et al at the Karlsruhe Nuclear Research Centre (later Research Centre Karlsruhe FZK) in 1982. This has allowed usage of the metal structures obtained after the primary metal deposition for fabricating multiple moulds, typically by injection moulding or hot embossing, to be used for the secondary metal deposition. The resulting nanofabrication technology was christened LIGA, which is a German acronym, where LI stands for "Roentgen-Lithographie" – X-ray lithography, G – "Galvanoformung" – electrodeposition, A – "Abformung" – moulding. Since its invention, LIGA has been used in a wide variety of applications, including fluidics, photonics, micromechanics, and recently RF engineering.

The LIGA process begins with application of a thin metal film on the substrate as shown in Fig. 1.6. The film is called "seed layer" and it acts as a negative electrode attracting metal ions to the substrate during electroplating. In case an electroless metal deposition technique is used, the first step is omitted. After that, the seed layer is covered with a thick layer of X-ray sensitive polymer photoresist, typically PMMA (poly-methyl-methacrylate), which is then exposed to collimated high-energy X-ray radiation through a patterned mask. X-ray radiation causes scission of the photoresist polymer chains in the areas not shaded by the mask. Following X-ray exposure, the photoresist is developed by immersion, which is essentially flushing of short polymer chains broken by X-ray radiation in unshaded areas, see Fig. 1.6. The ensuing three-dimensional photoresist structure is filled with deposited metal and the photoresist is subsequently removed via X-ray flood irradiation followed by secondary development to reveal a freestanding metal structure. Finally, the seed layer is etched away with hydrofluoric acid and reactive ion etching (RIE) to electrically isolate metal conductors as demonstrated in Fig. 1.6.

The fabrication process implemented up to the last step is called "direct LIGA" and it is primarily used for research purposes or prototyping, or in case when extremely precise parts are needed. In order to increase throughput and decrease cost of fabrication, the requirement for X-ray exposure in the fabrication process may be reduced. A method of doing this is using one of the precision moulding techniques: hot embossing or injection

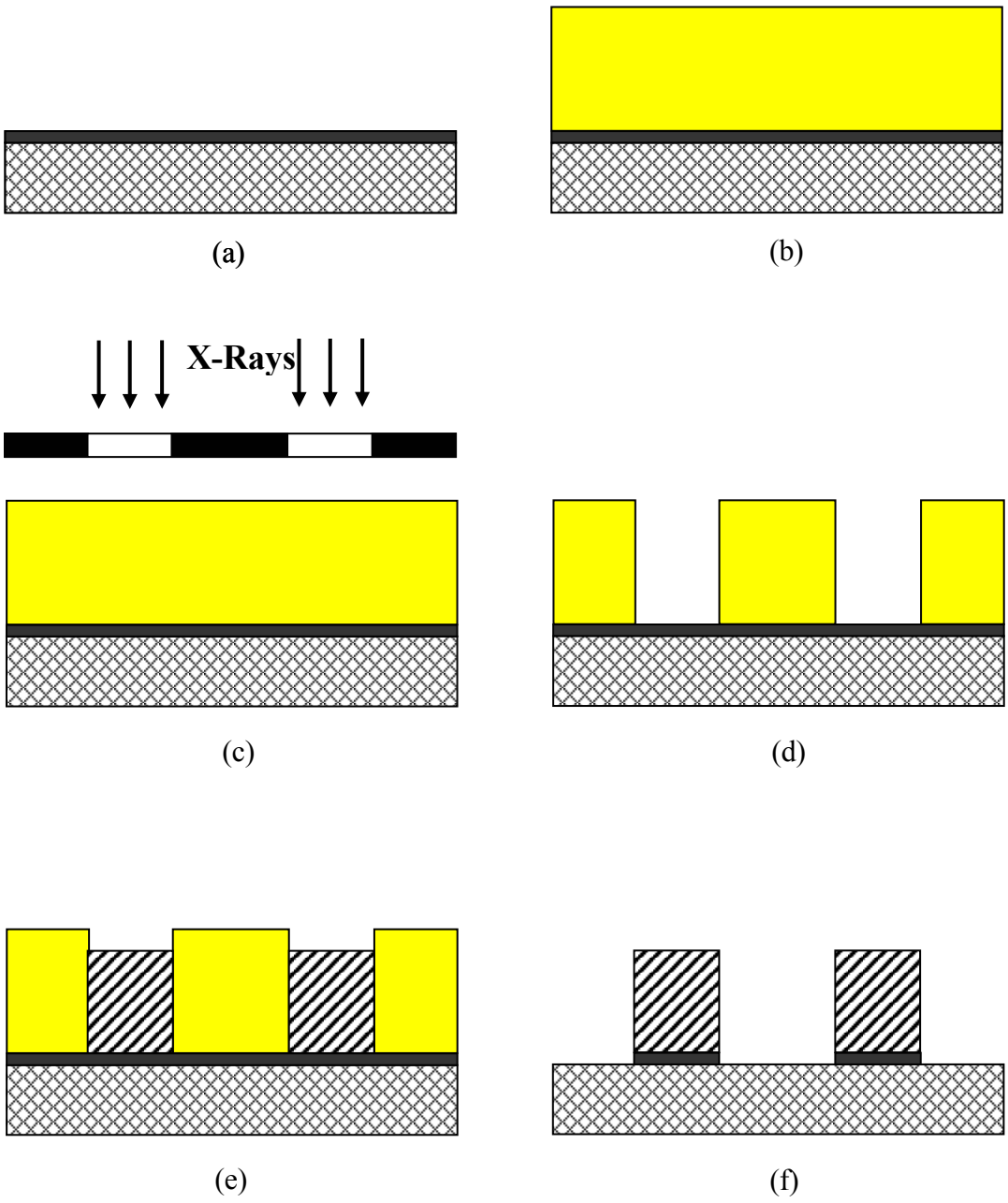

Figure 1.6 Direct LIGA Process:
a) Application of seed layer on substrate;
b) Application of photoresist;
c) X-ray exposure;
d) Photoresist development;
e) Metal deposition;
f) Removal of photoresist and seed layer.

moulding, which is in effect what makes LIGA more amenable to mass production than other X-ray lithography technologies.

The hot embossing procedure is illustrated in Fig. 1.7. Hot embossing is performed with the use of the metal mould insert obtained by electroplating metal into X-ray patterned photoresist over its top to create metal bridges between the metal fillings. This process is called “overplating”. The metal mould insert is impressed into softened plastic applied on a substrate to create the shape complimentary to the mould insert. The received plastic mould is cured and then filled with metal, which is called “secondary metal deposition”. This step is performed in the context of fabricating metal parts and may not be necessary in other cases. Lastly, the plastic and seed layer are stripped to obtain the final microstructure. The alternative to hot embossing is injection moulding and it basically differs from the former by the way the plastic mould is created. The LIGA replication techniques allow relatively inexpensive fabrication of parts precisely replicating the shape and size of the original X-ray-patterned part with minimum feature sizes as small as 0.1 μm and yields of up to 85 % without special clean-air premises [6]. Injection moulding is the preferred technique for large production volumes and hot embossing is the replication technique of choice when higher quality of parts is desired.

The structures discussed in this dissertation have been fabricated at the Institute for Microstructure Technology (IMT) in Karlsruhe, Germany using the ANKA synchrotron facility under one of its most developed processes of nickel electroplating into X-ray patterned PMMA photoresist spun on the Ti/TiOx seed layer applied onto alumina substrate. Nickel is one of the most widely used metals in LIGA for electroplating due to its ability to form deposits with extremely low internal stresses that result during electroplating (unlike other metals, such as silver or iron-nickel ferrimagnetic alloy that electroplate with significant internal stresses [5], thereby making fabrication of structures with fine features difficult). Alumina may also be considered a good choice of material for the substrate for the reason that it displays a low electrical loss tangent and a relatively high thermal conductivity as compared with other microwave-suitable dielectric materials, which renders it appropriate for high-power applications requiring good heat removal.

Speaking about the LIGA process in terms of its advantages and disadvantages, it is worth mentioning that LIGA is among few nanofabrication technologies capable of offering

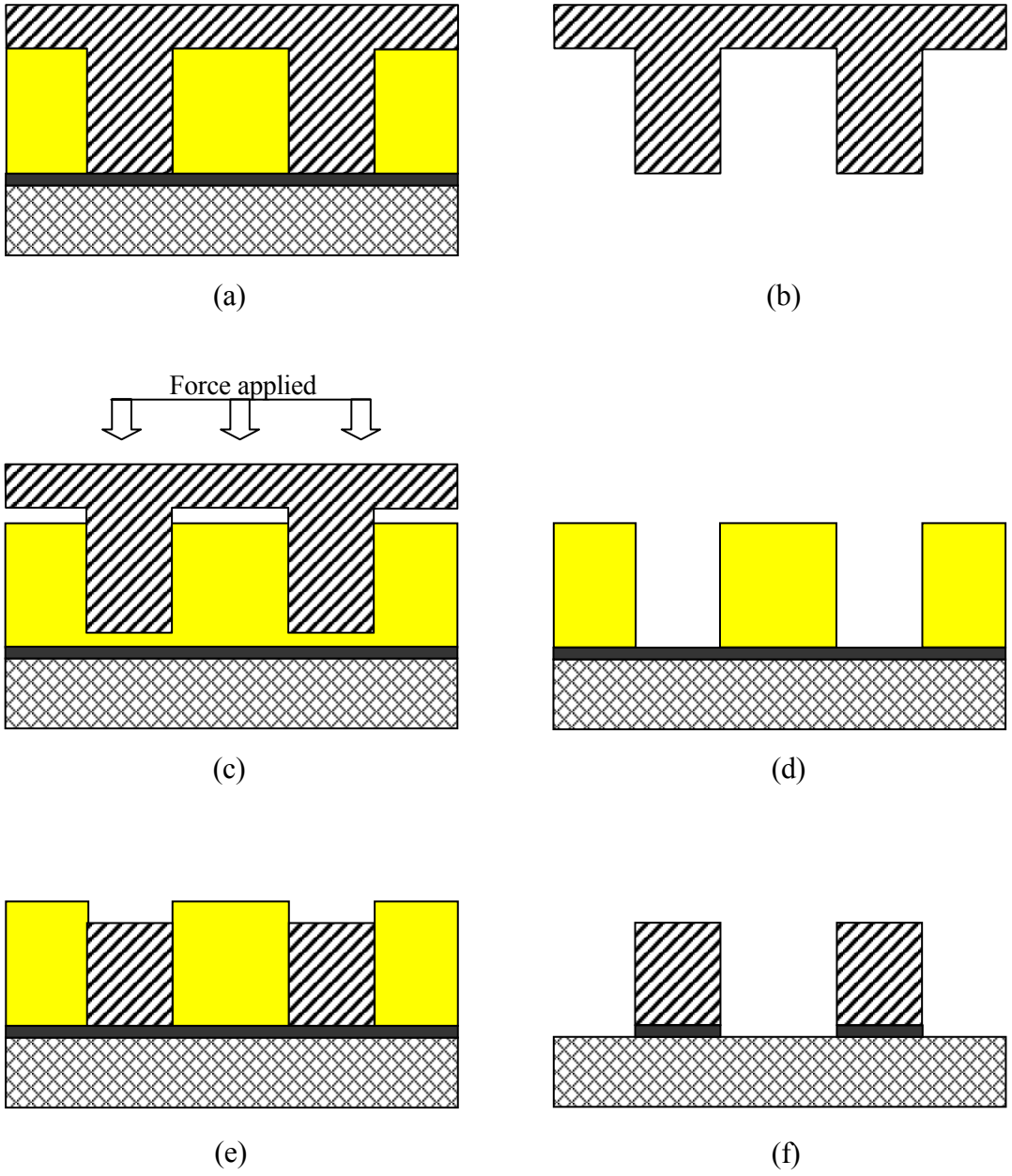

Figure 1.7 LIGA Process with Replication by Hot Embossing:
a) Metal overplating into X-ray patterned photoresist;
b) Release of metal mold insert;
c) Hot embossing;
d) Plastic mold;
e) Secondary metal deposition;
f) Release of final metal structure.

extreme vertical aspect ratios: ratios of several hundreds have been reported, whereas other lithography-based techniques, such as deep ultraviolet lithography (DUV), can only provide vertical aspect ratios of up to 22 [5]. Thanks to the high penetrating capacity of X-ray radiation, LIGA allows creating extremely high microstructures: the largest attempted so far at IMT was a 3.1-mm microstructure [6]. Together with being tall, LIGA microstructures feature excellent verticality: sidewall vertical slopes are ordinarily better than 89.9°. In addition to that, the LIGA process stands out with its possible minimum feature size of as low as 0.1 μm even in case of parts fabricated through plastic replication [6], as well as its achievable sidewall roughness of about 20 to 30 nm, which permits fabrication of structures with optical quality.

These LIGA properties make feasible many microwave devices with high-end performance. For instance, increased area of metal interface allows construction of structures with higher capacitance and higher power handling provided that there is an adequate heat removal. Also, LIGA has a great potential of drastically reducing manufacturing costs, size, weight, and improving performance and power consumption of RF systems by further eliminating off-chip passive components and meliorating their characteristics thanks to promising compatibility of LIGA with existing MMIC and CMOS processes [7] due to the fact the fabrication process does not involve high temperatures. For example, LIGA acceleration and vibration sensors have been fabricated on CMOS wafers by hot embossing using LIGA-fabricated mould inserts [6]. Bonding of LIGA microstructures to semiconductor wafers has also been attempted [6].

The chief disadvantages of LIGA stem from expensiveness of the X-ray exposure related procedures. They, however, are offset by the possibility of inexpensive replication using precision moulding techniques without resorting to X-ray exposure, which firstly requires access to the sources of high-energy collimated X-ray radiation that can be generated only by synchrotrons, facilities demanding high capital investments (there are only 47 synchrotrons around the world to date), and secondly only special masks can be used to shade selected areas and leave remaining areas exposed to X-rays. Fabrication of such masks is a costly multi-step procedure involving patterning of resist and electroplating. LIGA masks are created by electroplating metals with high atomic number, typically gold, that act as X-ray absorber into voids in resist patterned by optical lithography, electron-

beam lithography, or reactive ion etching [8]. The resist is spun on the carrier foil made of metals with low atomic number, typically titanium, which are X-ray transparent. The mask areas occupied by the absorber correspond to void areas in fabricated microstructures in case of positive photoresists such as PMMA or metal-filled areas in case of negative photoresists. Further reference on the LIGA technology may be found in [5] and [8].

1.4 Literature Survey

A very limited number of works dealing with research of application of LIGA for RF devices have been reported in the open sources to date. Most of the publications describe the RF LIGA projects undertaken at the University of Wisconsin-Madison, such as [9] and [10]. The first publication reports on X-band (8 – 12.4 GHz) stepped-impedance low-pass and broadband bandpass filters based on LIGA microstrip lines. The filters were realized with 200-μm thick nickel conductors on 420-μm thick fused quartz (relative permittivity 3.81 at 30 GHz) polished substrate. The nickel conductors were electroplated into X-ray patterned voids in the PMMA photoresist on a tri-layer metal film of titanium, copper, and titanium acting as the seed layer and stress buffer for the quartz and PMMA interface. Optical and SEM characterization revealed that structural heights had better than 1% thickness variation and average height variance within the batch yield was 10%. The sidewall surface roughness was less than 0.1 μm, while the top surface roughness was 1 – 2 μm. Sidewall slope was greater than 200:1. Theoretical design of the structures was performed using a quasi-static finite difference analysis.

A work similar to [9] is reported in [11], where a LIGA microstrip bandpass filter for the Ka-band (26.5 – 40 GHz) is described. The filter represents a five-stage coupled-line section designed under a Chebyshev polynomial. It was built on a 625-μm thick quartz substrate using 100-μm copper conductors electroplated into the X-ray patterned SU-8 photoresist on the seed layer of titanium-copper-titanium.

The only reference on the CPW-based microwave structures was found in [10]. It reports on a 6-dB CPW coupler and a single bandpass filter section designed for the centre frequency of 15 GHz. The structures were built using the LIGA process described in [9] with the only difference that 80-μm thick nickel conductors were electroplated.

1.5 Research Objectives

The purpose of the research described hereby has been the study of the advantages presented by the LIGA fabrication technology to microwave engineering. The ability to build tall metal structures with high vertical aspect ratio has been the primary LIGA feature under investigation. A microwave coupler with equal division of power, or 3-dB coupler, has been selected as the exemplary microwave device, whose design might be simplified and performance improved, if fabricated using LIGA. It was investigated whether the coupler would prove to be feasible if built using the simple and compact single-metal layer edge-coupling topology, transformed into the side-coupling topology by LIGA. Fabrication was carried out at the Institute for Microstructure Technology (IMT), Karlsruhe Research Centre, Germany using one of their most developed LIGA processes.

It was decided that the research would be conducted in the Ku and K frequency bands, which totally span from 12.4 to 26.5 GHz, due to the possibility of creating very small passive devices and availability of appropriate testing equipment. Yet, this frequency range was high enough to reveal the benefits of LIGA to MMIC applications with the emphasis on possible improvement of their performance and dimensions.

In order to attain the stated goals, the research work concentrated on the following objectives:

1. Characterization of HVAR LIGA structures, viz. transmission lines and coupled-line sections, to establish relation between their geometrical and electrical parameters. This had to be performed since no analytical closed-form expressions could be found in the literature.
2. Design and fabrication of power-bifurcating, or 3-dB coupler representing a coupled-line section complete with feeding transmission lines.
3. Design and fabrication of auxiliary structures required to carry out the testing and measurement of the primary structures.
4. Testing and measurement of the primary structures to verify the approaches used for their design.

1.6 Thesis Organization

This present thesis has been composed of the following chapters:

Chapter 2 discusses the mechanism of electromagnetic coupling between closely spaced conductors and gives a brief review of directional couplers. It then proceeds with a discussion of the modal analysis of coupled lines, followed by description of backward-wave directional couplers. The chapter concludes with presentation of the case for the HVAR couplers required to reach the tight levels of coupling.

Chapter 3 demonstrates characterization and its results for the HVAR transmission and coupled lines to provide relations between their geometrical and electrical parameters.

Chapter 4 describes design of a 3-dB HVAR coupling structure, shows simulation results, and finally gives details of the fabrication process.

Chapter 5 illustrates the used measurement procedure and results.

Finally, Chapter 6 concludes this dissertation with a discussion of project results and description of possible future work.

Chapter 2
COUPLED-LINE DIRECTIONAL COUPLERS

2.1 Principle of Electromagnetic Coupling

A transmission line representing a system of *N+1* non-touching conductors, where one of the conductors acts as the reference of zero potential (in other words, *N* transmission lines with a common reference placed in proximity to each other) can generally support *N* independent, or normal, propagation modes, each one described with a unique propagation constant and nonzero voltages and currents [12]. When the media, where the system is located is homogeneous, i.e. electromagnetic waves propagating along the conductors do not experience refraction, the modes will be transverse electromagnetic (TEM) and they, still being independent, will have identical propagation constants [12]. When one of the *N* transmission lines is excited with a time-varying signal, *N* sets of voltages and currents will be excited in the system due to the electromagnetic coupling. The essence of the electromagnetic coupling may be readily seen from Faraday's Law (2.1) stating that any change in the magnetic environment produces opposing electromotive force:

$$\oint_C \vec{E} \cdot d\vec{l} = -\frac{\partial}{\partial t} \int_S \vec{B} \cdot \hat{n} ds \tag{2.1}$$

where electric field intensity *E* is tangential to contour *C* and normal to magnetic flux density *B* passing through an arbitrary surface *S* bounded by *C*. For a stationary system, counteracting electromotive force will be induced by any temporal change of perpendicular magnetic field. Written in terms of field components after performing vector operations, Faraday's Law may be presented as follows:

$$emf = \oint_C E_t dl = -\frac{\partial}{\partial t} \int_S B_n ds \tag{2.2}$$

where E_t and B_n are mutually orthogonal components of electric and magnetic fields respectively. One of the implications of (2.2) is that if there are two closely spaced conduc-

tors and the first one is acted upon by magnetic field produced by current in the second conductor, there will be induced electromotive force *emf* causing flow of current in the first conductor in the direction opposing the change of magnetic field. Thus, electromagnetic coupling is established between the two conductors via magnetic-flux linkage as shown in Fig. 2.1.

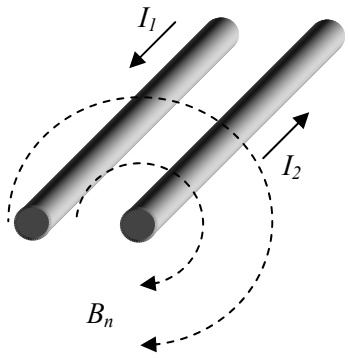

Figure 2.1 Magnetic-flux linkage between two conductors

In case if time-varying magnetic flux is caused by harmonic current, (2.2) may be written in the phasor form as:

$$emf = -j\omega \int_S B_n ds \tag{2.3}$$

where ω is the operating angular frequency. It is clear from (2.3) that in order for electromagnetic coupling to exist in a stationary system of conductors, one of them must be driven from an AC source.

2.2 Review of Directional Couplers

A four-port microwave device demonstrating electromagnetic coupling is called a "directional coupler". The simplest example of the directional coupler is a pair of unshielded transmission lines placed closely to each other and having a common reference of zero potential. Assuming that the lines are identical and the cross section of the coupled part does not change along its entire length, i.e. the coupled part is uniform and symmetrical, as shown in Fig. 2.2, then the scattering matrix, [S], of such a network will be as follows,

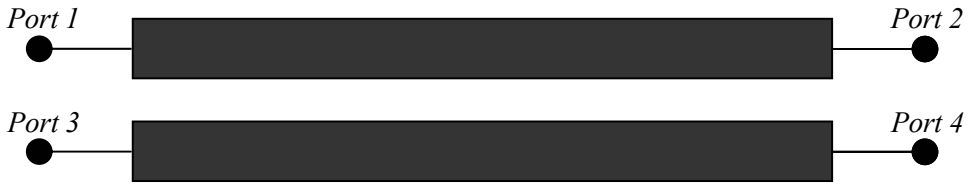

Figure 2.2 A two-line four-port uniformly coupled symmetrical section

provided the network is ideally matched to the characteristic impedance of the network at all four ports:

$$[S] = \begin{bmatrix} 0 & S_{12} & S_{13} & S_{14} \\ S_{12} & 0 & S_{23} & S_{24} \\ S_{13} & S_{23} & 0 & S_{34} \\ S_{14} & S_{24} & S_{34} & 0 \end{bmatrix} \tag{2.4}$$

If the network is not built of any nonreciprocal media, it shows reciprocal properties, which means that any port can serve as input and remaining ports will serve as appropriate output ports. Depending on the direction that the coupled wave travels, which in its turn depends on the geometry of the coupler [12], coupled power will appear either at *Port 3* or at *Port 4* as shown in Fig. 2.2. In the former case, the coupler will be backward-wave, and in the latter – forward-wave. Assuming a backward-wave directional coupler, i.e. the coupler where the coupled wave on the secondary line propagates in the direction opposite to the direction of the wave on the primary line, the elements of matrix (2.4) will have the following meaning when Port 1 acts as the input: S_{12} – throughput, S_{13} – coupling, S_{14} – isolation. By the virtue of reciprocity, the remaining elements of matrix (2.4) correspond to the above as follows: $S_{23} = S_{14}$, $S_{24} = S_{13}$, $S_{34} = S_{12}$. So when the input is assigned to Port 1, Port 2 becomes direct (through) port, Port 3 – coupled port, and Port 4 – isolated. Ideally, no power should appear at the isolated port or S_{14} should be zero, i.e. all power should be divided between the direct and coupled ports with the following relation being true:

$$|S_{12}|^2 + |S_{13}|^2 = 1 \tag{2.5}$$

In this case, the [S] matrix of the coupler looks like:

$$[S] = \begin{bmatrix} 0 & S_{12} & S_{13} & 0 \\ S_{12} & 0 & 0 & S_{13} \\ S_{13} & 0 & 0 & S_{12} \\ 0 & S_{13} & S_{12} & 0 \end{bmatrix} \tag{2.6}$$

Performance of couplers is described with the help of the following four main parameters [13]:

$$\text{1) Coupling, } K = 10\log\frac{P_1}{P_3} = 20\log|S_{13}|, \text{ dB;} \tag{2.7a}$$

$$\text{2) Directivity, } D = 10\log\frac{P_3}{P_4} = 20\log\left|\frac{S_{13}}{S_{14}}\right|, \text{ dB;} \tag{2.7b}$$

$$\text{3) Isolation, } I = 10\log\frac{P_1}{P_4} = -20\log|S_{14}|, \text{ dB;} \tag{2.7c}$$

$$\text{4) Throughput, } G = 10\log\frac{P_1}{P_2} = 20\log|S_{12}|, \text{ dB;} \tag{2.7d}$$

where P_1, P_2, P_3, and P_4 are levels of power at the input, direct, coupled, and isolated ports respectively.

The coupling factor K shows the fraction of input power that is electromagnetically coupled to the output port; the directivity factor D indicates the ability of the coupler to isolate between the forward and backward waves, where one of them is the coupled wave depending on the coupler type; and isolation factor I is the measure of the coupler's ability to deter the useful power from traveling to the isolated port. The isolation factor is linearly connected to the above quantities as follows:

$$I = K + D, \text{ dB} \tag{2.8}$$

The ideal coupler, as described by [S]-matrix (2.6), would have infinite isolation and directivity.

From the energy conservation law, in order for a network to be lossless its [S] matrix should be unitary [13], which means that each matrix column should be orthogonal to the conjugates of other columns and parallel to its conjugate. It can be easily seen from (2.5) and (2.6) that a directional coupler matched at all four ports is ideally lossless. Complimentarily, it may be inferred from the energy conservation condition that any lossless, reciprocal four-port network matched at all ports is a directional coupler [13]. Therefore, directional couplers may be designed for the condition of being simultaneously lossless,

reciprocal, and matched at all ports. Unlike directional couplers, three-port couplers, such as Wilkinson coupler, have to be lossy in order to be reciprocal and matched at all ports [13].

A special case of the directional coupler in which the signals at the two output ports are equal (which corresponds to the 3-dB level of coupling) and differ in phase by 90 degrees is called “hybrid”.

2.3 Even- and Odd-Mode Analysis

As stated in Section 2.1, a system of *N+1* conductors may generally support *N* main propagation modes. Therefore, a system of three conductors with one conductor acting as the ground, or alternatively two transmission lines with a common ground, can support two main modes of propagation, or bimodal propagation. The modes are called “even mode” and “odd mode” [12]. Linear combination of these modes can adequately describe coupling between uniform symmetric coupled structures [12]. An example of a two-line coupled section implemented in coplanar waveguide is presented in Fig. 2.3.

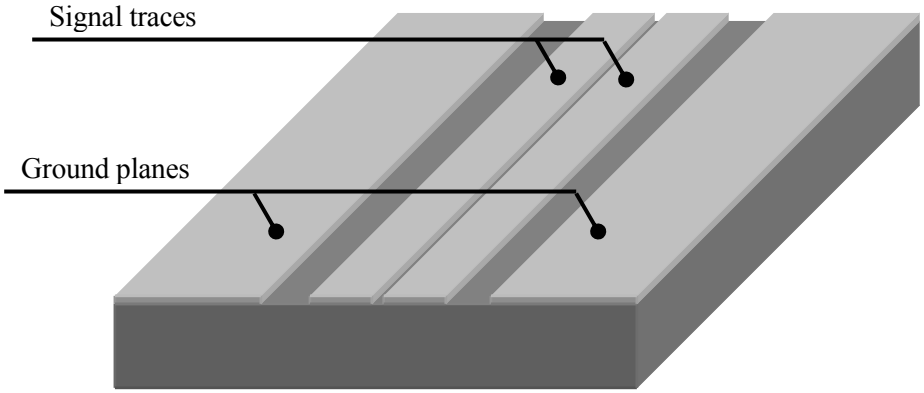

Figure 2.3 An example of CPW coupled-line section

Even mode exists alone in a coupled-line section when both lines are at the same potential. In this case, the lines may be said to be separated by the magnetic wall, which means that the tangential component of the magnetic field and the normal component of the electric

field vanish at the surface of the wall, while the normal component of the magnetic field and the tangential component of the electric field remain unchanged while being at the wall interface [13]. The appropriate even-mode field distribution is displayed in Fig. 2.4.

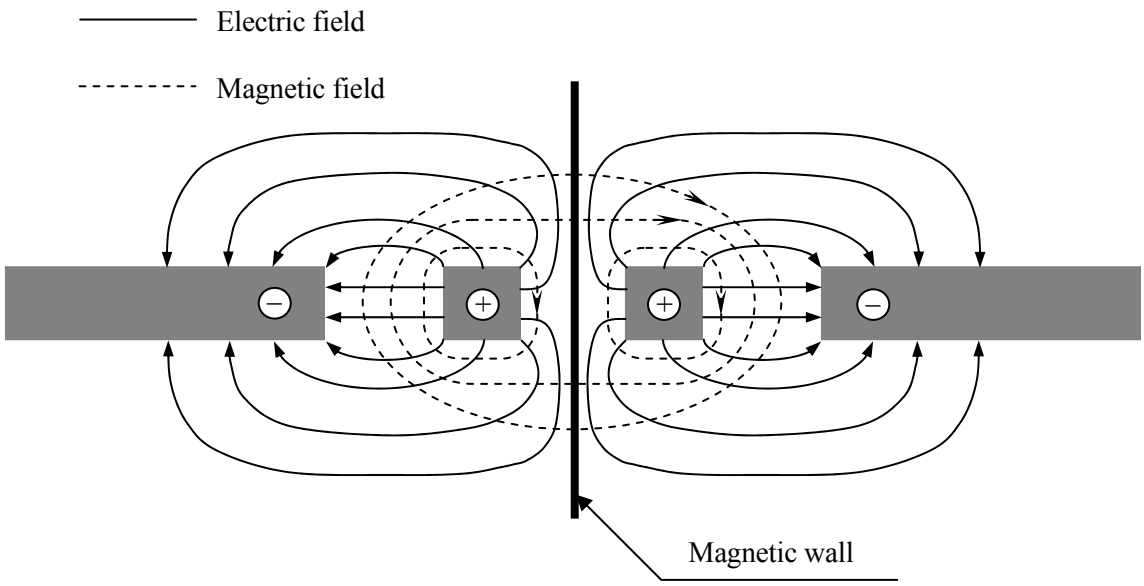

Figure 2.4 Cross section of CPW coupled lines supporting the even mode

Odd mode may be excited in a coupled-line section when the lines are at a potential of the same magnitude but opposite polarity. In this case, the lines may be said to be separated by the electric wall, which is dual to the magnetic wall. At the electric wall interface, the tangential magnetic field and normal electric field exist, while the normal magnetic field and tangential electric field disappear [13]. The appropriate odd-mode field distribution is shown in Fig. 2.5.

The coupling between the lines may also be presented in terms of self and mutual capacitances as shown in Fig. 2.6. Capacitances between the lines and the ground planes are self-capacitances. In Fig. 2.6, those are C_1 for the first line and C_2 for the second line. Capacitance between the lines, C_m in Fig. 2.6, is the mutual capacitance.

In the even mode, the magnetic wall prevents the electric field from passing between the signal lines and mutual capacitance C_m disappears. Even-mode capacitance C_e therefore

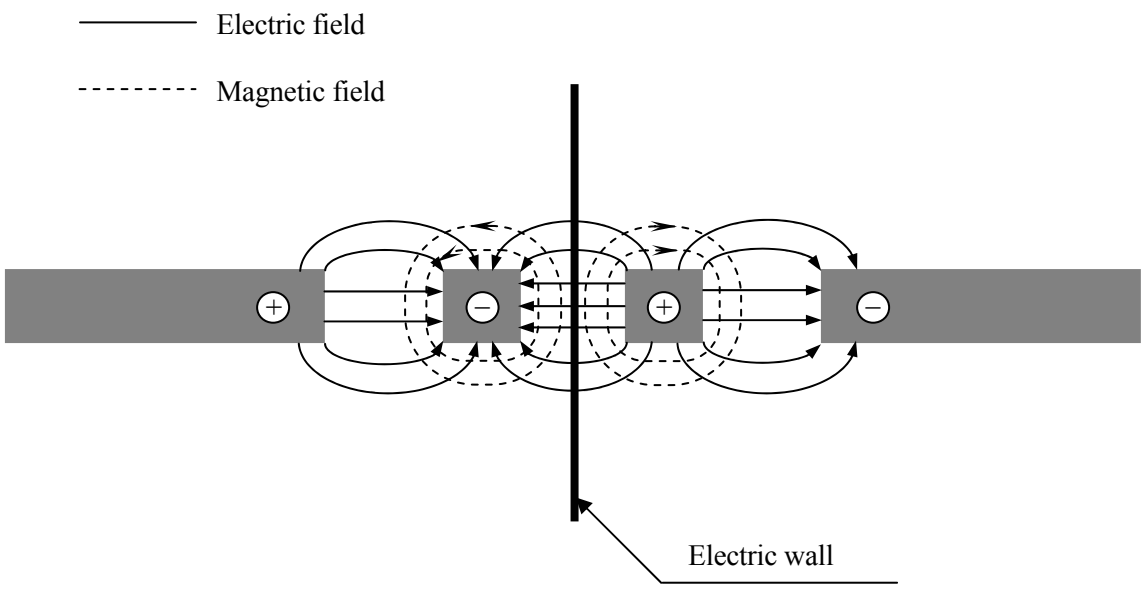

Figure 2.5 Cross section of CPW coupled lines supporting the odd mode

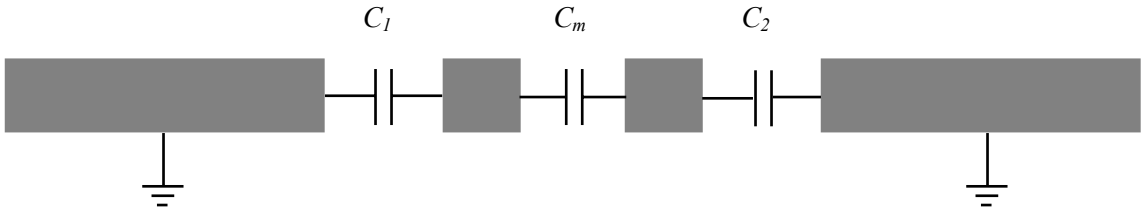

Figure 2.6 Representation of CPW coupled lines in terms of capacitances

may be expressed in terms of only self-capacitances, or per-unit-length capacitances of each line. For uniform symmetrical lines [12]:

$$C_e = C_1 = C_2 \tag{2.9}$$

In the odd mode, capacitance of the network is a combination of self-capacitances and the mutual capacitance. For uniform symmetrical lines, the odd-mode capacitance C_o is defined as [12]:

$$C_o = C_1 + C_m = C_2 + C_m \tag{2.10}$$

All capacitances given here must be expressed on a per-unit-length basis.

Characteristic impedance Z_0, which depends solely on physical properties of the transmission line, may be related to generalized per-unit-length capacitance C as follows [12]:

$$Z_0 = \frac{1}{v_{ph} C} \tag{2.11}$$

where v_{ph} is the wave phase velocity along the transmission line.

Considering expressions (2.9-2.11) and Figs. 2.3-2.4, the following may be inferred about bimodal propagation in a two-line coupled section:

- The even-mode characteristic impedance is the impedance from one signal conductor to the ground when the conductors are separated by the magnetic wall, or when the lines are driven synchronously from equal voltage sources;
- The odd-mode characteristic impedance is the impedance from one signal conductor to the ground as well as to the other conductor when the conductors are separated by the electric wall, or when the lines are driven from equal voltage sources of opposite polarity;
- The even-mode characteristic impedance is always greater than the odd-mode characteristic impedance;
- The modal characteristic impedances may only become equal when the mutual capacitance disappears, which is equivalent to uncoupled lines.

If the coupled lines are embedded in a homogeneous dielectric medium, modal phase velocities will be equal [12]. Therefore, the modal effective permittivities, defined as the ratio of the velocity of light in free space c to phase velocity v_{ph} of wave propagation along the lines (2.12), will also be equal.

$$\varepsilon_{eff} = \left(\frac{c}{v_{ph}} \right)^2 \tag{2.12}$$

However, if the lines are constructed in such a way that propagation of the even-mode and odd-mode waves takes place in the regions of different permittivity, the modal phase velocities, and consequently modal effective permittivities will differ due to different degrees of refraction generally experienced by each modal wave in an inhomogeneous dielectric medium. The difference between the modal phase velocities usually depends on geometrical parameters of the lines and relative permittivities of used dielectrics.

2.4 Backward-Wave Directional Couplers

The backward-wave directional coupler owes its name to the fact that the coupled wave on the secondary line propagates in the direction opposite to the direction of the incident wave on the primary line. The block diagram of the backward-wave directional coupler and definition of its ports is shown in Fig. 2.7.

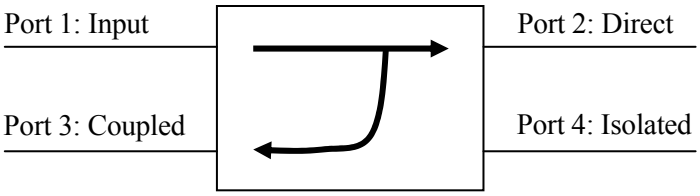

Figure 2.7 Block diagram of backward-wave directional coupler

According to [12], the necessary condition for the backward-wave directional coupler is the following balance of characteristic impedances:

$$\frac{Z_{0e}}{Z_0} = \frac{Z_0}{Z_{0o}} \tag{2.13}$$

which reduces to

$$Z_0 = \sqrt{Z_{0e} Z_{0o}} \tag{2.14}$$

where Z_0 is the characteristic impedance to which the coupled lines are terminated, Z_{0e} and Z_{0o} are the even-mode and odd-mode characteristic impedances of the coupled lines respectively.

For an ideal TEM backward-wave coupler described with (2.6), where no power is coupled to the isolated port, the main parameters represented by nonzero elements in (2.6) may be described using the relations given in [12]:

$$S_{12} = \frac{\sqrt{1-k^2}}{\sqrt{1-k^2}\cos\theta + j\sin\theta} \tag{2.15}$$

$$S_{13} = \frac{jk\sin\theta}{\sqrt{1-k^2}\cos\theta + j\sin\theta} \tag{2.16}$$

where S_{12} and S_{13} represent throughput and coupling, k is expressed as

$$k = \frac{Z_{0e} - Z_{0o}}{Z_{0e} + Z_{0o}} \tag{2.17}$$

and θ is the electrical length of the coupled-line section expressed in radians as

$$\theta = \beta l \tag{2.18}$$

with β being phase constant, and l – length of the coupled-line section.

Considering expressions (2.13-2.18), the following observations can be made:

- The maximum level of coupling S_{31} occurs when the electrical length θ is equal to $\pi/2$ or 90˚, which corresponds to physical length l being equal to $\lambda_{eff}/4$, where λ_{eff} is the effective wavelength in the waveguiding media. Therefore, it may be said that the maximum level of coupling occurs at the frequency when the length of the coupled-line section becomes equal to a quarter of the effective wavelength or odd multiple thereof.
- For a quarter wavelength long coupled-line section,

$$S_{12} = -j\sqrt{1-k^2} \tag{2.19a}$$

$$S_{13} = k = \frac{Z_{0e} - Z_{0o}}{Z_{0e} + Z_{0o}} \tag{2.19b}$$

- Since the electrical length of the coupled-line section changes with frequency, coupling and throughput, as well as other related parameters in a non-ideal coupler, are frequency dependent.
- When the length of the coupled-line section becomes equal to a half of the effective wavelength or multiple thereof, coupling in an ideal coupler disappears and all incident power proceeds to the direct port. The same happens at DC.
- Theoretically, the frequency response of such coupler is periodic and repeats every span of frequency equal to a half of the effective wavelength.
- For the given characteristic impedance of the network Z_0, the required level of coupling $k = S_{13}$ can be obtained if the following modal impedances are realized in a coupled-line section:

$$Z_{0e} = Z_0\sqrt{\frac{1+k}{1-k}} \tag{2.20a}$$

$$Z_{0o} = Z_0\sqrt{\frac{1-k}{1+k}} \qquad (2.20b)$$

For instance, if a coupler is required with the level of coupling $K = -3$ dB, which corresponds to $k = 10^{K/20} = 0.78$, in a 50-Ω system, then the even-mode and odd-mode impedances of 120.9 Ω and 20.7 Ω respectively have to be realized in a coupled-line section.

- Throughput S_{12} and coupling S_{13} are in phase quadrature irrespective of the length of the coupled-line section, which implies that backward-wave directional couplers may be used as quadrature phase shifters over a wide range of frequency.

2.5 Comparison of Tight Directional Couplers

Many applications, such as balanced mixers and amplifiers, require hybrid, or 3-dB couplers. It is difficult to reach this tight level of coupling in couplers realized in planar waveguiding media since very small gaps are required between the lines. Therefore, other types of couplers have to be used in order to obtain the tight levels of coupling. These usually include (1) branch-line and rat-race couplers, (2) interdigital and tandem couplers, (3) multilayer/broadside couplers, and (4) lumped-element couplers. Presented below is their brief description and comparison against the coupled-line coupler for usage in small-scale microwave circuits. The information is derived from [12], where further reference on these types of couplers may be found.

1. ***Branch-line and rat-race couplers.*** These are principally the same types of couplers differing only in the phase difference between the direct and coupled ports: 90 degrees for branch-line couplers and 0 or 180 degrees for rat-race couplers. They represent a pair of transmission lines interconnected by a pair of shunt branches at their outputs. The length of all branches in the branch-line coupler makes a quarter of a wavelength. In the rat-race coupler all branches but one, which is three quarters of a wavelength, are a quarter of a wavelength long. Required properties of the couplers are obtained by proper selection of characteristic impedances of the branches. Comparing these types of couplers with the coupled-line backward-wave coupler, it should be noted that they are intrinsically larger in the area occupied on the substrate and they have inconvenient shapes that are very

wasteful of the substrate space. Since all the ports of these couplers are electrically connected, they do not provide separation of DC from the input at the coupled port, which prevents them from usage in some applications. More importantly, the branch-line and rat-race couplers are perfectly matched at ports only at their centre frequency, at which there is also complete isolation between decoupled ports. In addition, they are able to provide phase quadrature between the signals at the direct and coupled ports also only at their centre frequency. The coupled-line backward-wave coupler satisfies these properties independently of the operating frequency. Therefore, usage of the branch-line and rate-race couplers is limited to the applications requiring less than about a 20 % frequency bandwidth only. An example of a branch-line coupler is shown in Fig. 1.4c.

2. ***Interdigital and tandem couplers.*** Both types of these couplers reach tight levels of coupling through increase of the mutual capacitance by using a greater number of coupled lines electrically interconnected with bonding wires. These couplers intrinsically suffer from a larger area occupied on the substrate as well as from the necessity to use bonding wires adding parasitic inductances, which limits their application in MMICs. An example of an interdigital coupler is shown in Fig. 1.4b.
3. ***Multilayer/broadside couplers.*** The main principle employed in these couplers is creation of a number of conductors on top of each other separated by layers of dielectric. Tight levels of coupling are achieved owing to the fact that the conductors face each other with their broad sides, which increases their mutual capacitance. These couplers require a more involved fabrication technology capable of creating multiple metal and dielectric layers, with ensuing consequences such as interconnects between the metal layers prone to parasitic resonances. An example of multilayer/broadside coupler is shown in Fig. 1.4a.
4. ***Lumped-element couplers.*** These couplers are composed of single reactive elements. Being the couplers of choice in the applications operating at frequencies below 3 GHz due to their exclusively small dimensions, they start to exhibit poor quality (Q) factor at higher frequencies, where their dimension advantage also shrinks.

2.6 Tight Coupling: The Need for High Vertical Aspect Ratio Couplers

As mentioned before, realization of tight couplers in a simple edge-coupled planar topology with a single metal layer requires very narrow gaps between the lines that are below the capabilities of existing fabrication technologies. For instance, a 4-μm gap is required to realize a 3-dB coupler on a 75-μm GaAs substrate (and less gaps on substrates with lower relative permittivity), whereas a typical MMIC plating metallization process can only achieve gaps greater than 8 μm for 4 to 5-μm thick conductors in order not to compromise production yields [12, p. 287].

In order to reach tight levels of coupling, low values of the odd-mode impedance must be provided, which in its turn requires high values of the mutual capacitance, see Sections 2.3 and 2.4. Higher mutual capacitance may be provided at the expense of using either larger area of metallic interface, or dielectrics with higher relative permittivity. The latter approach might not facilitate good dispersive characteristics for quasi-TEM transmission lines, where wave propagation takes place in at least two different dielectric regions, as it results in a greater discontinuity in the dielectric environment. Creating larger areas of metallic interface is difficult in planar circuits, as it requires conductors that are prohibitively wide for small-scale microwave networks. Therefore, single-metal layer planar coupled-line couplers are usually not considered the optimum choice in achieving tight levels of coupling. The answer to this problem might be exploring the third dimension, or height, by building tall conductors with high vertical aspect ratio (HVAR), reaching thereby high values of the mutual capacitance without wasting the area of the substrate. One of the fabrication technologies that permits creation of such conductors is LIGA, see Section 1.3. SML couplers that use HVAR tall conductors become side-coupled, rather than edge-coupled. Further in the thesis, research on the LIGA-fabricated HVAR lines and coupled sections conducted to explore the feasibility of reaching the tight levels of coupling is described. The structures under research were single-metal layer lines and coupled sections fabricated using the LIGA technology at the Institute for Microstructure Technology (IMT), Research Centre Karlsruhe, Germany.

2.7 Chapter Summary

Electromagnetic coupling is established in a system of closely spaced transmission lines, where one or several lines are driven from an AC source. It is only in the case of time-varying fields, that the electromagnetic coupling may exist in a system of stationary conductors. N main propagation modes may be supported in a system of $N+1$ conductors, with one conductor acting as the reference of the zero potential. In a system of two closely spaced symmetric and uniform transmission lines with a common ground, two main propagation modes, viz. the even mode and odd mode, may be supported.

Any four-port structure that simultaneously demonstrates reciprocity, losslessness, and ability to be matched at all ports is a directional coupler. This condition stems from the energy conservation law and it does not hold true for the three-port couplers.

Ideally, all the power entering a directional coupler should flow to the direct and coupled ports. In actual directional couplers, a fraction of incident power flows to the fourth port, called "isolated port". This degree of imperfection is described with the isolation factor, which is the ratio of the incident power to the power at the isolated port and is ideally infinite.

Depending on the direction where the coupled wave propagates with respect to the incident wave, directional couplers are classified as forward-wave and backward-wave. The coupling in a backward-wave coupled-line coupler is frequency dependent and reaches its maximum level when the coupled-line section becomes quarter-wavelength long.

A special case of the directional coupler that exhibits equal division of the incoming power, or whose coupling is equal to 3 dB, is called "hybrid". Hybrids also feature the phase quadrature between the direct and coupled waves irrespective of the operating frequency, which renders them suitable for the role of a fixed quadrature phase shifter. The hybrids are indispensable in a wide variety of microwave applications. However, they are difficult to realize in a compact single-section, single metal layer planar topology due to required high mutual capacitance between the coupled lines. This problem may be remedied by application of fabrication technologies capable of creating closer spaced conductors with larger surface area. One of the technologies permitting this is LIGA.

The following chapters characterize the LIGA microwave coupled-line structures and show how application of LIGA allows fabrication of simple and compact hybrids.

Chapter 3
CHARACTERIZATION OF HIGH VERTICAL ASPECT RATIO STRUCTURES

3.1 Selection of Waveguiding Structure: Coplanar Waveguide

The majority of small-scale microwave networks are built based on microstrip, slotline, or coplanar waveguide (CPW) lines*. Among these, CPW has been recently gaining increased popularity as the transmission line of choice for MMIC applications [14] due to a number of benefits, which are listed below [15]:

- Devices and components can be grounded on CPW directly on the front face without vias, which are prone to parasitic resonances;
- CPW lines suffer from much less dispersion than microstrip lines, making them more suitable for millimetre-wave networks;
- Required characteristic impedance can be realized with almost any trace width and spacing combination, unlike microstrip lines that only have one degree of design freedom;
- Substantially higher packing density is possible because the ground planes provide shielding between adjacent CPW lines;

*Note: *1. A microstrip waveguide consists of a signal conductor and a ground plate carried by a substrate and located on its opposite sides.*
2. A slotline waveguide consists of two closely placed metal plates on a substrate, where wave propagation takes place in the slot between the plates.
3. A coplanar waveguide consists of a dielectric substrate that carries a signal conductor placed between two ground planes, see Fig. 3.1.

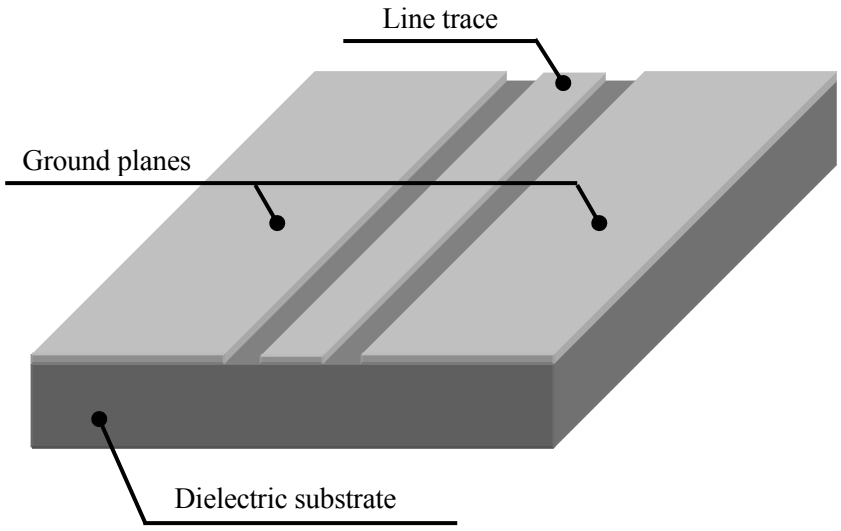

Figure 3.1 An example of CPW line

- Without the bottom-face ground plane, lumped elements exhibit less parasitic capacitance.

Additional advantage of the CPW is that the minimum loss for a given cross section occurs at about 60-Ω characteristic impedance, whereas the minimum loss for microstrip occurs at about 25 Ω [15]. This renders the CPW potentially less lossy when applied in standard 50-Ω networks.

Unlike microstrip lines, CPW electric field lines can terminate to the ground without passing the dielectric. Therefore, the CPW networks built using tall LIGA conductors may possibly allow further separation of the field from the dielectric with positive effect on dispersive characteristics of the lines. With respect to the aforementioned, it was decided that application of the CPW, rather than other types of waveguides such as microstrip lines, would better exemplify advantages given by LIGA.

3.2 Design of CPW-based structures

Since coplanar waveguides typically represent metal conductors supported by a dielectric substrate, the field propagating along the line is not entirely contained in a homogeneous dielectric region, see Fig. 3.2. Therefore, the field propagation properties and the line per-unit-length parameters may not be accurately determined from the relative permittivities

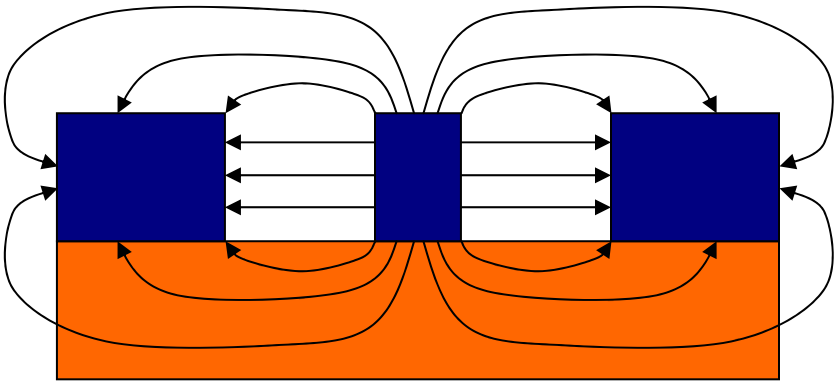

Figure 3.2 Approximate distribution of electric field in a CPW

of either region, which most typically are the air and substrate. For inhomogeneous dielectric media, another quantity known as "effective permittivity" is used. The magnitude of the effective permittivity lies between the magnitudes of the relative permittivities of the used dielectrics. For the case of CPW in air (or vacuum), the following relation holds true:

$$1 < \varepsilon_{eff} < \varepsilon_r \tag{3.1}$$

where 1 is the relative permittivity of air (or vacuum), ε_{eff} – effective permittivity of the dielectric medium, and ε_r – relative permittivity of the substrate.

The most accurate way to find the effective permittivity is the ratio given in (2.12), where the phase velocity must be found using some rigorous technique.

Another ramification of the field propagation in an inhomogeneous dielectric medium is that pure TEM waves cannot be supported, since the phase match at the air-dielectric interface is impossible due to refraction. This means that determination of the important electrical characteristics of the transmission line, such as characteristic impedance and phase velocity, cannot be reduced to finding the per-unit length parameters associated with the structure. However, CPW may support so called "quasi-TEM" modes, which are close to TEM. For the case of quasi-TEM modes, the electrical characteristics of the line cannot be determined from static solutions accurately, but have to be approximated instead. The quasi-TEM assumption is valid for CPW as long as its cross-sectional dimensions are much shorter than the effective wavelength [16]. In most cases, accurate determination of

fields in non-TEM structures has to be performed numerically, especially when complex geometries are involved.

3.2.1 Review of Published Techniques

Since the CPW cannot support the pure TEM mode, providing accurate closed-form expressions allowing synthesis or analysis of the CPW, let alone CPW-based structures, is difficult and in most cases is impossible. As the analysis of the publications treating design of the CPW and CPW-based structures shows, the majority of the design approaches have to rely on some kind of assumptions, the most common being the quasistatic assumption (in a quasistatic system, signal time variations are so slow that the corresponding wavelength is much greater than the system's dimensions, in which case the quasistatic solution is very close to the static solution when fields do not vary in time), which is valid in the frames given in [16]. All analyzed design techniques found in the literature proceed from the assumption that one or several geometrical parameters are infinite or zero. The zero conductor height and/or infinite substrate thickness are the most critical assumptions found in the literature. Early treatments of the CPW used both of these geometrical assumptions [17]. Subsequent treatments considered the substrate thickness to be finite, though still assuming the metal height to be zero, e.g. [18-22]. The zero-thick conductor assumption is obviously not suitable for describing the LIGA CPW structures, where the influence of increased conductor height is the major focus of research. Other references proceed on the assumption that the substrate thickness is infinite, e.g. [14], [16], [20], [23], [24], [25]. The infinitely thick substrate assumption is also likely to cause severe errors for the case of commensurable conductor height and substrate thickness encountered in LIGA. In addition, the substrate thickness must not be neglected as it approaches the waveguide slot width [17, 24].

The general approach applied in these techniques is solving two-dimensional Laplace's equation to find distribution of potentials in the cross-section of the transmission line once the quasistatic assumption has been considered valid. Depending on the geometry of the line cross section and its symmetry, the solution of Laplace's equation can be reduced to a closed-form expression, but this occurs only in exceptional cases. In most practical cases, Laplace's equation must be solved using numerical techniques. Once solution of Laplace's

equation is finished, the computed distribution of potentials is used to find distribution of the electric field. More detailed information on this may be found in numerous references, e.g. [26]. A very powerful technique for solving Laplace's equation that is capable of accounting for the finite metal thickness is the conformal mapping, allowing to find fields for virtually any lengthwise uniform waveguiding shapes by transforming the initial cross section topology into a simpler one, provided that the quasi-TEM propagation might be assumed. A very good treatment of one of the conformal mapping analysis approaches, the Schwarz–Christoffel conformal transformation, as applied to coplanar waveguides is presented in [27]. This approach is exact insofar as the quasistatic in vacuo capacitance, inductance, and characteristic impedance are concerned. However versatile this technique is, it, firstly, leads to closed-form expressions in rare cases only and, secondly, it does not account accurately for the effective permittivity of an inhomogeneous waveguiding media hence approximate definitions of the effective permittivity have to be used.

The sources referred to above consider only CPW transmission line design issues. The number of publications treating design of coupled CPW lines is rather scarce and very few analytical formulas are available in the literature [12], with the majority of them being quasistatic and relying on geometrical assumptions. For instance, [28] assumes zero metal height and infinite substrate thickness, and [29] considers the metal height to be zero. Application of all these quasistatic approaches is limited to specific narrow ranges of dimensions. Unfortunately, the LIGA conductors do not fit into these limits, especially as far as their height is concerned. Therefore, using these approaches for characterization and analysis of microwave LIGA CPW-based structures may not even be a good starting point.

Under these conditions, accurate analysis of the LIGA CPW-based structures must be sought via direct application of numeric techniques to the solution region. Numerical analysis is used in this research to characterize the LIGA CPW structures in focus, or, in other words, to establish direct numerical relations between the geometrical parameters, treated as variables, and electrical characteristics, treated as functions. This has been done via parametric full-wave simulations of the LIGA CPW structures, viz. transmission line and quarter-wavelength coupled-line section, using commercially available Ansoft HFSS^{TM} 3-D electromagnetic simulation software (hereinafter referred to as HFSS).

3.2.2 Finite Element Method

The finite element method (FEM) is one of the numerical techniques used to solve partial differential equations describing physical systems, which generally are defined with three spatial variables and a temporal variable. The FEM is a very flexible numerical technique capable of being adapted to the problems dealing with very complex geometries and material distributions where the underlying partial differential equations cannot be solved analytically. This makes the FEM a universal tool in a wide variety of engineering disciplines, including electrical, mechanical, civil, power, heat, aerospace and other branches of engineering. In general, an FEM solution contains the following principal steps:

- Discretization or meshing of the solution region into a finite number of sub-regions or elements as in Fig. 3.3, where only the nodes on the visible outer faces of the cube are shown for clarity;
- Approximation of continuous quantities with a set of discrete quantities in the finite elements;
- Assembling all elements in the solution region;
- Solving the system of algebraic equations.

A more profound reference on the FEM as applied to electromagnetic problems may be found in [30, 31].

HFSS (High Frequency Structure Simulator) employs the FEM to solve Maxwell's equations for the distribution of electromagnetic fields inside arbitrarily shaped solution regions. It belongs to the class of full-wave 3-D electromagnetic simulators capable of finding 3-D fields and currents associated with arbitrary 3-D passive structures. Capable of the full-wave analysis, the software takes into account all propagation modes and predicts most of high-frequency effects such as dispersion, conversion between modes, losses, and radiation. HFSS automatically divides the solution region into a finite element mesh, which is a collection of a large number of tetrahedra, then finds vector field quantities at the vertices or nodal values, and interpolates field quantities inside tetrahedra from the nodal values. HFSS stores at each vertex the vector field components that are tangential to the three converging edges of the tetrahedron. Additionally, the software can store the vector field components at the midpoint of the edges that are also used for interpolation of the

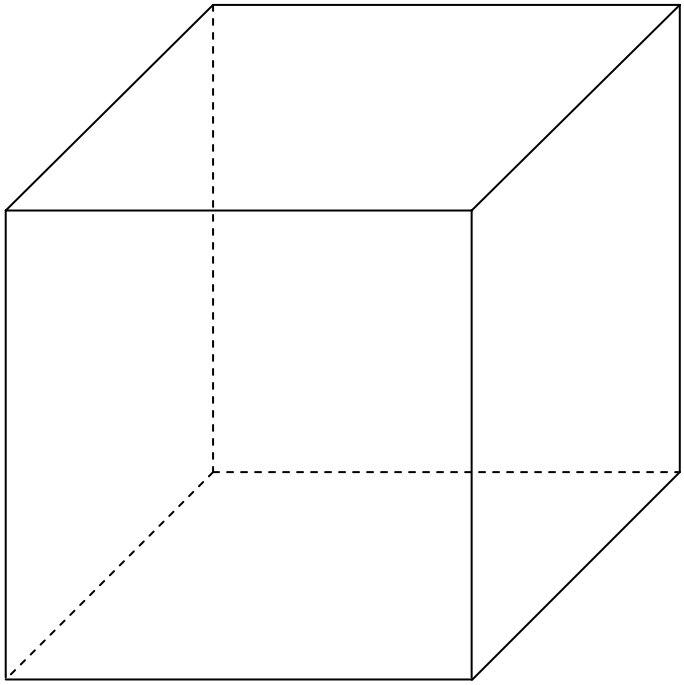

(a)

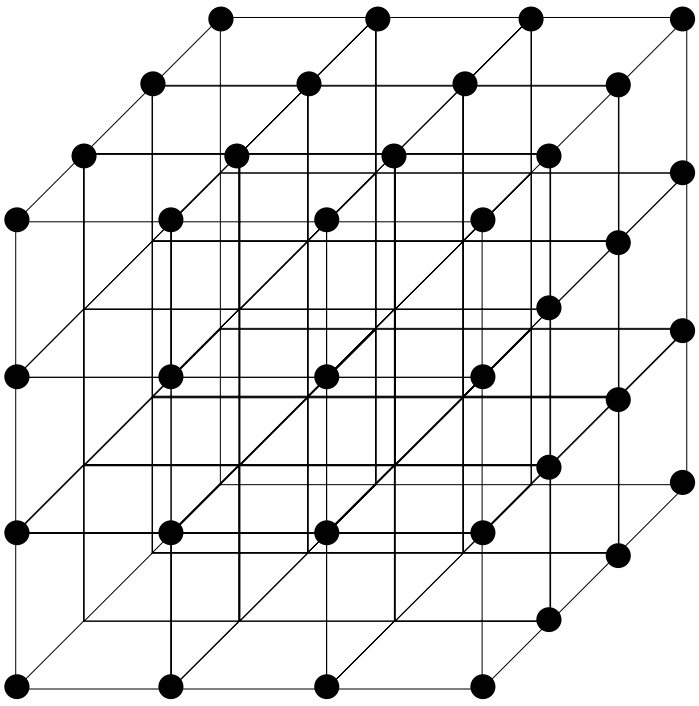

(b)

Figure 3.3 Meshing of an object:
a) Before;
b) After.

fields inside the tetrahedron. By converting the continuous field quantities into the discrete in this way, the software represents Maxwell's equations as sets of algebraic equations and then solves them using conventional matrix methods. If a more accurate solution is desired, a denser mesh with a greater number of smaller finite elements should be generated. However, the density of the mesh is limited to the amount of available computing resources, as more nodal field values need to be stored in the memory and more computing power is required for matrix operations. Therefore, the tradeoff between the level of accuracy and the mesh density is sought proceeding from availability of the computing resources. Generally, a finite element should be at least smaller than the wavelength, but advisably small enough to adequately interpolate the field inside the element. At the beginning of the solution process, the software produces a coarse initial mesh and finds an approximate field solution. Then it optimizes the mesh during subsequent iterations by refining it in the regions with high solution error density. The solution error is found by comparing the solution results of the current iteration with the results of the previous iteration. This iterative process of mesh adaptation continues until the solution results converge to the defined level of accuracy or the number of permitted iterations is reached. The main output data provided by HFSS are the [S]-matrix, characteristic impedances at ports, and the complex propagation constant. From the imaginary part of the complex propagation constant, the effective permittivity and wavelength are found.

3.3 Characterization of LIGA CPW Transmission Line

The two main electrical parameters that are characterized, or in other words related to geometrical parameters of the structure, are the characteristic impedance of the line and its effective permittivity, which is defined by the phase velocity of the wave propagation along the line. They are generally the functions of the four following variables shown in Fig. 3.4: trace width W, spacing between the trace and the ground plane S, conductor height H, and substrate thickness T. Unlike most published CPW design techniques, conductor height H may not be assumed zero and substrate thickness T may not be assumed infinite in case of LIGA CPW due to the reasons outlined in Section 3.2.1. The LIGA CPW line is characterized using parametric sweeps for all four variables performed with

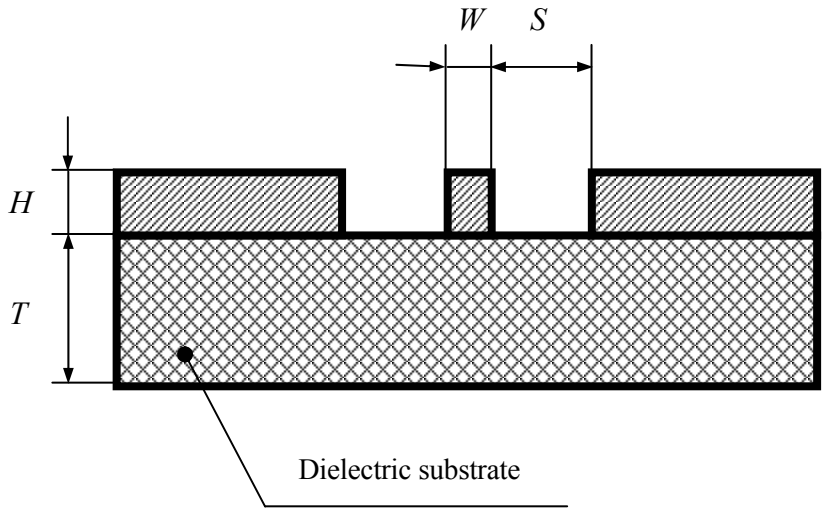

Figure 3.4 Cross section of LIGA CPW transmission line

Ansoft Optimetrics™ (hereinafter referred to as Optimetrics), which is a plug-in for HFSS allowing quick and handy alteration of the model geometry and material properties.
The variable sweep ranges have been selected with respect to the expected electrical characteristics and also the fabrication capabilities of LIGA. They are given in Table 3.1.

Table 3.1 Variable sweep ranges for the LIGA CPW line

Variables	***Ranges, mm***
1. Trace width *W*	0.1 to 0.8
2. Spacing *S*	0.1 to 1.0
3. Conductor height *H*	0.2 to 0.8
4. Substrate thickness *T*	0.4 to 1.2

3.3.1 Model

The HFSS simulation model for the LIGA CPW used for the parametric sweeps is presented in Fig. 3.5. The model is composed of both real and virtual objects. The former include the dielectric substrate and the conductors. The latter are the ports and the air box. The ports must be defined as the surfaces of the model that can pass power into and out of

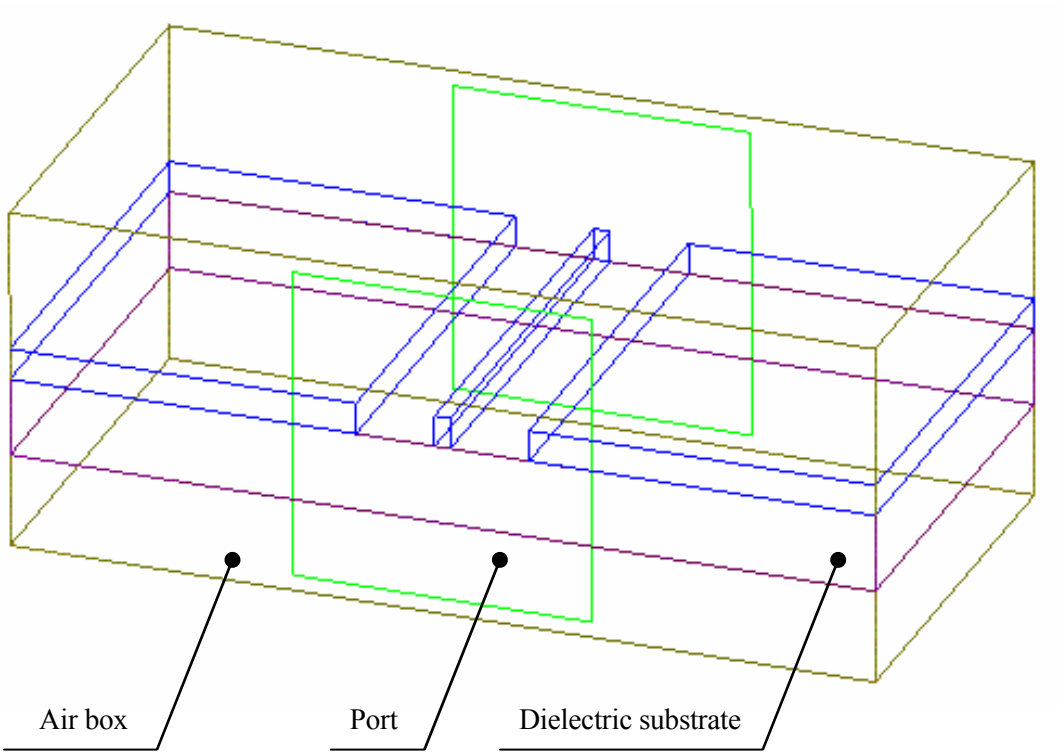

Figure 3.5 HFSS simulation model for the LIGA CPW

the model. The size of the ports is selected so that the ports are not too large to permit excitation of a rectangular waveguide mode, with the air box being the rectangular waveguide, yet not too small to confine the electric field between the port borders, thus modifying the intended model by introduction of the field-affecting elements. As a rule of thumb for planar CPW [32], the port width should be no less than three CPW propagation slot widths, which is the distance between the two ground planes, and the port height should be no less than four substrate heights. At the same time, no port dimension should exceed effective half-wavelength. In case the former requirement contradicts the latter, the latter prevails. In order for the CPW propagation mode to be excited correctly, the port must touch all three conductors. Therefore, the port sizes are set automatically at each setup depending on the model geometry and the above requirements according to the relations introduced into the routine.

All other outer surfaces of the model interfacing the background are by default assumed perfect E boundaries (tangential component of the electric field is zero), which do not permit any energy to enter or leave. The solutions are generated in succession by exciting each individual port with 1 W of time-averaged power while setting all other ports to zero power. The ports must be perfectly matched to the characteristic impedance of the waveguide that each port faces in order not to allow reflection of power back into the model. This is realized by HFSS automatically by assuming that each port is virtually connected to a semi-infinitely long waveguide having the same cross-section and material properties as the part of the model exposed to the port. The two-dimensional field distributions generated for each port are used as the boundary conditions for the three-dimensional model.

The air box is included into the model to introduce the space where the investigated electromagnetic field will exist in the structure. Otherwise, all the object surfaces touching the background would be considered perfect conductors, which would prevent the fields in focus from being excited. As the air box touches the background and it is considered a perfect conductor, it should be large enough in order for its walls not to affect the field patterns along the line. The size of the air box is defined such that its walls do not interact with the fields inside the model and, therefore, do not modify the intended behaviour of the model. Usually, the size of the air box is set initially to exceed the dimensions of the field-containing volumes by a number of times and then checked by visualizing the solved fields to see if they interact with the air box walls. If they do, the air box is made larger.

For the sake of generality, the conductors are assumed perfect and the model is assumed being placed in a box of vacuum. The substrate used for characterization is alumina with the relative permittivity of 9.8.

The simulations were performed on a computer platform based on Intel Pentium 4 processor running at 1.5 GHz with no other concurrently running applications. Simulation of each setup required building a mesh of approximately 3000 tetrahedra and took approximately 5 minutes.

3.3.2 Results

The simulation results are presented in this section in the form of characteristic graphs. Their interpretation is given in the next section.

All the graphs represent the simulation results as characteristic impedances and effective permittivities being functions of the geometrical parameters of the model, viz. spacing *S* and width *W*. The characteristic impedance and effective permittivity are computed by HFSS automatically based on the found electric and magnetic field quantities in the model. The characteristic impedance of a port is found from the values of power passing through the port and current around it. As noted earlier, the effective permittivity is calculated from the imaginary part of the complex propagation constant.

Figure 3.6 demonstrates dependence of characteristic impedance Z_0 and effective permittivity ε_{eff} of the LIGA CPW transmission line on signal trace width *W*, established for various conductor heights *H* and fixed values of spacing *S* of 0.3 mm and substrate thickness *T* of 1 mm.

Figure 3.7 reveals dependence of the LIGA CPW electrical characteristics on the spacing *S* between the signal trace and the grounds for various substrate thicknesses *T* and fixed values of trace width *W* of 0.2 mm and metal height *H* of 0.2 mm.

Figures 3.6 and 3.7 also provide comparison of the electrical characteristics of the LIGA CPW with the electrical characteristics of the planar CPW built using metal conductors with a typical value of height of 5 μm. The planar CPW was characterized using the "LineCalc" tool from the "Advanced Design System 2002" (hereinafter referred to as ADS 2002) software package developed by Agilent Technologies. The "LineCalc" tool is used for analysis and synthesis of transmission lines and is based on models and design approaches published in the relevant literature. ADS 2002 LineCalc was selected for this purpose owing to two reasons:

Firstly, HFSS simulations of the thin conductors would not be accurate since HFSS does not create optimum meshes for the objects with one dimension significantly less than the others, which would be the case for the long conductors used in the coupler model. The HFSS developers recommend to define such objects as zero-thickness surfaces.

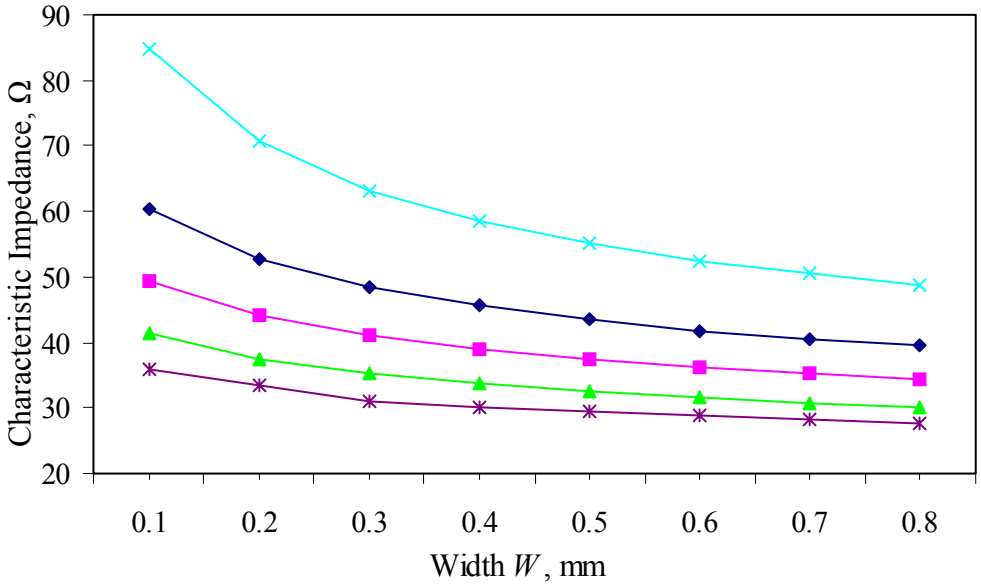

(a)

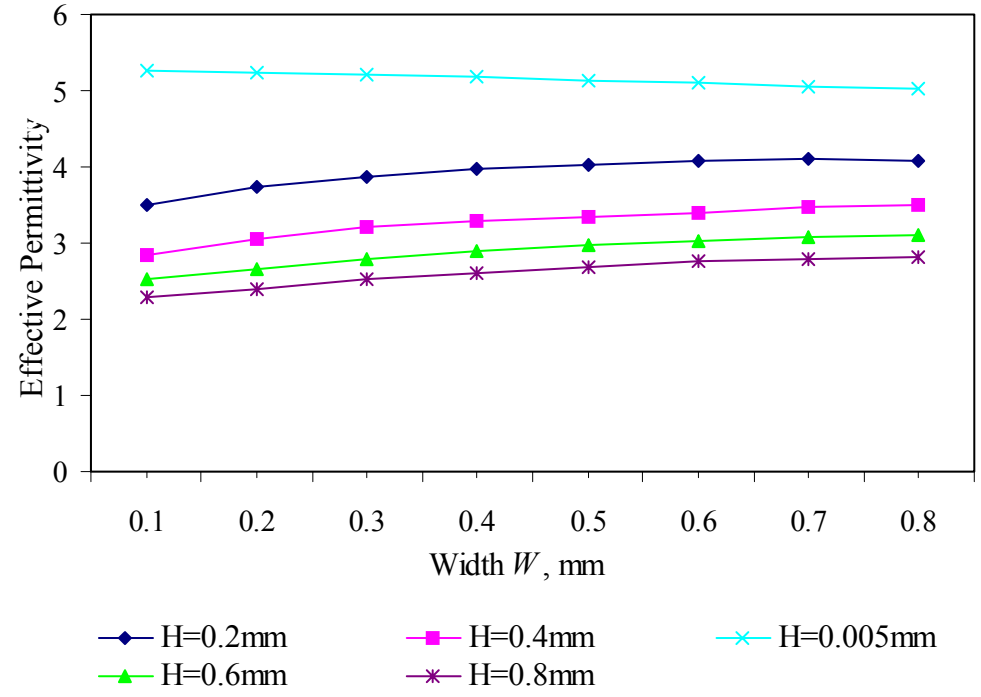

(b)

Figure 3.6 Characteristic impedance Z_0 (a) and effective permittivity ε_{eff} (b) of the LIGA CPW transmission line versus trace width W for various conductor heights H, spacing S of 0.3 mm, and thickness T of 1 mm

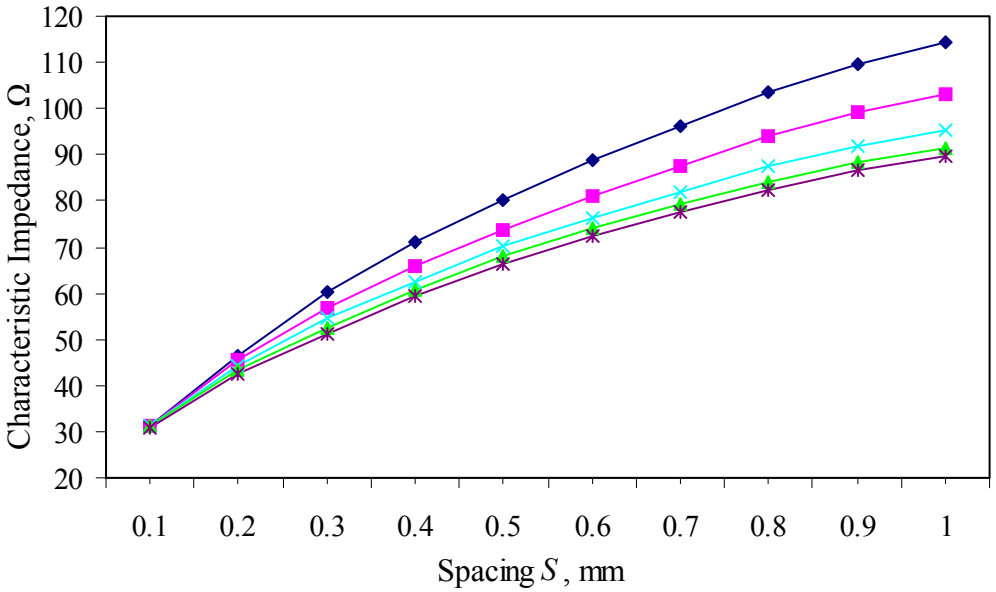

(a)

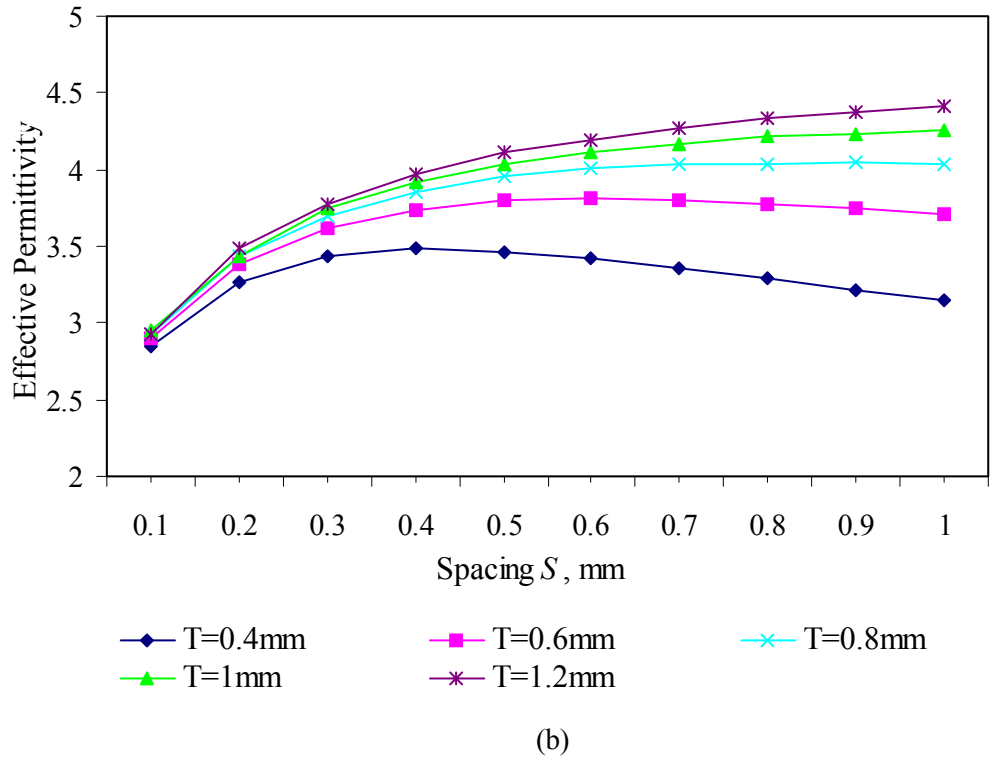

(b)

Figure 3.7 Characteristic impedance Z_0 (a) and effective permittivity ε_{eff} (b) of the LIGA CPW transmission line versus spacing S for various substrate thicknesses T, trace width W of 0.2 mm, and height H of 0.2 mm

Secondly, since ADS 2002 LineCalc uses closed formulae, it is much faster than HFSS, which uses the numerical technique requiring significant computer time. The thin-conductor coupler models calculated with ADS 2002 LineCalc are within the validity limits of the formulae used by the software.

3.3.3 Discussion

As may be seen from Fig. 3.6a, showing the relation $Z_0 = f(W, H)$, where W is the trace width and H is the conductor height, greater conductor heights result in lower values of characteristic impedance. This occurs due to the fact that taller conductors create larger metal surfaces that increase per-unit-length capacitance, which is inversely related to characteristic impedance as follows from (2.11). As the trace width W grows, the rate of impedance change slows down, ostensibly due to the fact that the bigger fraction of the fields is concentrated near the gaps between the trace and the grounds and further increase of the trace width does not significantly affect the characteristic impedance. This is also true for the effective permittivity, whose dependence on trace width W is shown in Fig. 3.6b. This assertion is corroborated by Fig. 3.8, generated using the HFSS post-processing module and showing the distribution of the electric field in the LIGA CPW cross section for the varied trace widths W of 0.1 and 0.8 mm, and fixed values of spacing S of 0.3 mm, metal height H of 0.4 mm and substrate thickness T of 1.0 mm. The distribution of the electric field is shown in Fig. 3.8 as the areas of equal electric intensity magnitudes separated by equipotential lines. Lighter area show greater electric intensity magnitudes. It is evident from the figure that at larger trace widths the areas of high electric intensity are concentrated only around the areas of the top and bottom surfaces of the conductors that are adjacent to the air gaps, while at narrower trace widths the whole areas of the said surfaces are at high potentials. It may be noted that the symmetry in this and the field plots to follow is not perfect. This might be happening due to the fact that the HFSS solves the problems irrespective of the symmetry of the structures under consideration.

Figure 3.6b shows that greater values of conductor height H result in lower effective permittivity and, consequently, higher phase velocity of the wave propagating across the line. The rate of reduction of the effective permittivity, however, slows down at greater values of conductor height H. The diagram for the effective permittivity in Fig. 3.6b also reveals

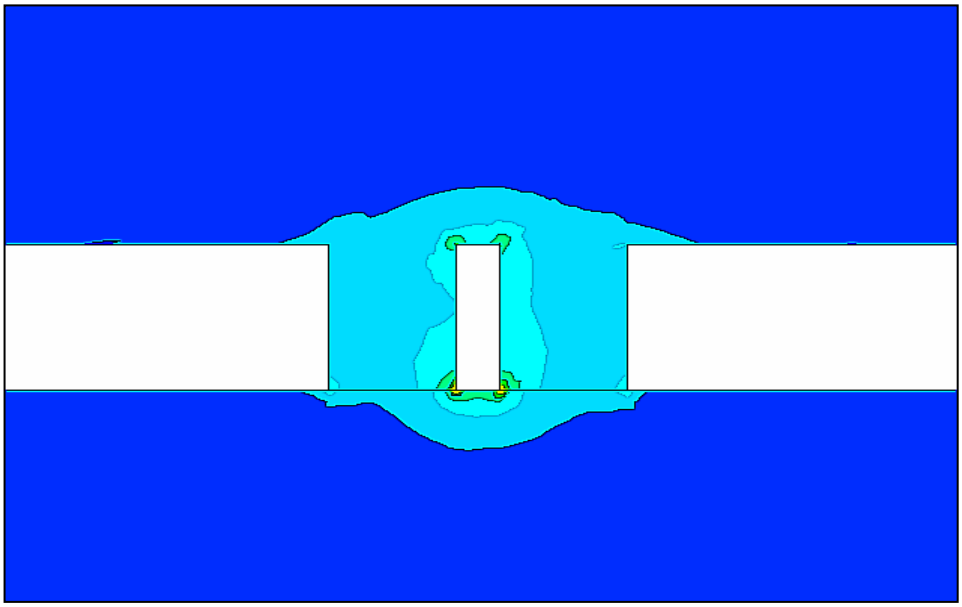

(a)

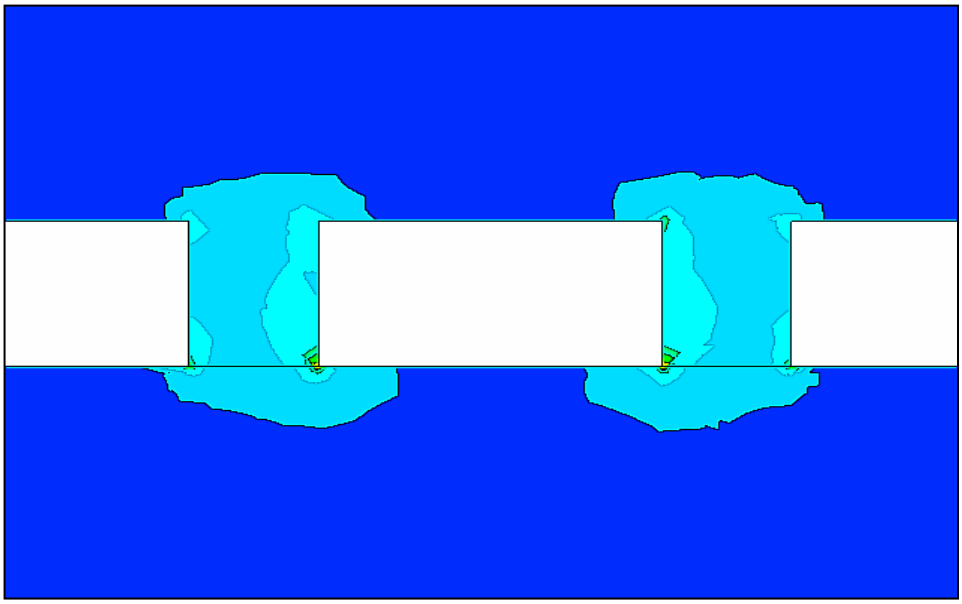

(b)

Figure 3.8 A plot of electric field intensity magnitude in the cross section of the LIGA CPW line for various trace widths:
a) W = 0.1 mm, b) W = 0.8 mm.

that the slopes of all the curves are insignificant. However, the slope for the planar CPW is negative, whereas the slope for HVAR CPW is positive. Generally, application of tall conductors (i.e. 0.4 – 0.8 mm) allows reduction of the effective permittivity and characteristic impedance by approximately one and a half times.

A very important conclusion on the characteristics of the LIGA CPW is that it attains the standard values of characteristic impedance (50 Ω and 75 Ω) at lower values of the trace width, which renders the line more compact widthwise as compared to its conventional planar counterpart. This means that desired characteristics are achieved by expansion in the third dimension, viz. height, rather than increase in the lateral dimensions.

Figure 3.7 displays the functional dependence of the LIGA CPW electrical characteristics on spacing S between the signal trace and the ground planes and substrate thickness T: $Z_0, \varepsilon_{eff} = f(S, T)$. As evident from Fig. 3.7a, increase in spacing S results in greater values of the characteristic impedance, since greater distances between the signal trace and the grounds lead to lower values of the per-unit-length capacitance, which, in its turn brings about lower characteristic impedance according to (2.11). The general trend of the substrate thickness increase is the growth of the effective permittivity and, consequently, reduction in the characteristic impedance as follows from (2.11), where the per-unit-length capacitance grows due to higher permittivity. However, it may be observed from Fig. 3.7 that at narrow spacings S substrate thickness T has little effect on both characteristic impedance and effective permittivity and the curves on both diagrams take origin from almost the same point. This is a result of the fact that at low values of S, the larger fraction of the fields is concentrated between the conductor sidewalls and top surfaces and little field penetrates the substrate down to the bottom, therefore variation of thickness T almost does not influence both characteristic impedance and effective permittivity. It is corroborated by Fig. 3.9, showing distribution of the electric field in the LIGA CPW cross section, generated by HFSS for substrate thicknesses T of 0.4 mm and 1.2 mm and fixed values of trace width W of 0.2 mm, metal height H of 0.2 mm, and spacing S of 0.2 mm. As evident from the figure, the change of substrate thickness T does not change the penetration depth of the electric field into the substrate. At greater values of S, effect of the thickness growth on characteristic impedance Z_0 saturates and does not cause large variations of Z_0 once T reaches 1 mm. This is also true for the effective permittivity.

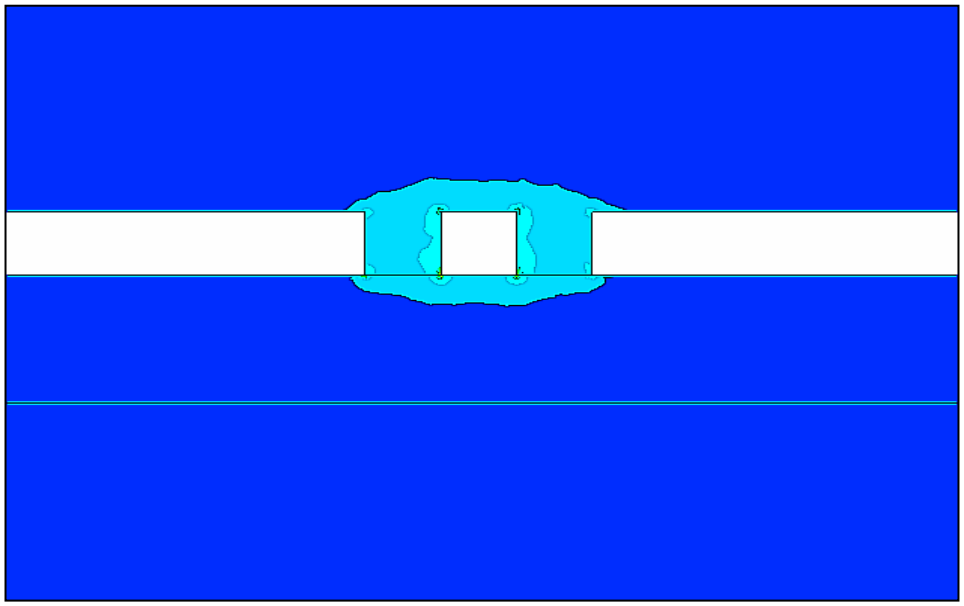

(a)

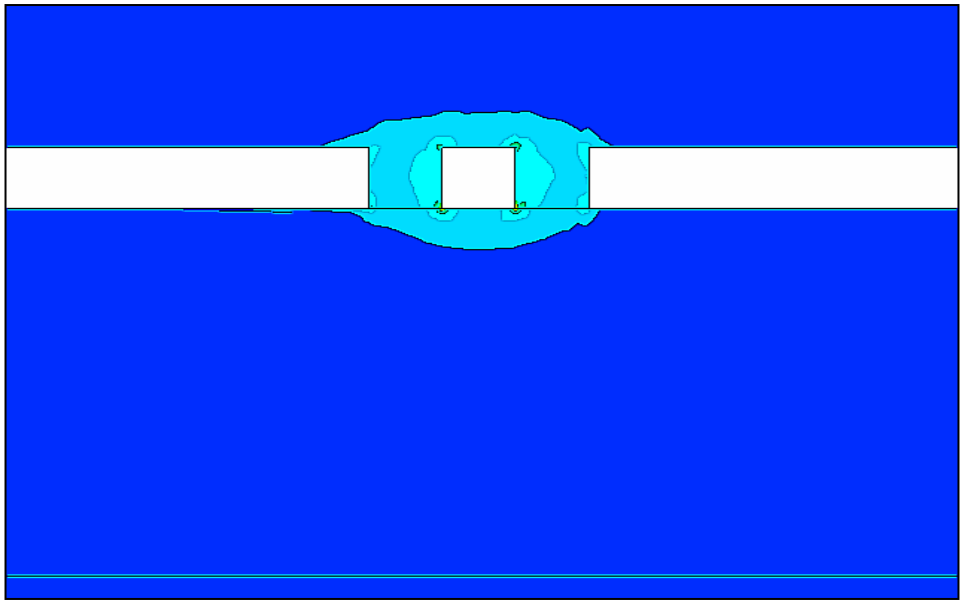

(b)

Figure 3.9 A plot of electric field intensity magnitude in the cross section of the LIGA CPW line for various substrate thicknesses *T*: a) T = 0.4 mm, b) T = 1.2 mm.

The characteristic curves for the effective permittivity depicted in Fig. 3.7b may be divided in the following three regions: in the first region, increase in spacing S causes growth of the effective permittivity ε_{eff} and the curve slope is positive; in the second region, the growth of ε_{eff} saturates and the slope becomes zero; and in the last region, ε_{eff} falls and the slope becomes negative. These regions may be delineated by the areas where spacing S becomes equal to substrate thickness T. After spacing S exceeds thickness T, the fields start to reach the bottom substrate surface and penetrate into the air below, which increases the phase velocity indicated by the reduction of the effective permittivity. In this case, the fields will be experiencing another refraction at the interface between the bottom substrate surface and the air below in addition to the refraction along the top substrate surface, which will entail further departure from the TEM propagation and, possibly, higher dispersion. Therefore, structures with wide spacings on thin substrates should be avoided. The described behaviour may be seen in Fig. 3.10, showing the electric field distributions generated by the HFSS post-processing module for various spacings S, where fixed values of trace width W of 0.2 mm, metal height H of 0.2 mm and substrate thickness T of 0.4 mm as well as two different values of spacing S of 0.1 and 1.0 mm are used. In the figure, the lighter areas stand for the areas with higher magnitude of the electric field intensity. It may be seen in Fig. 3.10 that the electric intensity is higher under the LIGA CPW where spacing S is greater than substrate thickness T and a substantial fraction of the electric field appears under the bottom and in the substrate itself than in the case of the LIGA CPW where spacing S is less than substrate thickness T.

3.4 Characterization of LIGA CPW-Based Coupled-Line Structure

The LIGA CPW two-line coupled section has been characterized for its two main electrical parameters: characteristic impedance and effective permittivity. Since the section is two-line, with both lines having a common ground, it can support two main modes, called "even" and "odd" for the case of symmetric uniform lines (see Section 2.3). Each of the modes is described with its own characteristic impedance and effective permittivity: Z_{0e} and $\varepsilon_{eff.e}$ for the even mode, and Z_{0o} and $\varepsilon_{eff.o}$ for the odd mode. These characteristics are generally the functions of the five variables shown in Fig. 3.11: gap between the traces G, trace width W, spacing between the trace and the ground plane S, conductor height H, and

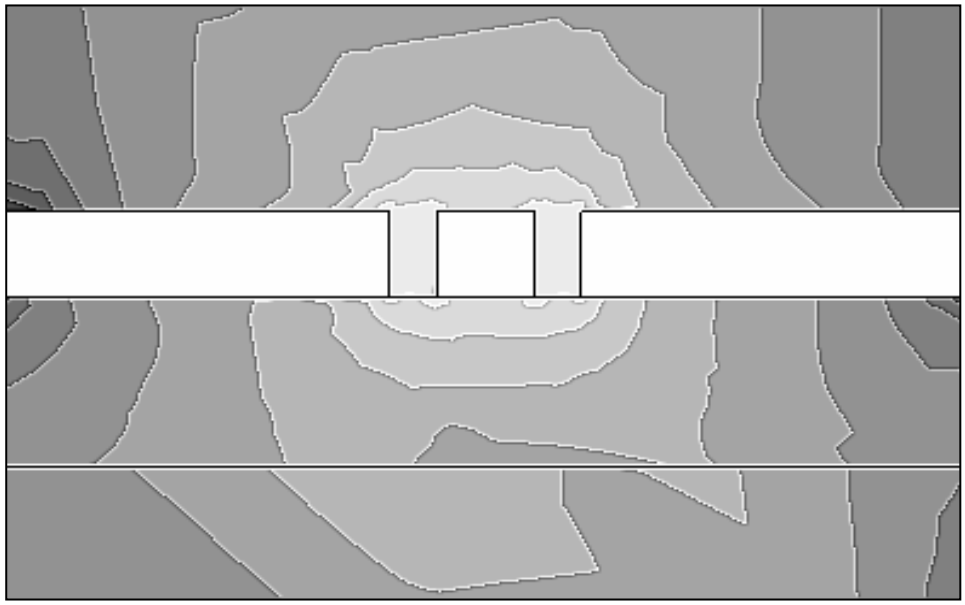

(a)

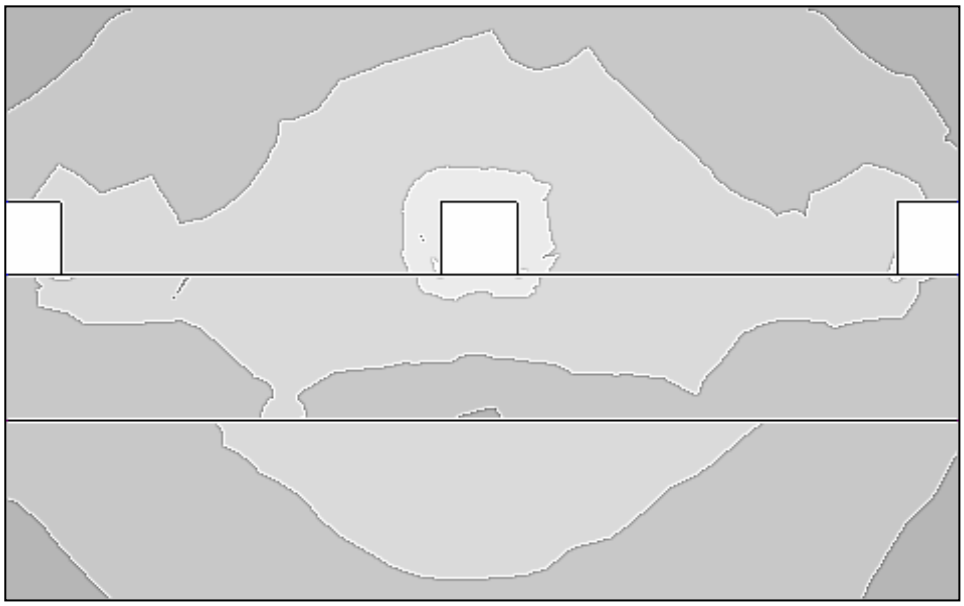

(b)

Figure 3.10 A plot of electric field intensity magnitude in the cross section of the LIGA CPW line for various spacings *S*:
a) S = 0.1 mm, b) S = 1.0 mm.

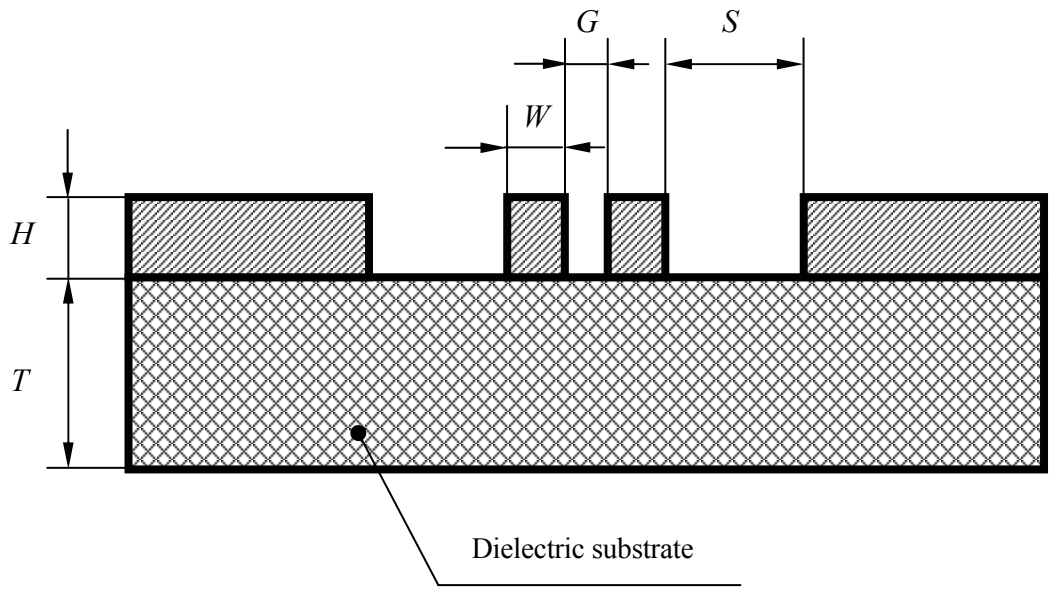

Figure 3.11 Cross section of LIGA CPW coupled lines

substrate thickness *T*. When characterizing the LIGA structures with HVAR conductors, substrate thickness *T* may not be assumed infinite and conductor height *H* may not be assumed zero according to the reasons given in Section 3.2.1.

Characterization was performed using HFSS, described in Section 3.2.2, together with Optimetrics by sweeping all five variables in the ranges given in Table 3.2.

Table 3.2 Variable sweep ranges for the LIGA CPW coupled-line section

Variables	***Ranges, mm***
1. Trace width *W*	0.1 to 0.8
2. Spacing *S*	0.3 to 1.2
3. Conductor height *H*	0.2 to 0.6
4. Substrate thickness *T*	0.4 to 1.2
5. Gap *G*	0.02 to 0.2

In order to provide comparison of the HVAR coupled lines against the planar coupled lines, the latter were characterized in the ranges from Table 3.2, except for the conductor

height, for which a typical value of 0.005 mm was selected. The planar coupled lines were characterized using "LineCalc" from ADS 2002 due to the fact that HFSS simulations of the thin conductors would not be accurate since HFSS does not create optimum meshes for the objects with one dimension significantly less than the others, which would be the case for the long conductors used in the coupler model. Since ADS 2002 LineCalc uses closed formulae, it is much faster than HFSS, which uses the numerical technique requiring significant computer time.

3.4.1 Model

The HFSS simulation model of the LIGA CPW coupled-line section used for the parametric sweeps is shown in Fig. 3.12. The major principles taken into account during its design are similar to those of the LIGA CPW transmission line model described in Section 3.3.1. The only difference is that the coupled-line section is computed for two modes of propaga-

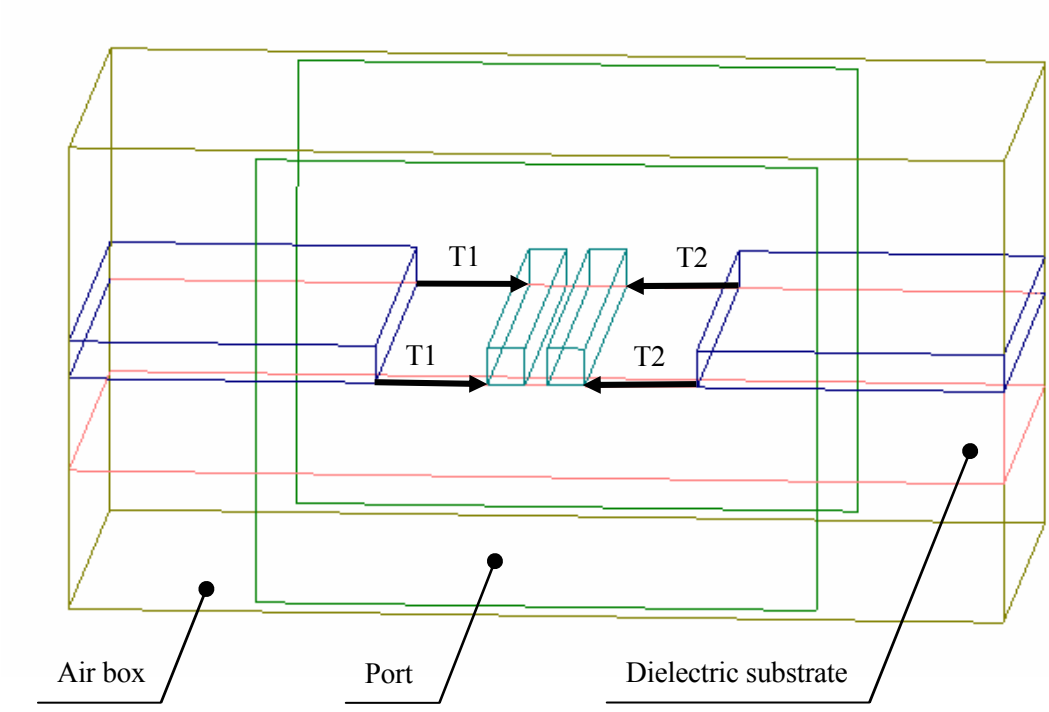

Figure 3.12 HFSS simulation model for the LIGA CPW coupled-line section

tion at each geometrical setup. In HFSS, terminals in the amount equal to the number of modes must be set up on the port surfaces if modal propagation is expected. The number of major modes and, therefore, the number of used terminals is defined by the number of non-touching conductors according to Section 2.1: if there are $N+1$ conductors, N major propagation modes are to be expected. The terminals are set up in HFSS using "terminal voltage lines", which are the designated paths along which modal voltages are computed on the port surfaces. The terminal lines are drawn between non-touching conductors facing the port, with one of the conductors being the zero-potential reference. In this work, two terminals are defined for each port by drawing terminal lines T1 and T2 between the grounds and the signal traces, see Fig. 3.12.

For the sake of generality, the conductors are assumed perfect and the model is assumed being placed in a box of vacuum. The substrate used for characterization is alumina with the relative permittivity of 9.8.

The simulations were performed on a computer platform based on Intel Pentium 4 processor running at 1.5 GHz with no other concurrently running applications. Simulation of each setup required building a mesh of approximately 3600 tetrahedra and took approximately 8 minutes.

3.4.2 Results

The characterization results are provided in this section in the form of characteristic graphs, followed by their interpretation in the next section.

Figures 3.13 demonstrates the curves for the even-mode and odd-mode characteristic impedances Z_{0e} and Z_{0o} versus gap G between the signal traces, varied from 20 to 200 μm. The curves were computed for conductor height H varied from 0.2 to 0.6 mm, and fixed values of trace width W of 0.2 mm, spacing S between the trace and the ground of 0.5 mm, and substrate thickness T of 1 mm. The same variables and parameters were used for constructing the characteristic curves for the even-mode and odd-mode permittivities $\varepsilon_{eff.e}$ and $\varepsilon_{eff.o}$ shown in Fig. 3.14.

Figures 3.15 shows the curves for Z_{0e} and Z_{0o} versus spacing S between the signal traces, varied from 0.3 to 1.2 mm. The curves are presented for conductor height H varied from 0.2 to 0.6 mm, and fixed values of gap G of 0.05 mm, trace width W of 0.2 mm, and sub-

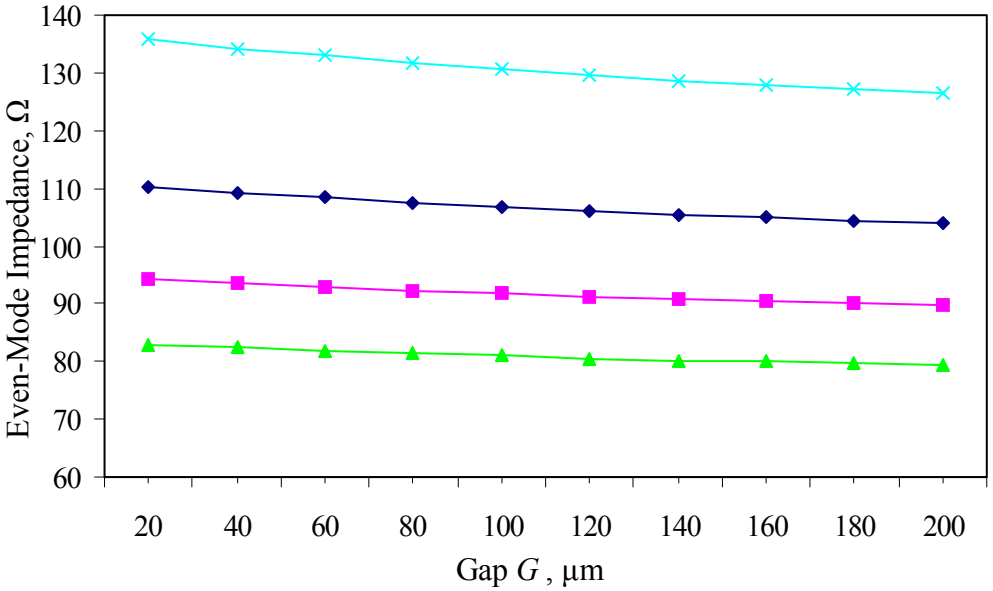

(a)

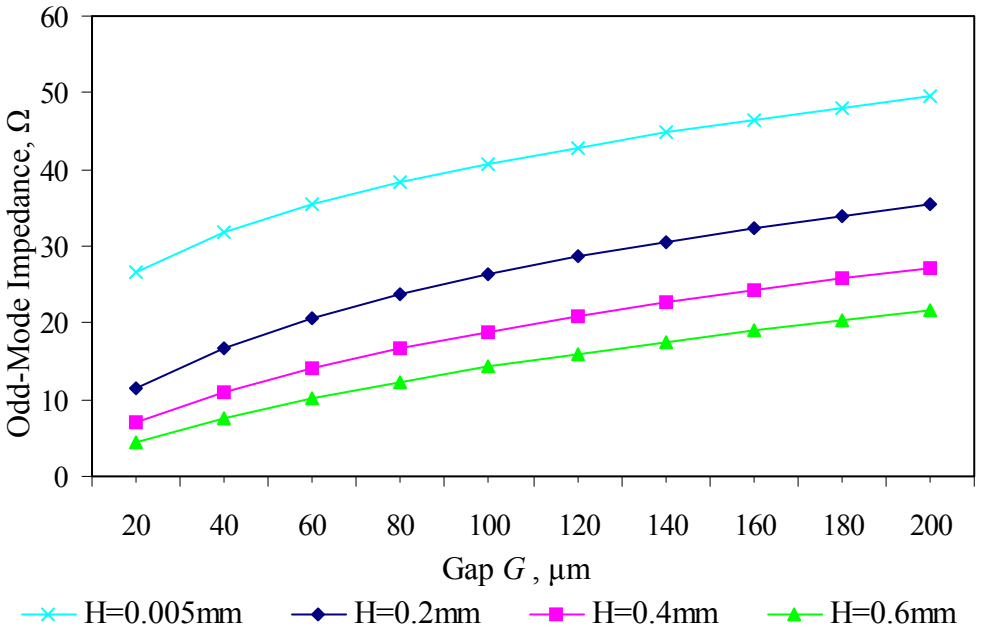

(b)

Figure 3.13 Modal characteristic impedances of the LIGA CPW coupled-line section versus gap G for various conductor heights H:
(a) even-mode, (b) odd-mode

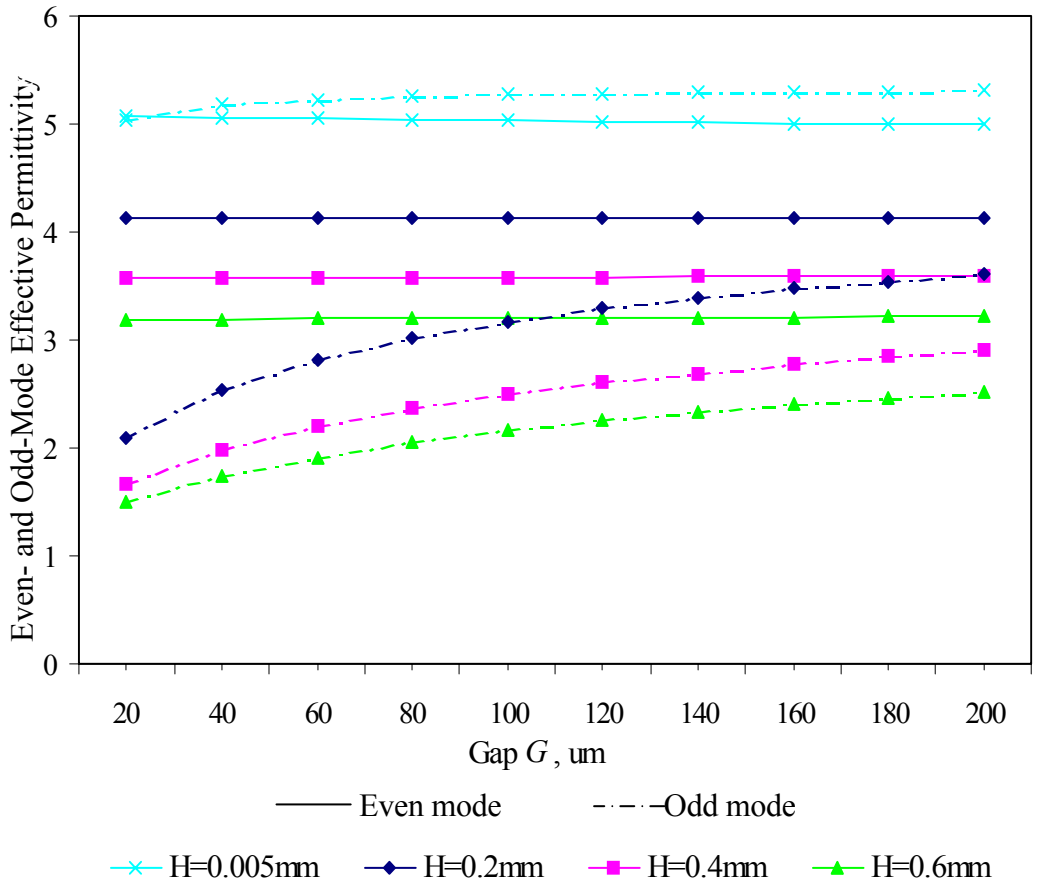

Figure 3.14 Modal effective permittivities of the LIGA CPW coupled-line section versus gap G for various conductor heights H

strate thickness T of 1 mm. The same variables and parameters were used for constructing the characteristic curves for $\varepsilon_{eff.e}$ and $\varepsilon_{eff.o}$ shown in Fig. 3.16.

Figures 3.17 shows the curves for Z_{0e} and Z_{0o}, versus substrate thickness T, varied from 0.4 to 1.2 mm. The curves are presented for conductor height H varied from 0.2 to 0.6 mm, and fixed values of gap G of 0.05 mm, trace width W of 0.2 mm, and spacing S of 0.5 mm. The same variables and parameters were used for constructing the characteristic curves for $\varepsilon_{eff.e}$ and $\varepsilon_{eff.o}$ shown in Fig. 3.18. All the characteristic graphs in Figs. 3.13-3.18 also include the curves for the similar planar structures with 0.005-mm tall conductors.

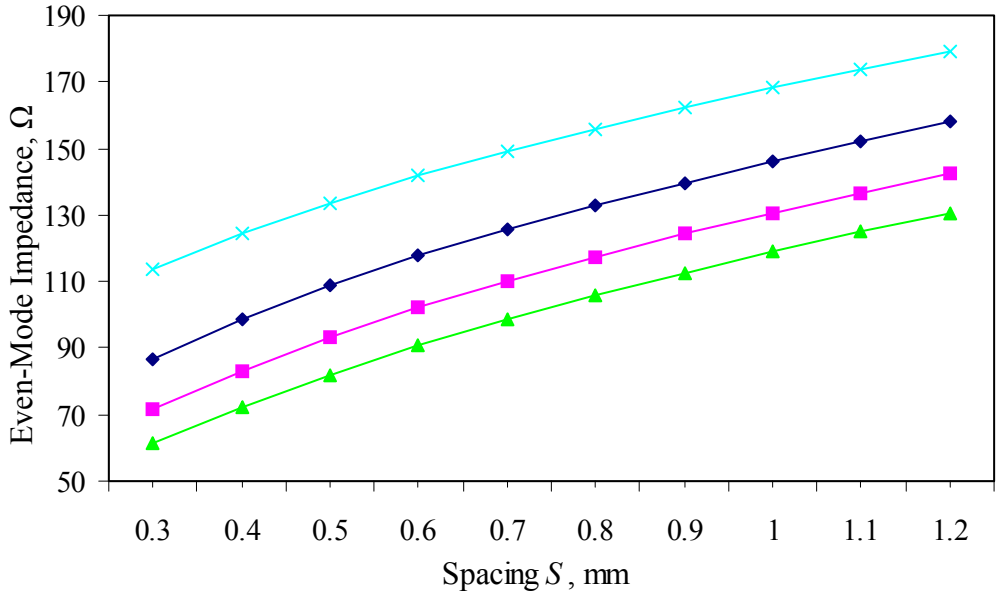

(a)

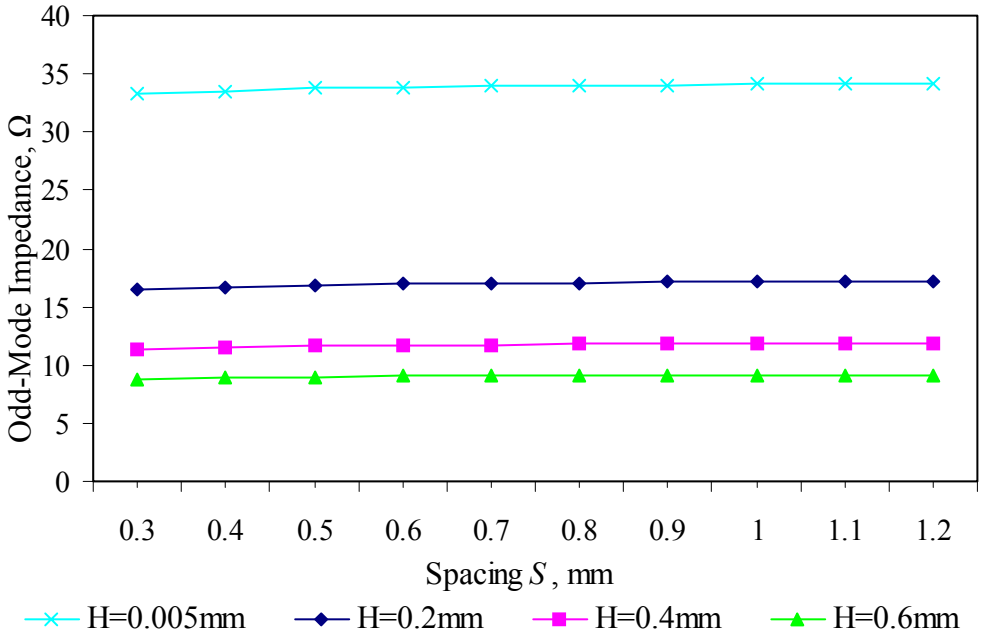

(b)

Figure 3.15 Modal characteristic impedances of the LIGA CPW coupled-line section versus spacing S for various conductor heights H:
(a) even-mode, (b) odd-mode

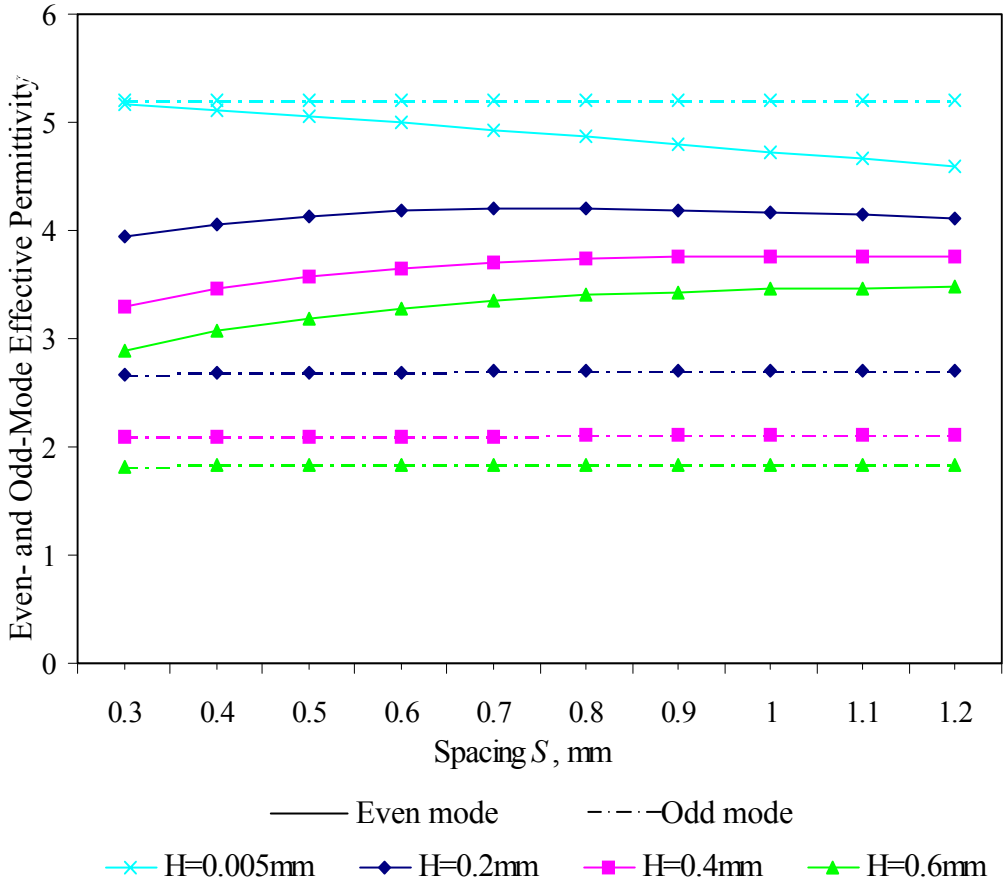

Figure 3.16 Modal effective permittivities of the LIGA CPW coupled-line section versus spacing S for various conductor heights H

3.4.3 Discussion

Comparison of the curves for the even-mode and odd-mode characteristic impedances Z_{0e} and Z_{0o} versus gap G shown in Fig. 3.13 reveals that Z_{0e} is only slightly affected by variation of gap G and has the tendency to decrease as gap G widens. At the same time, the odd-mode impedance Z_{0o} undergoes a significant growth as gap G becomes larger. To compare, the change in value for Z_{0e} and Z_{0o} constitutes –5.6% and 206.8% respectively as gap G grows from 0.02 mm to 0.2 mm for the conductor height H of 0.2 mm. At greater conductor heights, the even-mode impedance displays a weaker dependence on gap variation, whereas the odd-mode impedance becomes even more affected by changes in gap G, e.g. at H = 0.6 mm the variation of G from 0.02 mm to 0.2 mm causes a 383.5% change in

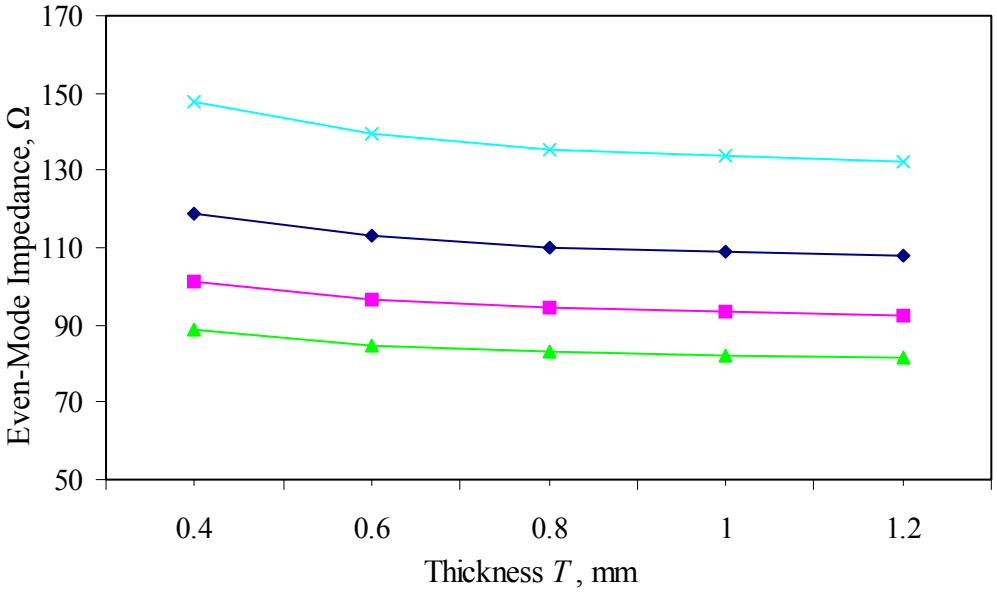

(a)

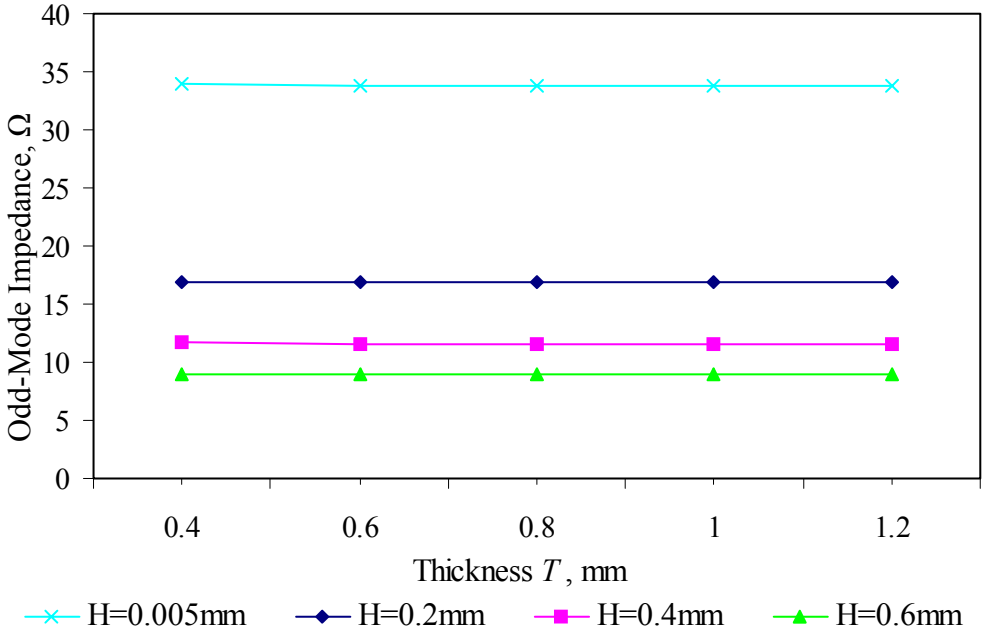

(b)

Figure 3.17 Modal characteristic impedances of the LIGA CPW coupled-line section versus substrate thickness T for various conductor heights H: (a) even-mode, (b) odd-mode

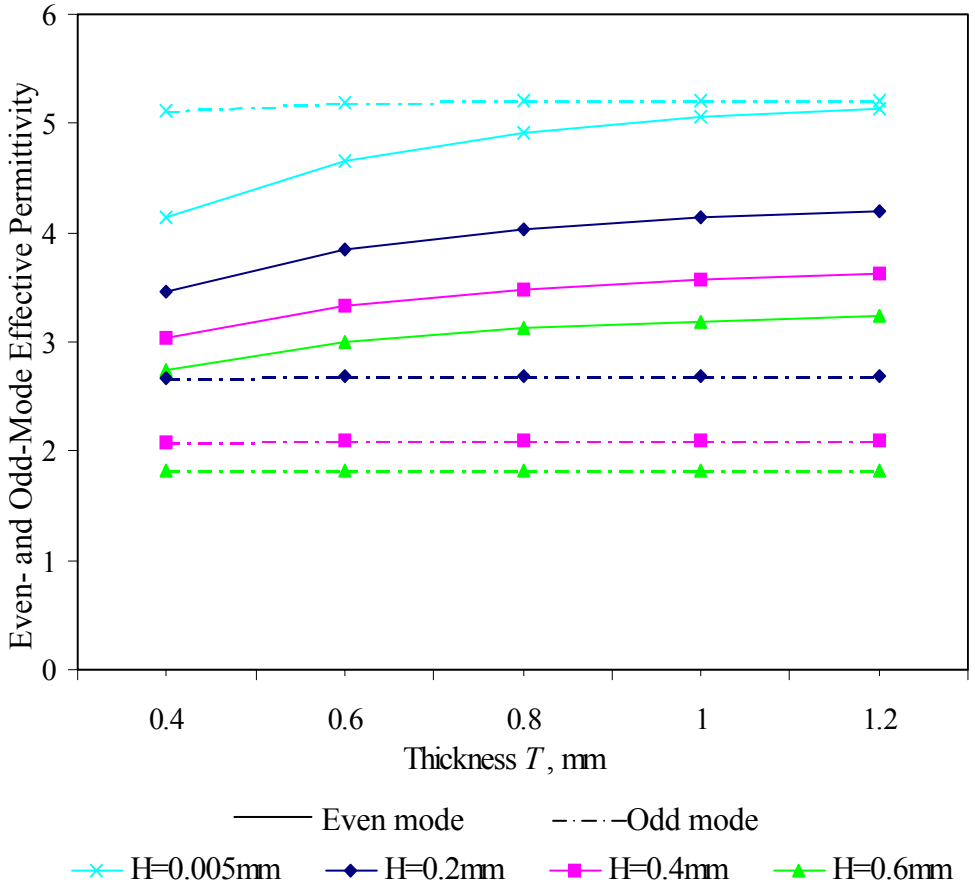

Figure 3.18 Modal effective permittivities of the LIGA CPW coupled-line section versus substrate thickness T for various conductor heights H

Z_{0o} and only a –4.32% change in Z_{0e}. Dependence of both impedances on conductor height H shows that higher values of H entail lower impedances since higher conductors give rise to larger conductor sidewall areas, which increases the per-unit-length capacitance and, consequently, reduces the characteristic impedances as follows from (2.11). The characteristic curves for the planar coupled lines are significantly separated from the curves for the HVAR coupled lines in both diagrams in Fig. 3.13. It shows that the planar lines may not be used to built tight couplers with gaps suitable for fabrication with reasonable yields, since, according to Section 2.4, the odd-mode impedance should be 20.9 Ω in order to reach 3-dB coupling in a 50-Ω system and the odd-mode impedance curve for the planar lines does not attain this value in the region of narrow gaps. But in case of HVAR LIGA

conductors, the odd-mode impedance curves reach the values required for tight couplings at the gap values well above the fabrication limits of LIGA.

The functional dependence of the effective permittivities on the same variables and parameters as in Fig. 3.13 is illustrated in Fig. 3.14. Similarly to the case of the even-mode characteristic impedance, the even-mode effective permittivity $\varepsilon_{eff.e}$ is not significantly affected by the variation of gap G between the signal traces, whereas the odd-mode effective permittivity $\varepsilon_{eff.o}$ is subjected to increase as gap G grows due to the fact that a greater fraction of the fields concentrated between the traces penetrates into the substrate. The same reason is behind the fact that higher conductors result in lower values of the effective permittivities for both modes. This is corroborated by Fig. 3.19 that shows the electric field distribution combined for both modes in a coupled-line section with varied metal heights H of 0.2 and 0.8 mm as well as fixed values of gap G of 0.1 mm, spacing S of 0.5 mm, trace width W of 0.2 mm, and substrate thickness T of 1 mm. It is clear from Fig. 3.19b that in case of taller conductors, a larger fraction of the fields is concentrated outside of the substrate. The characteristic dependences in Figs. 3.13 and 3.14 indicate that the geometrical configuration between the coupled lines is the major contributor to the propagation of the odd-mode wave and it does not largely affect the propagation of the even-mode wave.

The relationship between the modal impedances and spacing S is shown in Fig. 3.15. It reveals that variation of spacing S largely affects the even-mode characteristic impedance Z_{0e} and does not significantly influence the odd-mode characteristic impedance Z_{0o}. Quantitatively, variation of S from 0.3 mm to 1.2 mm produces a 82.2% change in Z_{0e}, whereas Z_{0o} changes only by 4.6% at conductor height H of 0.2 mm. Higher values of H bring about a stronger sensitivity of Z_{0e} and a slight increase in sensitivity of Z_{0o} to variation of S within the stated limits: 113.1% and 5.28% changes respectively at conductor height H of 0.6 mm. Figure 3.15 also indicates that both modal impedances reduce as conductors become taller due to greater per-unit-length capacitance increased by larger sidewalls.

The modal effective permittivity curves plotted versus the same variables and parameters as above in Fig. 3.16 demonstrate behaviour similar to that of the characteristic impedance curves: increase in spacing S results in greater even-mode effective permittivity, while the odd-mode permittivity remains virtually unchanged. The increase in $\varepsilon_{eff.e}$ occurs as a greater fraction of the fields concentrated between the signal traces and the ground planes

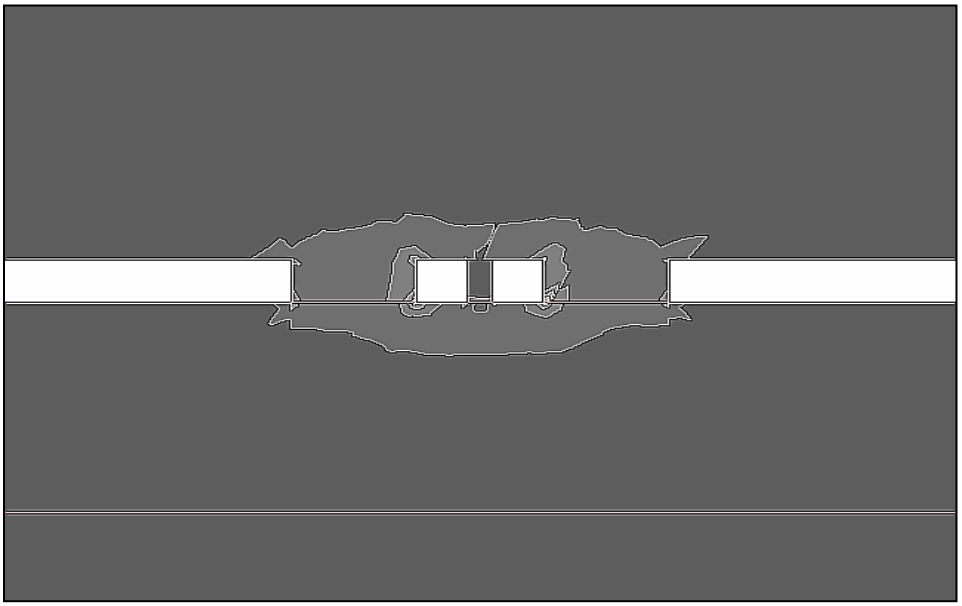

(a)

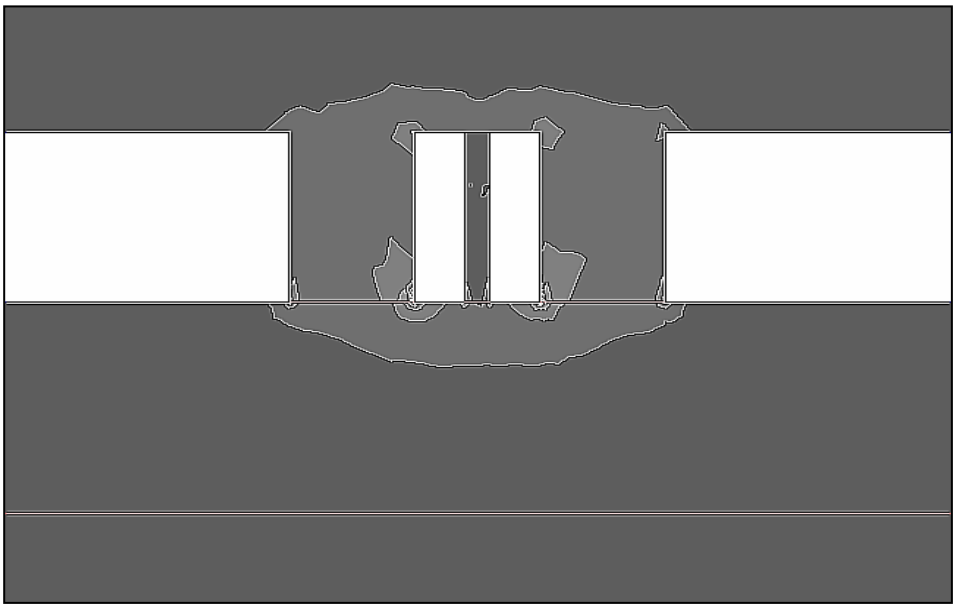

(b)

Figure 3.19 A plot of electric field intensity magnitude in the cross section of the LIGA coupled-line section for various metal heights *H*:
a) H = 0.2 mm, b) H = 0.8 mm.

starts to penetrate into the substrate when spacing *S* becomes greater, which is similar to the case depicted in Fig. 3.10. Conversely, greater conductor heights *H* result in a higher separation of the fields from the substrate, therefore both modal permittivities diminish as the conductors become taller.

The characteristic dependences in Figs. 3.15 and 3.16 indicate that the geometrical configuration between the signal traces and the ground planes is the major contributor to the propagation of the even-mode wave and it does not largely affect the propagation of the odd-mode wave.

The manner in which variation of the substrate thickness *T* affects the electrical characteristics of the CPW coupled-line section is displayed in Figs. 3.17 and 3.18. Fig. 3.17 shows that increase in thickness *T* causes a slight decrease in the even-mode characteristic impedance due the growth of the relevant effective permittivity as indicated in Fig. 3.18, which leads to higher per-unit-length capacitance. The odd-mode characteristics remain unaffected by the variation of *T* from 0.4 mm to 1.2 mm as follows from Figs 3.17 and 3.18, apparently due to the fact the odd-mode fields do not reach the bottom of the substrate, which is similar to the case depicted in Fig. 3.9. Similar to the functional dependences of the electrical characteristics described above, taller conductors result in lower impedances and effective permittivities.

3.5 Validation of the FEM Simulation

Validation of the FEM analyses was performed by comparing simulation results from HFSS and ADS for the same problems. One set of problems was solved for both the CPW transmission line and the coupler. In each set of problems, one parameter was varied while the rest of the parameters were fixed: for the transmission line, the signal trace width *W* was varied from 0.1 to 0.8 mm, while spacing *S* was fixed at 0.3 mm and substrate thickness *T* at 1.0 mm; and for the coupler, the gap between the signal traces *G* was varied from 0.02 to 0.2 mm, while trace width *W* was fixed at 0.2 mm, spacing *S* at 0.5mm, and substrate thickness *T* at 1.0 mm. It was assumed that the closest match between the simulation software packages would be for the case of the zero-thickness conductors, since neither HFSS was amenable to generating accurate meshes for thin conductors, nor ADS was expected to be accurate for simulation of the thick HVAR conductors. The zero-thickness

conductors were modelled in HFSS as the electric walls (see Section 2.3), which are used to designate the metallic surfaces in electromagnetic problems. The ADS simulation results were selected as the reference since the ADS solutions were based on the well-studied techniques, including [28].

The validation results for the single main mode of the CPW transmission line and the two main modes of the CPW coupler are presented in Fig. 3.20. It is evident from the validation plots that the ADS and HFSS results agree within 5 to 15 %, with the characteristic impedance as per HFSS being somewhat greater. The latter might possibly be explained by the fact that ADS assumes some parameters to be infinite, such as the width of the ground planes, while the HFSS simulates the all-finite environment.

Proceeding from the validation results, the FEM analyses were deemed sufficiently accurate to represent the electrical behaviour of the CPW HVAR structures with respect to their geometry.

3.6 Chapter Summary

In this chapter, the rationale of application of the CPW was given, which included easiness of accommodation of lumped elements on CPW, less dispersion, and more degrees of freedom during design. This was followed by a review of the existing CPW design approaches for transmission lines and CPW-based structures published in the open literature. The prevailing majority of the approaches rely on geometrical assumptions, such as metal conductors with zero thickness or infinitely thick substrates. This precluded them from using for characterization of the LIGA CPW structures, where the main focus was investigation of the effects brought about by tall conductors. In addition, the substrates used for LIGA structures are usually not thick enough to disregard the effects of their finite thickness. After considering the available design options, it was found that numerical techniques had to be applied directly to the geometrical models in order to find their performance accurately. One of the direct numerical techniques is the finite element method (FEM), whose essence is division of a designed structure into smaller elements, solving the underlying physical equations in the vertices of the elements with interpolation inside the elements if necessary, and solving sets of algebraic equations for the entire structure assembled from the finite elements. More accurate FEM solutions are obtained

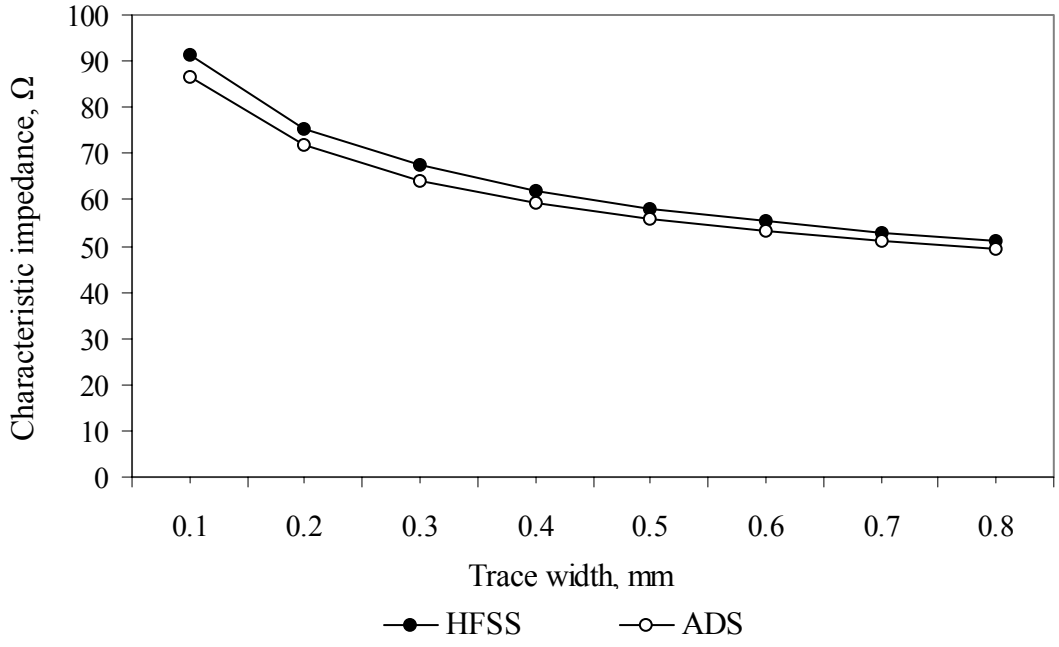

(a)

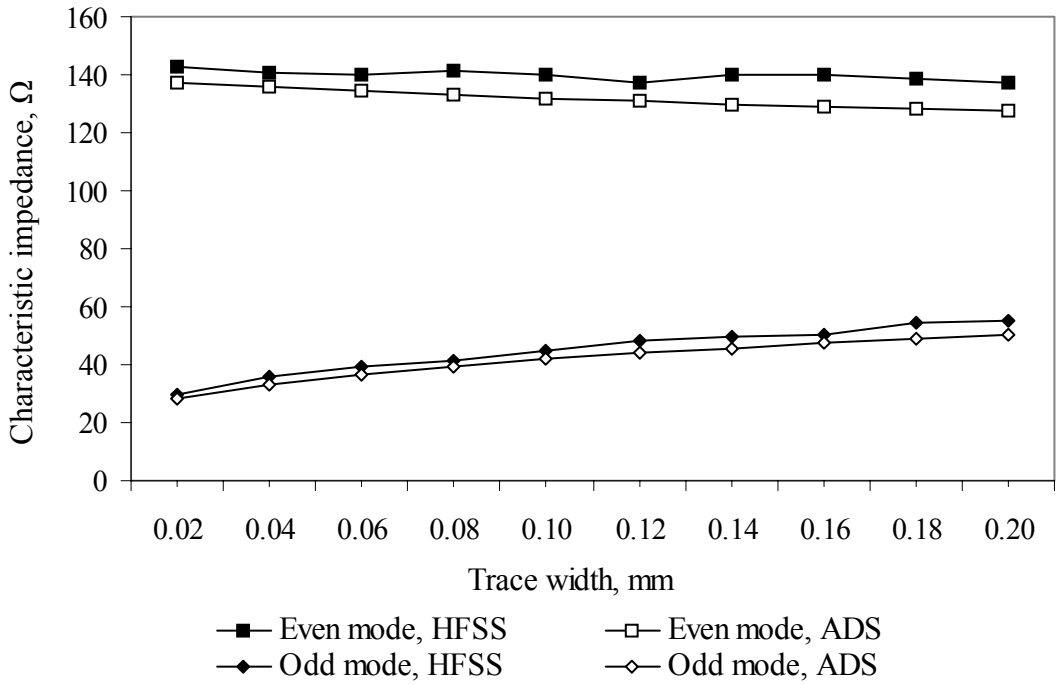

(b)

Figure 3.20 Validation plots for CPW transmission line (a) and coupler (b)

by division of the structure into smaller elements. However, this results in bigger matrices to solve, and, consequently, in more extensive computing resources to consume.

The characterization of the LIGA CPW transmission lines has revealed that they are capable of achieving the standard values of the characteristic impedance (50 Ω and 75 Ω) with narrower signal traces or spacings between the traces and the ground planes, which renders the LIGA CPW lines more compact laterally when compared with the planar CPW lines.

The characterization of the LIGA CPW coupled lines has detected that they may be designed to the desired specification by almost independent control over the characteristics of the two main propagation modes supported by the coupled lines, viz. the even mode and the odd mode. It was found that the properties of the even-mode wave are largely affected by the geometrical configuration between the signal traces and the ground planes, while the properties of the odd-mode wave are influenced by the geometrical configuration between the traces. The planar CPW coupled lines were shown to be not capable of reaching the required values of the modal impedances in order to fabricate the tightly coupled lines with maintaining the dimensions suitable for a high-yield production. The LIGA HVAR CPW coupled lines attain the required modal impedance values with the dimensions well above the fabrication capabilities of the LIGA technology.

Chapter 4
DESIGN, SIMULATION, AND FABRICATION OF 3-dB HVAR COUPLER

4.1 Design of 3-dB LIGA HVAR Coupler

The advantages presented by the LIGA technology to microwave engineering are investigated in this research by the example of a 3-dB coupler, which was required to be built using a simple single metal layer configuration. The edge-coupled, or rather side-coupled in case of LIGA, configuration with the coupled wave traveling backwards was selected as the one with potentially compact dimensions both widthwise and lengthwise – in order to attain the maximum level of coupling, the backward-wave coupled lines should be made a quarter-wavelength long according to Section 2.4. The centre operating frequency was chosen to be 18 GHz to make a fuller use of LIGA's capabilities to produce small-scaled structures, yet not to go beyond the capabilities of the available test equipment.

The final design represents a 3-dB quarter-wavelength long coupled-line section whose ports are extended via 50-Ω transmission lines in order to make microprobe measurements possible.

4.1.1 Transmission Line

The transmission lines used for extension of the ports of the coupled-line section were designed using the characterization data from Section 3.3 as the starting point. The conductor height was selected to be 0.22 mm with respect to standard structural heights offered at IMT and an alumina substrate was selected with a standard thickness of 1 mm. The trace width was set to 0.2 mm. Then the characterization data in the vicinity of the desired characteristic impedance of 50 Ω was refined via a separate HFSS simulation to find the proper spacing between the trace and the ground planes. The length of the extension

transmission lines was set to a half of the effective wavelength, calculated from the effective permittivity on the basis of (2.12) as follows:

$$\lambda_{eff} = \frac{\lambda}{\sqrt{\varepsilon_{eff}}} = \frac{c}{f\sqrt{\varepsilon_{eff}}} \tag{4.1}$$

The HFSS simulation procedure and the model used were similar to those described in Section 3.3. The simulation results are presented in Table 4.1.

Table 4.1 The simulation results for a LIGA HVAR CPW 50-Ω transmission line

Quantities	***Values***
1. Trace width W	0.20 mm
2. Spacing between the trace and the ground planes S	0.25 mm
3. Conductor height H	0.22 mm
4. Substrate thickness T	1.00 mm
5. Characteristic impedance Z_0	50.05 Ω
6. Relative permittivity of the substrate (alumina) ε_r	9.8
7. Effective permittivity ε_{eff}	3.59
8. Frequency f	18 GHz
9. Effective wavelength λ	8.79 mm

4.1.2 Coupled-Line Section

As follows from expressions (2.20) in Section 2.4, the level of coupling $K = -3$ dB, which corresponds to $k = 10^{-K/20} = 0.78$, in a 50-Ω system is attained when the coupled lines are designed so that the even-mode and odd-mode impedances are 120.9 Ω and 20.7 Ω respectively. The shortest length of the coupled-line section at which the designed maximum level of coupling is reached is a quarter of the effective wavelength.

The quarter-wavelength coupled-line section was designed using the characterization data from Section 3.4 as the starting point. The conductor height and the trace width were set to the same values as those for the extension transmission lines: 0.22 mm and 0.2 mm respectively. The same substrate was also used: 1-mm thick alumina with the relative permittivity of 9.8. Then the characterization data in the vicinity of the desired modal characteristic impedances of 120.9 Ω and 20.7 Ω was refined via a separate HFSS simulation to

find the proper gap between the traces and spacing between the traces and the ground planes.

Since the phase velocities for the even and the odd propagation modes differ, the modal effective permittivities and, consequently, the modal effective wavelengths are different. Therefore, the length of the coupled-line section was set to the geometric mean between the even-mode and the odd-mode effective wavelengths found using (4.1).

The HFSS simulation procedure and the model used were similar to those described in Section 3.4. The simulation results are summarized in Table 4.2.

Table 4.2 The simulation results for a LIGA HVAR CPW 3-dB quarter-wavelength coupled-line section

Quantities	***Values***
1. Trace width W	0.20 mm
2. Gap between the traces G	0.06 mm
3. Spacing between the traces and the ground planes S	0.56 mm
4. Length L	2.26 mm
5. Conductor height H	0.22 mm
6. Substrate thickness T	1.00 mm
7. Characteristic impedance Z_0 at ports	50 Ω
8. Even-mode characteristic impedance Z_{0e}	121.4 Ω
9. Odd-mode characteristic impedance Z_{0o}	20.2 Ω
10. Relative permittivity of the substrate (alumina) ε_r	9.8
11. Even-mode effective permittivity $\varepsilon_{eff.e}$	4.27
12. Odd-mode effective permittivity $\varepsilon_{eff.o}$	2.7
13. Frequency f	18 GHz
14. Even-mode effective wavelength $\lambda_{eff.e}$	8.06 mm
15. Odd-mode effective wavelength $\lambda_{eff.o}$	10.1 mm

4.2 Simulation of 3-dB LIGA HVAR Coupler

Using the design data from Section 4.1, the final structure including the quarter-wavelength coupled-line section and extension transmission lines has been designed and simulated. The solutions were sought for the centre operating frequency of 18 GHz as well as a range of frequencies around 18 GHz. The structure was fabricated at IMT in Karlsruhe, Germany.

4.2.1 Model

The simulation model of the 3-dB coupler is shown in Fig. 4.1 as a drawing generated by HFSS. In the model, the ports of the coupled-line section are extended to the four sides of the final structure in order to facilitate microprobe testing as well as to better decouple the extended ports from each other. The extension is made via half-wavelength transmission lines with the geometrical length of 4.4 mm. In consequence, the lateral dimensions of the final structure are 10.4 x 10.4 mm.

The model includes both actual and virtual objects. The latter are the air box, ports, and air inserts between the conductors.

The air box is required to separate the structure from the background, which is assumed to be the perfect conductor to provide continuity for the electric fields. Since the air box is interfaced with background, its walls are the perfect conductor. Therefore, the dimensions of the air box have to be selected such that they do not influence the major modes propagating in the structure. As in Section 3.3.1, selection of the air box dimensions is ad hoc and they are set to exceed the dimensions of the field-containing volumes. In this case, it is sufficient to select the lateral dimensions of the air box to enclose the structure laterally and the height of the air box to accommodate the ports.

The ports are the two-dimensional objects that are used to pass power from and into the structure. In order not to create reflection off the ports, they are perfectly matched to the structure, which is modeled by assuming that the ports are connected to semi-infinite waveguides that exactly repeat the cross-section and material properties of the regions of the structure adjoining the ports.

The air inserts between the conductors were included in the model in order to increase accuracy of the simulation. This is achieved by way of making the meshing denser in the

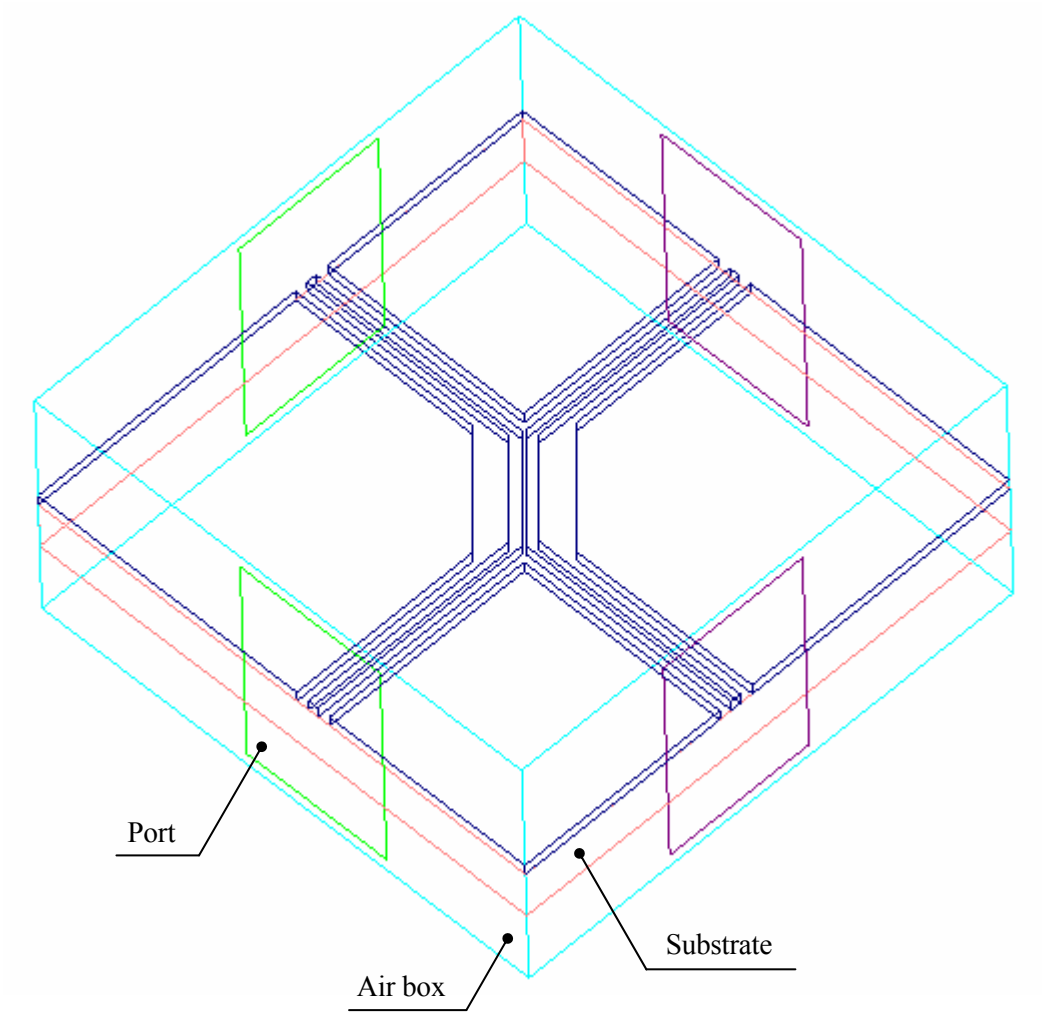

Figure 4.1 HFSS model of 3-dB coupler

regions of major field concentration, which is done by inserting virtual objects not affecting the fields in those regions. As HFSS meshes simulated structures automatically, usage of these virtual objects is a method to save valuable computer resources by instructing HFSS to mesh certain regions denser while leaving other, less critical, regions meshed sparsely. As one of the areas of the major field concentration in the studied structure are the spaces between the conductors, they are filled with the air inserts that are delineated by the conductors laterally and by the substrate top surface and the top surface of the conductors. The electrical properties of the air inserts exactly follow the electrical properties of

the air box and are those of air. For better clarity, the air inserts were made invisible in the drawing in Fig. 4.1.

The actual objects are the conductors and the substrate. The conductors were assumed to be nickel and the substrate was assumed to be alumina.

4.2.2 Results

The results of HFSS simulations of the entire 3-dB coupler structure, comprising the quarter-wavelength coupled-line section and extension transmission lines, are demonstrated in Figs. 4.2 – 4.5.

Figure 4.2 shows the HFSS generated graphical representation of the electric field traveling in the coupler.

Figure 4.3 displays the HFSS simulated frequency sweep for the entire structure over a range of 12 – 25 GHz. The figure includes the graphs for magnitude and phase of coupling (S_{31}) and throughput (S_{21}).

Figure 4.4 presents the ideal performance of the 3-dB quarter-wavelength coupled-line section without the extension transmission lines in terms of magnitude and phase of coupling (S_{31}) and throughput (S_{21}) over a range of 12 – 25 GHz.

Figure 4.5 shows the frequency-dependent behaviour of the remaining S-parameters of the entire structure simulated with HFSS: reflection (S_{11}) and isolation (S_{41}) presented in terms of their magnitudes and phases over a range of 12 – 25 GHz.

The simulated S-parameters of the entire coupler structure at the centre frequency of 18 GHz are summarized in Table 4.3.

Table 4.3 HFSS-simulated S-parameters of the entire coupler structure at 18 GHz

Parameter	Magnitude, dB	Phase, deg
S_{11}, Input reflection	–22.8	–163
S_{21}, Throughput	–3.36	–83.9
S_{31}, Coupling	–2.78	6.46
S_{41}, Isolation	–21.7	–86.5

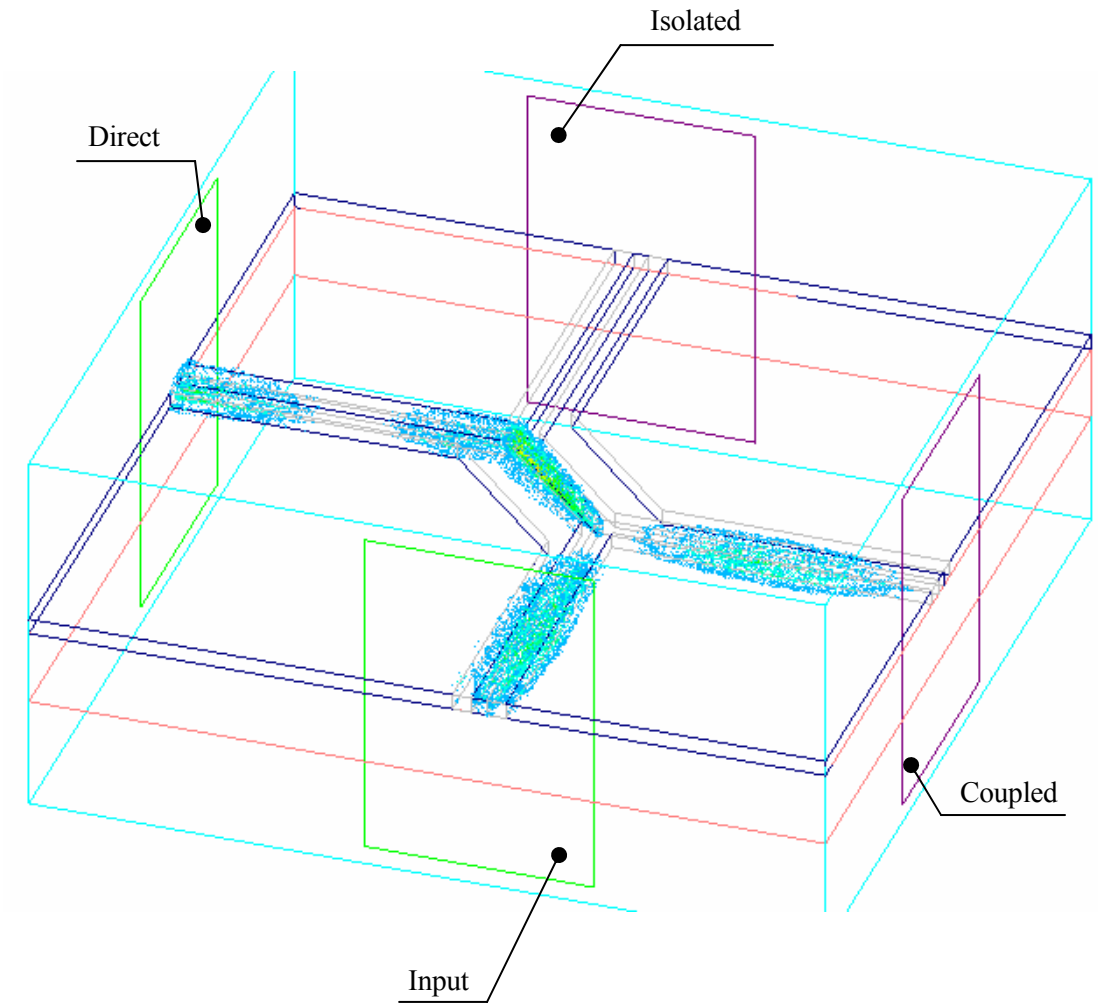

Figure 4.2 Distribution of the electric field in the coupler

4.2.3 Discussion

Figure 4.2 gives an illustrative insight into how the electric field propagates along the entire coupler structure. The illustration was generated by HFSS and represents the electric field in terms of its magnitude in the form of half-wave clouds. It may be seen that as a new half-wave is entering the coupled port, an old half-wave is crossing the direct port by its crest. This is an evidence that the phase difference between the direct and coupled ports is 90 degrees. It may also be seen that no visible field appears at the isolated port, which indicates good directivity, defined by (2.7b), of the structure.

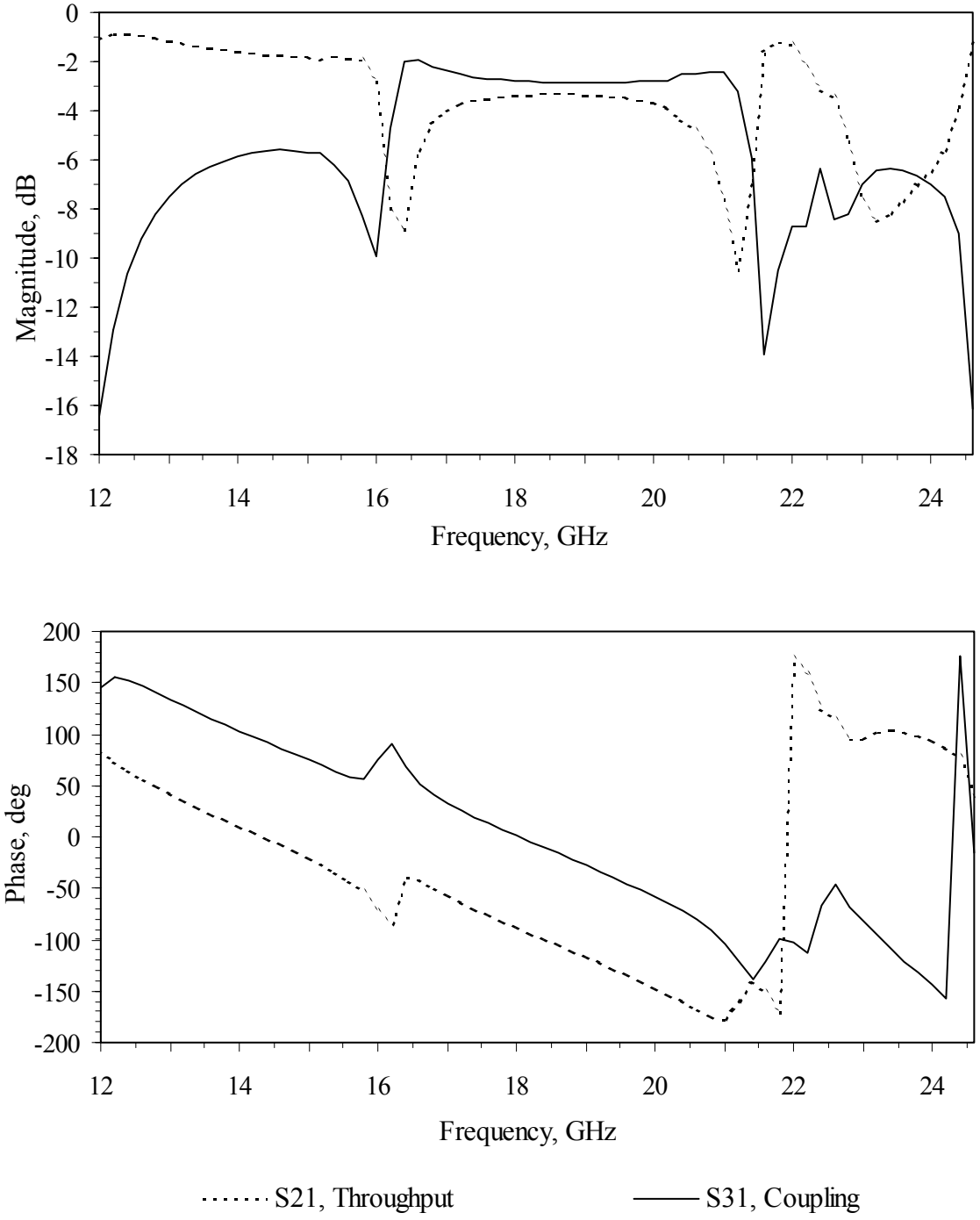

Figure 4.3 Simulated performance of the entire structure: Magnitude and phase of throughput and coupling

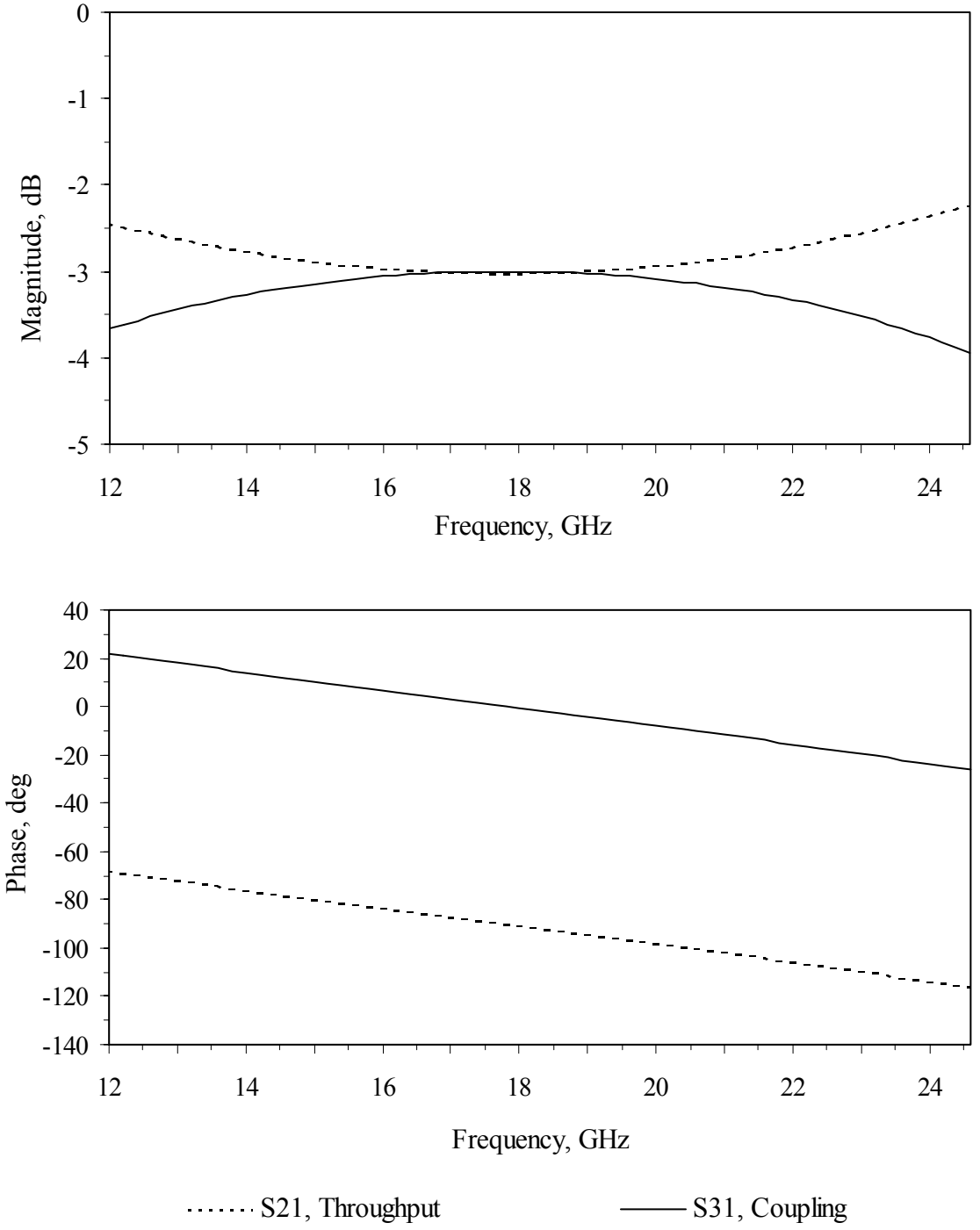

Figure 4.4 Ideal performance of the coupled-line section alone: Magnitude and phase of throughput and coupling

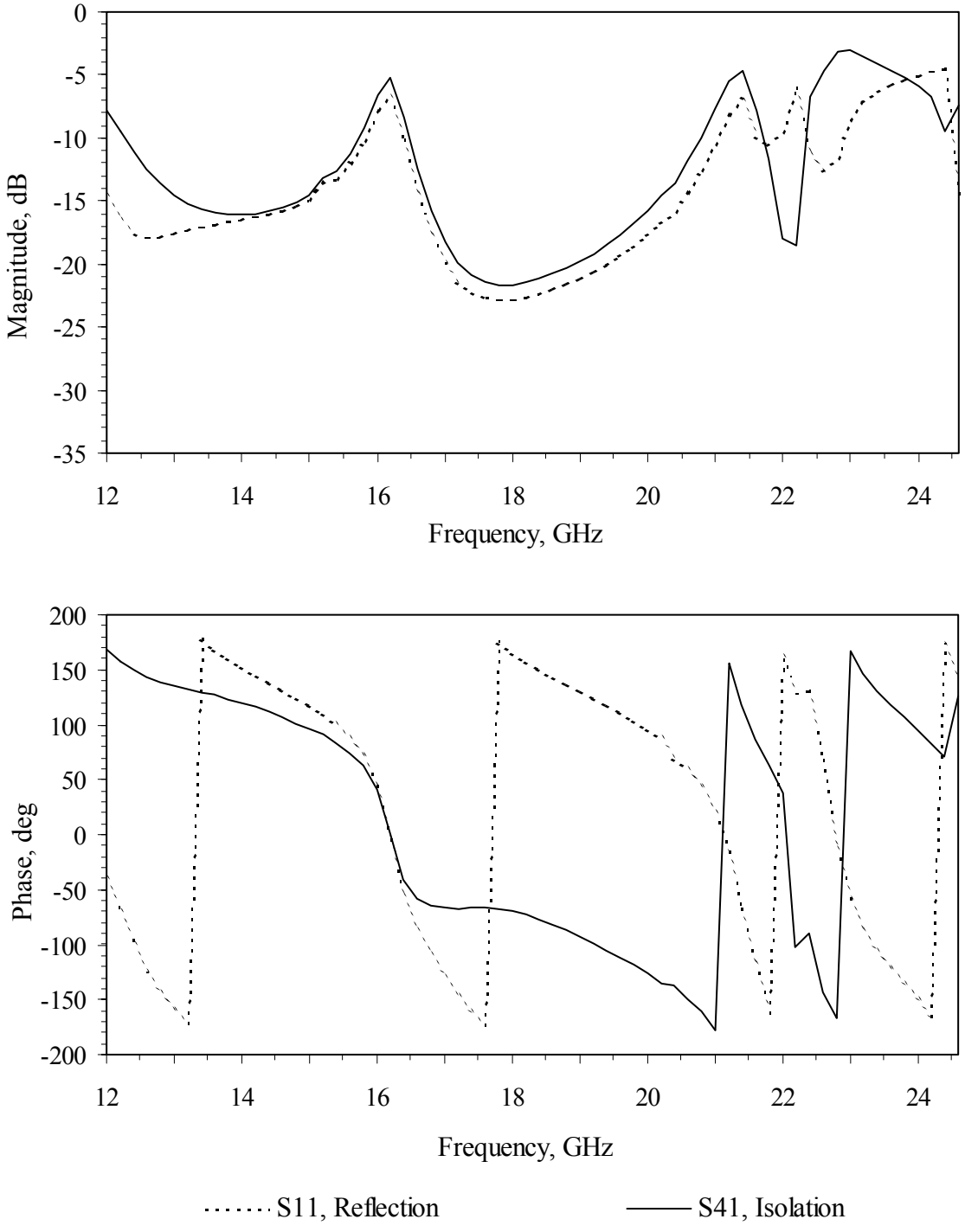

Figure 4.5 Simulated performance of the entire structure: Magnitude and phase of reflection and isolation

The major performance characteristics of the entire coupler structure simulated by HFSS, viz. coupling (S_{31}) and throughput (S_{21}), are plotted in Fig. 4.3 versus frequency over a range of 12 – 25 GHz in separate graphs for magnitude and phase. The same quantities for the ideal case of the 3-dB quarter-wavelength coupled-line section are plotted in Fig. 4.4. It may be seen that both magnitude and phase of coupling (S_{31}) and throughput (S_{21}) of the ideal coupler are smooth over the entire range of the simulated frequency, whereas these quantities have discontinuities for the case of the actual coupler with transmission lines. The ideal characteristics are plotted using (2.15) for (S_{21}) and (2.16) for (S_{31}). The electrical length θ in (2.15) and (2.16) was calculated via (2.18), where phase constant β was found using the average effective permittivity of 3.4, found as the geometrical mean between the even- and odd-mode effective permittivities, according to (4.1). The ideal coupling magnitude curve is at its maximum of –3 dB at the centre frequency of 18 GHz, where the throughput magnitude is at its minimum of –3 dB. In the frequency regions outside the centre frequency, coupling magnitude smoothly goes down reaching the level of about –3.7 dB while throughput magnitude smoothly raises to about –2.4 dB at the lower and upper simulated frequency points. The sum of magnitudes of coupling and throughput expressed without units is unity in every point of the frequency range, which suggests that ideally the entire incident power should be divided between the direct and coupled ports and no power should proceed to the isolated port, or reflected back to the input port (S_{11}, $S_{41} = 0$). The ideal coupling and throughput phases are represented by straight lines with negative slopes that are spaced 90 degrees apart over the entire frequency range, indicating that the signals at the coupled and direct ports are always in the phase quadrature.

Notwithstanding the fact that the characteristics of the actual coupling structure experience sudden transitions, there are smooth regions around the centre frequency of 18 GHz where the required specifications are met: between 16 and 21.6 GHz for coupling (S_{31}), where it goes down to –10 and –14 dB respectively; and between 16.4 and 21.2 GHz for throughput (S_{21}), where it goes down to –8.9 and –10.5 dB respectively. By measuring the useful operating bandwidth between the points where the frequency characteristic drops below the –3 dB level from the nominal operating level (between the –6 dB points for this case), it may be seen that the bandwidth by coupling makes 5.3 GHz (between 16.1 and 21.4 GHz) and the bandwidth by throughput makes 4.4 GHz (between 16.5 and 20.9 GHz).

Therefore, the structure's useful operating bandwidth, where the characteristics remain within the 3-dB band from the specified levels of –3 dB at centre frequency for both throughput and coupling, is 4.4 GHz, or 24.4%.

The dips in the frequency characteristics that delineate the useful operating bandwidth around the centre frequency may be explained by insertion of discontinuities in both characteristic impedance and phase velocity in the transitions between the coupled-line section and extension transmission lines, highlighted by the circle in Fig. 4.6.

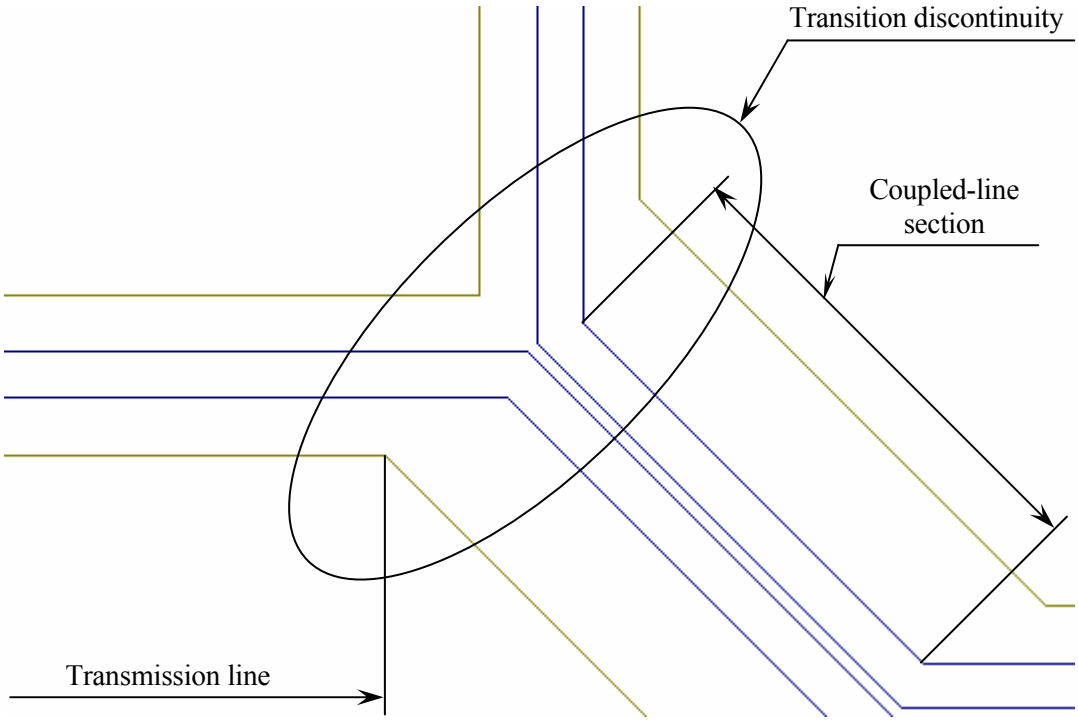

Figure 4.6 Transition discontinuity between the coupled-line section and transmission lines (in the circle)

It may be seen in Fig. 4.6 that there are pieces of the signal traces between the ends of the coupled-line section and transmission line where no ground planes are present at the distances required to provide the design characteristic impedance of 50 Ω. This entails characteristic impedances other than 50 Ω, which results in reflections off the mismatch discontinuities. The transition discontinuities may also be the reason of the slight shift of the

maximum coupling point off the centre frequency by 0.8 GHz to 18.8 GHz due to the change of the electrical length of the coupled-line section caused by reflections off the transition discontinuities.

The coupling and throughput phase characteristics in Fig. 4.3 are fairly linear and spaced approximately 90 degrees apart from each other in the useful operating bandwidth limited by the transitional discontinuities. Therefore, the signals at the direct and coupled port will be in phase quadrature.

The figures of merit of the entire coupler structure, viz. input reflection (S_{11}) and isolation (S_{41}) are plotted in Fig. 4.5 versus frequency. Presented are their magnitudes and phases. Fig. 4.5 reveals that both quantities reach their minimum levels exactly at the centre frequency and make –22.8 and –21.7 dB for the input reflection (S_{11}) and isolation (S_{41}) respectively. In the regions outside the centre frequency they smoothly grow and reach their maximum levels of –6.8 dB for S_{11} and –5.2 dB for S_{41} at 16.2 GHz as well as –7 dB for S_{11} and –4.72 dB for S_{41} at 21.4 GHz. However, the input reflection (S_{11}) and isolation (S_{41}) never exceed –11 and –9 dB respectively in the useful operating bandwidth of 4.4 GHz.

The phases of the input reflection (S_{11}) and isolation (S_{41}) are not critical quantities during nominal operation of the coupler.

The four S-parameters presented in Table 4.3 are adequate to represent the 4x4 [S] matrix of the four-port coupler structure since the structure is reciprocal and (4.2) holds true:

$$S_{ij} = S_{ji} \tag{4.2}$$

where i and j are the numbers of rows and columns in the [S] matrix.

The phase difference between the throughput and coupling makes 90.39 degrees at 18 GHz, hence the signals at the direct and coupled ports are in the phase quadrature.

4.3 Fabrication of 3-dB LIGA HVAR Coupler

The 3-dB HVAR coupler structure, as well as an HVAR CPW transmission line and the structures required for calibration of test equipment (calibration standards), have been fabricated at IMT in Karlsruhe, Germany. One of IMT's most developed LIGA processes was used for fabrication using the 2.5-GeV ANKA storage ring and beamline Litho-2 providing high-energy X-ray radiation of up to 8 keV. A 1-mm thick alumina wafer was

coated with a 3-μm Ti/TiOx plating base, followed by application of a 340-μm thick layer of PMMA photoresist, which was then exposed to X-ray radiation through a mask constructed of 20-μm gold absorbers on a 2.7-μm titanium membrane. Following that, the photoresist was developed by dipping in GG developer. Developed voids were filled with nickel to a height of 220 μm. Before being stripped away, the remaining photoresist underwent flood X-ray irradiation to ensure its solubility. Finally, the conductors were electrically isolated by removing the plating base with hydrofluoric (HF) acid and reactive ion etching (RIE). A scanning electron microscopy (SEM) micrograph showing the enlarged transition between the coupled-line section and the extension transmission lines is presented in Fig. 4.7. It may be noticed that all the sharp corners were rounded. This was done following the fabrication requirements in order not to crack the photoresist, which expands and contracts during processing, and also not to facilitate creation of the centres of internal stresses in electroplated nickel. An SEM micrograph highlighting the structural qualities of the coupler is demonstrated in Fig. 4.8. First of all, the micrograph features the conspicuous roughness of the top metal surface, which has not been polished and therefore it shows a natural grain distribution that forms on the nickel surface during electroplating. The surface roughness was measured using a profilometer, which showed a mean roughness (R_a) of 0.7 μm with a typical peak-to-valley roughness (R_t) of 7 μm.

After fabrication, an experimental procedure of polishing the conductor top surface of the coupler structure and calibration standards was carried out under the following procedure: first, the voids in all the structures were filled with liquid resist under vacuum to ensure structural stability; second, the remains of the resist were ground away; third, the top metal surfaces were polished with a fine polishing compound with 10-μm grains; fourth, the samples were flood irradiated with X-rays to facilitate solubility of the resist, which was finally removed via development. The polishing reduced the height of the metal structures down to approximately 200 μm and gave the following top surface finish results: mean roughness (R_a) of 35 nm and typical peak-to-valley roughness (R_t) of 200 nm, which is an optical surface quality. It should be noted though that the polishing will likely change the electrical performance of the coupler as compared with results of the simulation, which was done at the stage when the polishing was not anticipated.

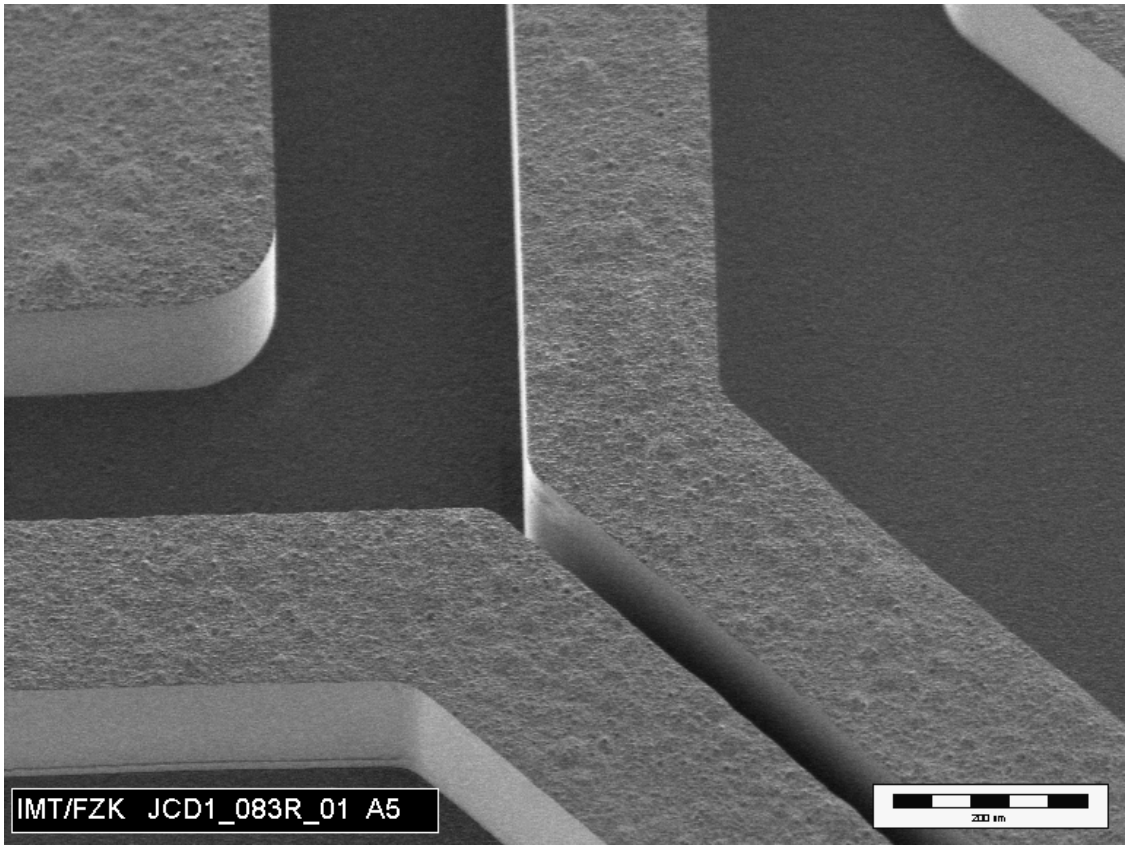

Figure 4.7 The LIGA HVAR coupled-line structure fabricated at IMT

The micrograph in Fig. 4.8 also reveals an excellent quality of the sidewalls that are visually flat and whose roughness cannot be judged by the micrograph, but is typically of the optical quality and less than 50 nm.

4.4 Chapter Summary

By using the LIGA microfabrication technology, a simple side-coupled 3-dB coupler implemented in a single metal layer has proved to be feasible with tall HVAR conductors.

The entire 3-dB coupling structure has been designed by combining the HVAR CPW 3-dB quarter-wave long coupled-line section and HVAR CPW extension lines to enable testing the structure using a microprobing station. The coupled-line section and extension lines were designed by refining their characterization data from Sections 3.3 and 3.4 via HFSS simulations to provide the characteristic impedances of 50 Ω for the extension lines,

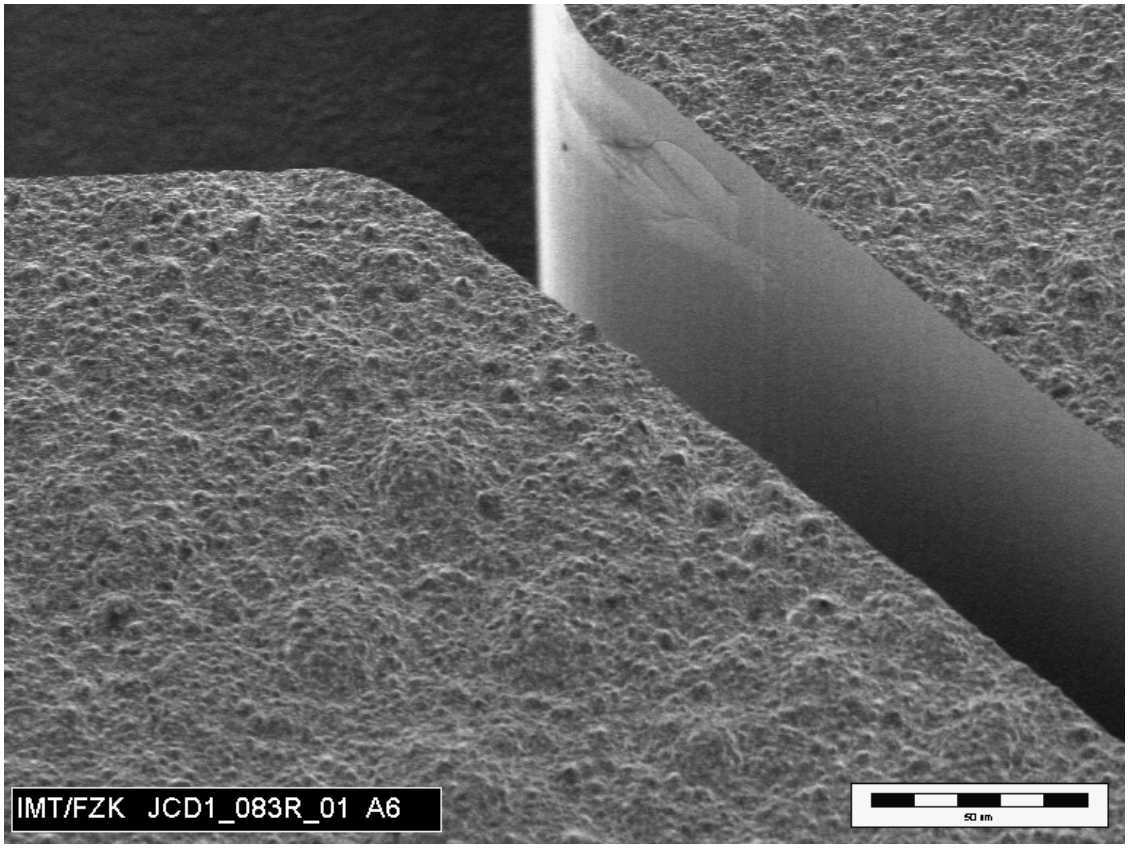

Figure 4.8 Enlarged top surface of the LIGA HVAR coupler conductors

and 120.9 Ω and 20.7 Ω for the coupled-line section. The length of the coupled-line section was selected to place the centre frequency at 18 GHz.

The resulting 10.4x10.4 mm 3-dB coupling structure was HFSS simulated to reveal that the initial design specifications were met at the centre frequency and in the 3-dB useful bandwidth of 4.4 GHz, or 24.4%, around it. The useful bandwidth was apparently limited by the discontinuities in characteristic impedance and phase velocity created by the transitions between the coupled-line section and extension lines. Further expansion of the useful bandwidth for this device should be sought by finding the ways to compensate the transitional discontinuities.

The designed HVAR structure was fabricated at IMT in Karlsruhe, Germany using a LIGA process where 0.22-mm high nickel conductors were electroplated on a 1-mm thick alumina substrate. Then the top surfaces of the structure were polished, which reduced the structure's height to approximately 200 μm.

The next chapter presents measurement results for the fabricated coupling structure.

Chapter 5
TESTING OF 3-dB HVAR COUPLER

5.1 TRL Standards and Calibration Procedures

The fabricated structures are tested using the Agilent 8722 ES vector network analyzer (hereinafter referred to as the VNA), which is usually connected to tested devices via coaxial cables. Since the structures do not have coaxial connectors, a test fixture is required to connect them to the VNA. With a test fixture inserted between the tested device and the VNA, the S-parameters seen by the VNA are not the parameters of the tested device. In order to eliminate the influence of the test fixture on the measurement results, the fixture characteristics must be known and taken into account during measurement. This is achieved by calibration procedure, which effectively is the measurement of calibration standards with pre-determined characteristics. In general, the calibration helps remove the systematic errors, which are repeatable errors that the VNA can measure. These errors include mismatch and leakage in the test setup, isolation between the reference and test signal paths, and system frequency response, which are the most significant sources of measurement uncertainty in most microwave measurements [33]. There are also other measurement errors such as drift errors and random errors, with the latter being due to instrument noise and connection repeatability [33]. They cannot be eliminated through calibration, but are generally reduced with three different noise reduction techniques provided by the VNA: sweep-to-sweep averaging, display smoothing, and variable IF bandwidth.

Distinguished by convenience of design, fabrication, and characterization of standards among other 2-port calibration methods is the thru, reflect, line (TRL) 2-port calibration procedure, where only three calibration standards are required: “thru”, “reflect”, and “line”. All TRL standards are based on the same type of transmission line as that used in the tested sample. The TRL method relies on the knowledge of the characteristic imped-

ance of the “thru” and “line” standards, which is found via simulation and is the measurement reference.

According to [33], the “thru” standard is a non-zero long transmission line whose characteristic impedance is equal to that of the “line” standard. Its insertion loss does not have to be known.

The “line” standard is a piece of the same transmission line as the one used in “thru”. By default, the calibration impedance is defined to be equal to the characteristic impedance of the “line”. However, if the characteristic impedance of the “line” is not of the desired value (e.g. not equal to the characteristic impedance of the measured device or the system’s standard 50 Ω), the difference between the calibration and measurement impedances may be preset in the VNA manually. In this project, the same design of CPW transmission line was used for both coupling structure and the calibration standards and all the structures underwent identical fabrication procedures. Therefore, the calibration impedance was defaulted to be equal to the characteristic impedance of the “line”. The electrical length of “line” must be greater than the electrical length of “thru”. Optimally, “line” should be longer than “thru” by a quarter-wavelength at the centre calibration frequency, or additional electrical length of “line” should be 90 degrees. The TRL calibration is valid for the frequency band where the additional electrical length of “line” relative “thru” stays within 20 to 160 degrees. As with “thru”, the insertion loss of “line” does not have to be known.

The “reflect” standard should optimally provide the reflection coefficient magnitude of unity, but does not have to be known exactly. The reflection coefficient must be identical at both ports. Its phase must be known and specified to within ±90 degrees.

The VNA provides automatic characterization of the calibration standards under the TRL procedure, calculation of the correction coefficients, and correction of actual measurement results for tested devices.

The TRL standards were designed using the LIGA CPW transmission line employed in the coupler according to the above requirements and geometrical data given in Table 4.1. The “thru” standard is 4-mm long and the “line” standard is a 6.2-mm long LIGA CPW transmission line. The “line” is 2.2 mm longer than the “thru”, therefore the calibration is valid in the range of frequency from 4 to 32 GHz. The “reflect” standard is the same piece

of LIGA CPW as the "line", except that the centre signal trace in the "reflect" has a 2.2-mm long missing section in the middle to provide open-port terminations (see Fig. 5.1), which in reality are slightly capacitive.

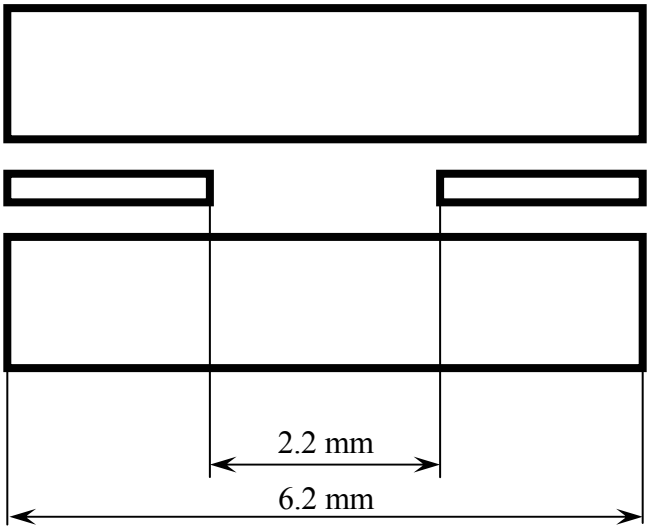

Figure 5.1 Top view of the "reflect" standard

5.2 Description of Test Fixture

The purpose of the test fixture is to connect two of the coupler ports to the VNA, while terminating the remaining two ports in 50-Ω terminations, as well as to constrain and support the samples. The test fixture comprises a heavy base plate, which carries four micropositioners and sample support. Micropositioners are the mechanical units that hold microprobes and terminations and provide their fine motion along the three coordinate axes. There are two micropositioners that hold 50-Ω terminations and two micropositioners that hold microprobes. A microprobe is the adapter that provides direct contact with the measured sample and transition between the microprobe transmission line and the coaxial connector that is used to connect the microprobes to the VNA via coaxial interconnecting cables. The microprobes used in test fixture are customized Cascade ACP40 air coplanar

probes with the distance between the coplanar pins of 750 μm. A photograph of the microprobes touching a LIGA HVAR sample is shown in Fig. 5.2. The 50-Ω termination microprobes were made at the TRLabs laboratory. The visual control was performed through a Dynascope optical magnification unit manufactured by Vision Engineering. A general view of the testing fixture and the VNA is presented in the photograph in Fig. 5.3.

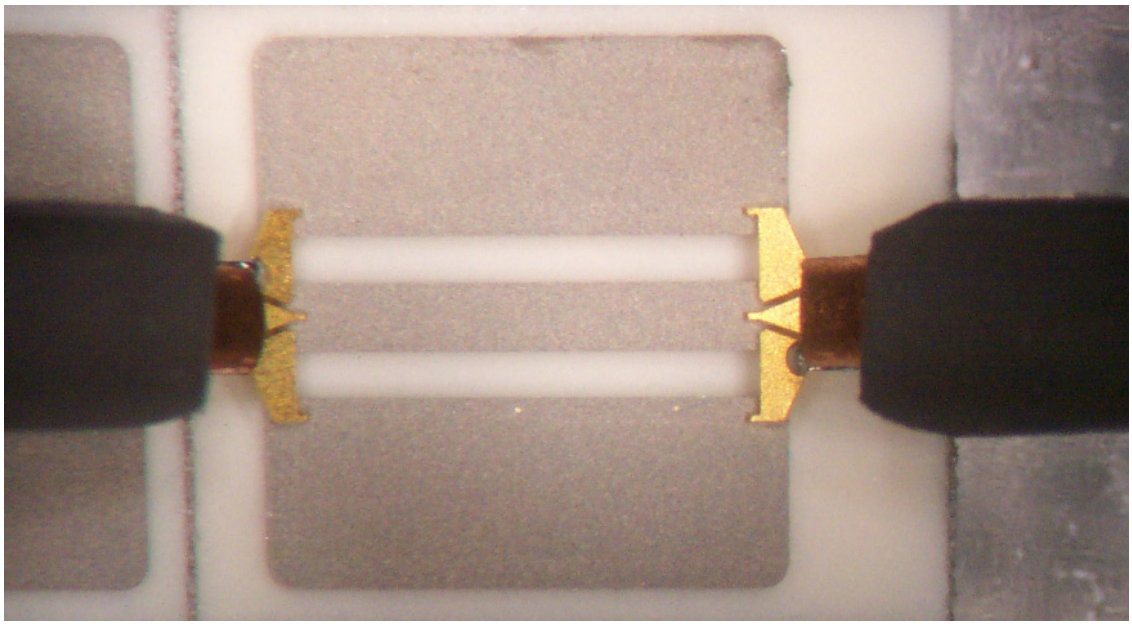

Figure 5.2 Air coplanar microprobes touching a sample

5.3 Measurement of the 3-dB HVAR Coupler

In order to test the 3-dB coupler, its three main parameters, described in Section 2.2, were measured: coupling, isolation, and throughput.

Each of the above parameters was measured in a two-port setting, where at any given time two ports were terminated with 50-Ω terminations and two other ports were touched by the microprobes.

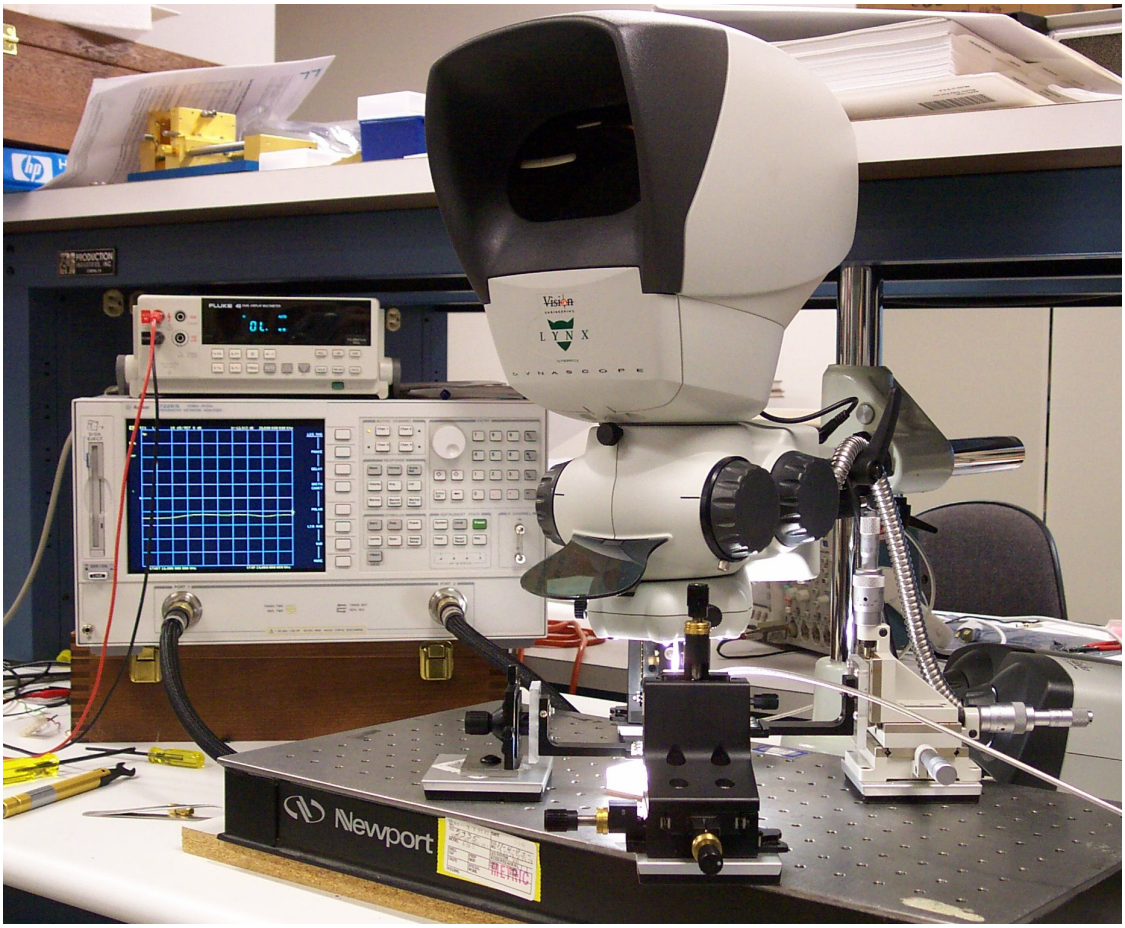

Figure 5.3 The testing fixture and vector network analyzer

When measuring coupling (S_{31}), the "Input" and "Coupled" ports were touched by the microprobes as per Fig. 4.2, while the "Direct" and "Isolated" ports were touched by the 50-Ω terminations.

When measuring throughput (S_{21}), the "Input" and "Direct" ports were touched by the microprobes, while the "Coupled" and "Isolated" ports were touched by the 50-Ω terminations.

When measuring isolation (S_{41}), the "Input" and "Isolated" ports were touched by the microprobes, while the "Direct" and "Coupled" ports were touched by the 50-Ω terminations.

The reflection losses in all the measurements may be considered equivalent to each other since all the ports were terminated with matching loads at all times. Therefore, the results for the reflection loss (S_{11}) of the coupler are given from the coupling measurement.

In order to see the coupler's broadband behaviour, the measurements were done in three narrower bands: 12 – 16 GHz, 16 – 20 GHz, and 20 – 24 GHz. This was required since accurate and stable calibration and measurement were difficult over the entire 12 – 24 GHz range in a single sweep due to the large frequency steps (limited number of measurement points) and therefore extremely large input bandwidth of the VNA's receiver, which influences the measurement accuracy. The three measurement bands were combined into a common broad band spanning from 12 to 24 GHz. Each of the three bands was measured in 201 frequency points, hence the coupler's combined broadband performance included 603 frequency points. Also, the measurement in each of the bands was preceded by a separate calibration. The measurement results are demonstrated in the combined plots: coupling (S_{31}) and throughput (S_{21}) in Fig. 5.4, and isolation (S_{41}) and reflection loss (S_{11}) in Fig. 5.5. As evident from the testing results, the coupler structure demonstrates the level of coupling that is close to the predicted coupling within the boundaries of measurement errors and other errors relevant to the testing issues discussed below. The maximum coupling is demonstrated at 18.2 GHz (the simulated centre frequency where the maximum coupling is expected is 18 GHz) and it is –4.07 dB, which is 1 dB less than predicted via simulation. The downgrade of the coupling observed in the higher end of the measurement band may be owing to higher impedance mismatch due to poorer quality of the 50-Ω terminations, whose return loss grows with frequency as evident from Fig. 5.6, where it may be seen that the reflection loss of the terminations becomes –10 dB at 17 GHz and continues to grow with higher frequencies, reaching –3.8 dB at 26 GHz. Since the quality of the terminations becomes poorer in the higher end of the defined 3-dB operating bandwidth, it may be inferred that the measurement errors are greater in the higher end of the bandwidth than in the lower and the lower end of the bandwidth is closer to the coupler's actual performance, while the higher end may be masked by measurement errors. With respect to the maximum coupling, the 3-dB operating bandwidth is 6.8 GHz and it spans from 13.3 to 20.1 GHz.

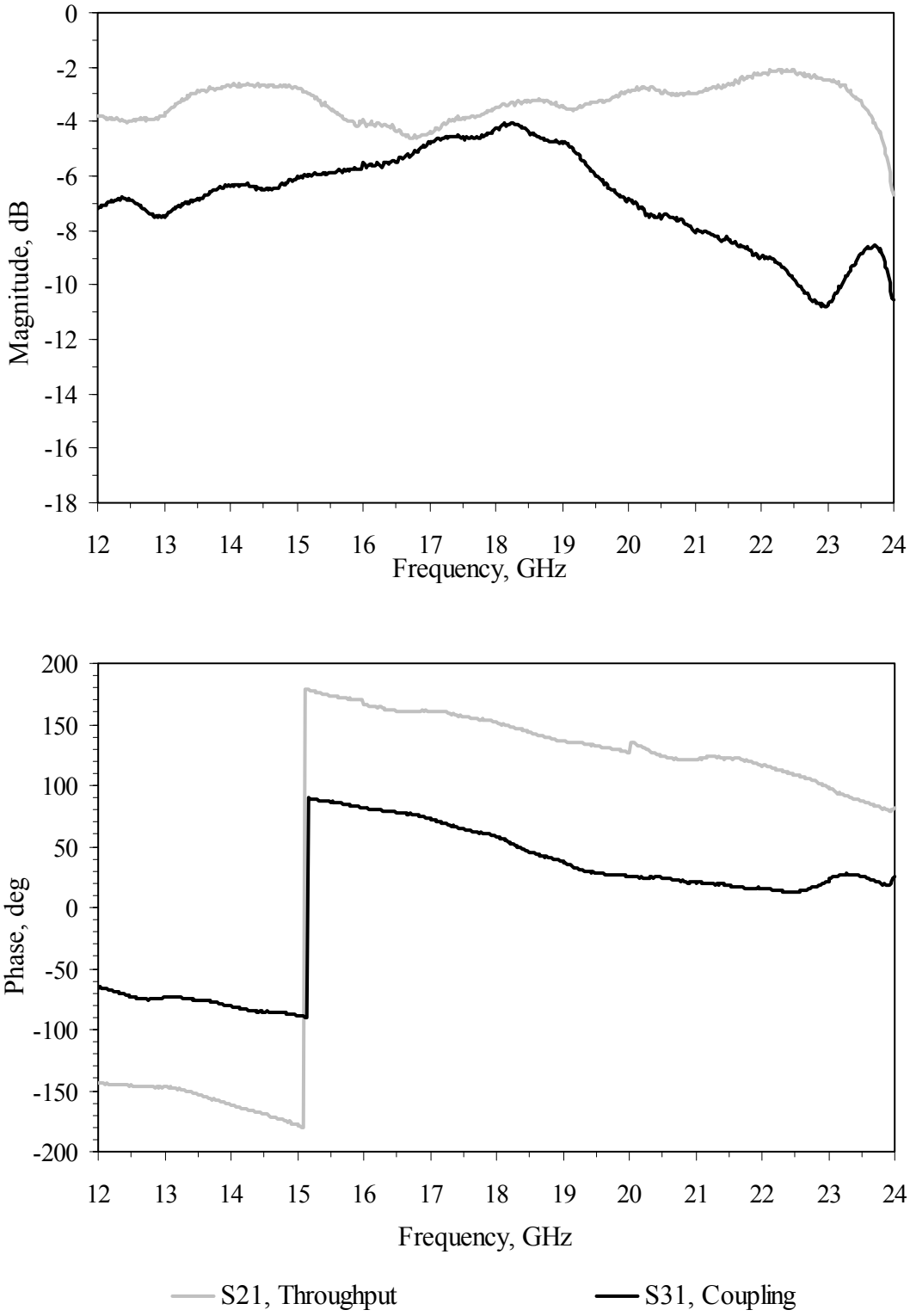

Figure 5.4 Measured performance of the entire structure: Magnitude and phase of coupling and throughput

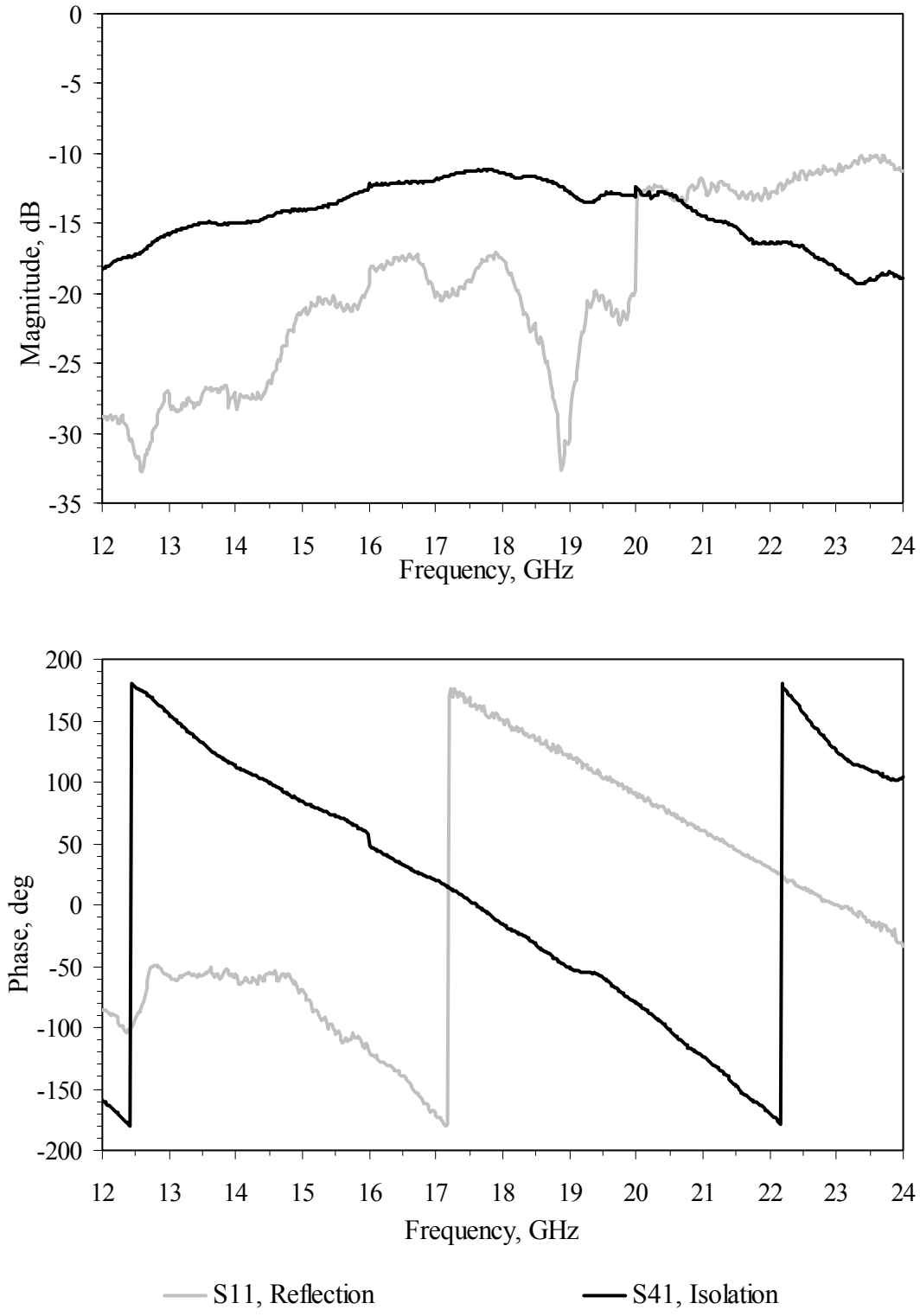

Figure 5.5 Measured performance of the entire structure: Magnitude and phase of reflection and isolation

The bandwidth for the throughput is yet wider. The measurement results show only the upper bandwidth limit at approximately 24 GHz, which may be still higher if a better matching of the ports terminated with the 50-Ω terminations at higher frequencies is achieved. Theoretically, it should not reduce below the lower measurement frequency of 12 GHz, on the contrary it should go up to 0 dB at DC. Overall, the experimental throughput is close to expected –3 dB almost in the entire measured range and only goes down at the higher end of the range, which might be caused by mismatches of the 50-Ω terminations. The highest throughput in the measured band is –2.07 dB.

The phase curves of the coupling and throughput are fairly linear and spaced approximately 90 degrees apart (i.e. the coupled and through signals are in phase quadrature) across the measured band, with the throughput phase lagging behind the coupling phase as expected. The linearity of the coupling and throughput phase curves renders the coupler suitable for applications with multi-carrier signals as their delay would be linear after passing the coupler. The spacing of the phase curves, which is close to 90 degrees, suggests that the coupler may also be used as a quadrature phase shifter, a device where the phase difference between the output signals is 90 degrees all over the operating bandwidth. The coupler's phase differential characteristic is demonstrated in Fig. 5.7, showing a plot of the modulus of the phase difference between the coupling and throughput over the range of 12 – 24 GHz. The plot reveals that the phase difference changes in the vicinity of the 90-degree line between approximately 70 and 110 degrees almost in the entire measured frequency range and goes down only at the higher end of the range, which corroborates that the coupler may in principle serve as a wide-bandwidth quadrature phase shifter provided its design is optimized for this specific purpose.

The measurement plots in Fig. 5.5 show that the reflection loss stays below approximately –17 dB and reaches its minimum level of –32.74 dB in the operating bandwidth, whereas it grows to –10.12 dB outside of it at 23.6 GHz, which might be a consequence of poorer impedance matching of the loaded ports due to poorer quality of the 50-Ω terminations at the higher frequency end, as may be seen in Fig. 5.6.

The coupler has demonstrated good isolation properties in the measured band of 12 – 24 GHz, where it always stays below –11 dB and becomes better when going away from the centre frequency.

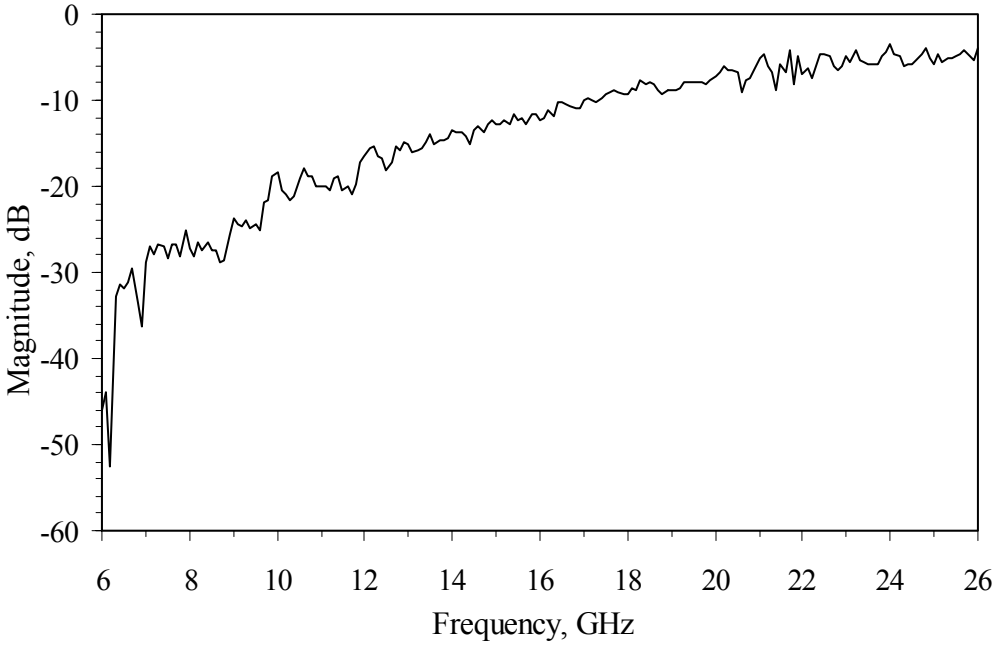

Figure 5.6 Reflection loss of the 50-Ω terminations used during testing

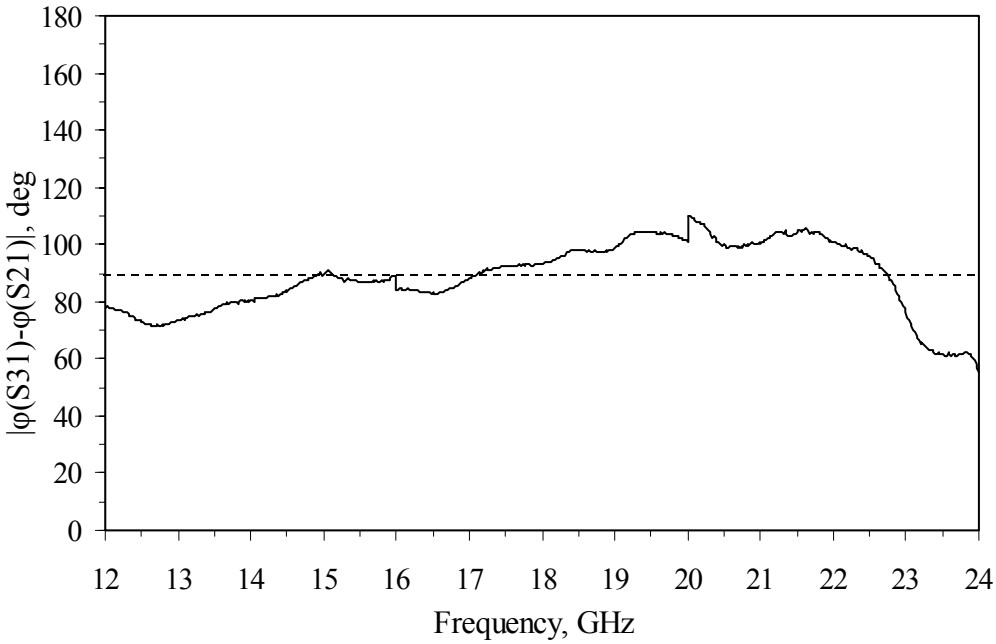

Figure 5.7 Phase difference between coupling (S31) and throughput (S21)

The departure of the measurement from the simulation, whose results are shown in Figs. 4.3 and 4.5, may be due to a number of reasons, which are explained below:

- Improper impedance matching of the ports loaded with the 50-Ω terminations due to poorer quality of the latter at higher frequencies, see Fig. 5.6. Poor impedance matching might change the electrical length of the coupler, which in its turn shifts the centre frequency.
- Nonoptimal excitation of the tall LIGA conductors with the air coplanar microprobes. The microprobes are designed to provide optimal transition from the microprobe air coplanar waveguide to planar circuits and might not be as suitable for the tall conductors.
- Polishing of the top surfaces of the conductors carried out in order to reduce roughness, resulting from natural grain distribution of nickel during electroplating, and improve thereby the microprobe-to-coupler contact and conductivity of the top surface. This polishing procedure was experimental and was not anticipated at the design stage of the project. The polishing reduced the metal height from the design height of 0.22 mm to 0.2 mm, which changed the electrical characteristics of the coupler by supposedly increasing the modal impedances and, therefore, the design level of coupling in a 50-Ω network. Alternatively, modified modal impedances result in a different characteristic impedance that the coupler ports should be terminated to in order to demonstrate the design level of coupling: if both modal impedances are changed by a certain factor, then the characteristic impedance of the network, where the coupler is connected, must be changed by the same factor in order for the coupler to show the specified coupling, as follows from (2.14) and (2.17).

5.4 Chapter Summary

Testing of the coupler structure under investigation has been carried out in a custom-made test fixture with air coplanar microprobes using the Agilent 8722 ES vector network analyzer. The testing was preceded by the TRL calibration procedure carried out to remove systematic errors from the measurement results. The testing procedure was comprised of sets of three two-port measurements performed in three different narrow frequency bands

to describe the main parameters of the coupler: coupling, isolation, and throughput. The narrow-band measurement results were combined into the broadband characteristics spanning from 12 to 24 GHz. The testing has revealed a close match between the coupler's simulated and experimental performance: the coupling is 1 dB less than simulated at the centre frequency of 18 GHz, with the measured passband of 6.8 GHz; and the throughput is in the vicinity of the expected level within ±1 dB almost in the entire measured range of 12 to 24 GHz. The noted departure of the measurement results from the simulation may be due to improper impedance matching of the coupler at higher frequencies in the test fixture, nonoptimal excitation of the tall LIGA conductors by the air coplanar microprobes designed for planar circuits, and polishing of the conductor top surface that shortened the design height and, therefore, modified the coupler's electrical characteristics.

The coupler has demonstrated the phase differential behaviour over a wide frequency range which suggests that the coupler may be employed as a wide-bandwidth quadrature phase shifter after its refinement for this purpose.

Chapter 6
SUMMARY AND CONCLUSIONS

6.1 Summary

This research has investigated the feasibility of using the LIGA technology for fabrication of RF structures, which has not received an extensive coverage in the published literature. This has been done with a simple and very wide-spread microwave device – the directional coupler. It was intended to use the LIGA technology to build a microwave directional coupler, with possibly improving its characteristics as compared with existing designs.

In the course of this dissertation, the fabrication procedures of the LIGA technology as well as its capabilities and limits were reviewed. This was followed by a description of the principles of the electromagnetic coupling and then the existing types of directional couplers and their parameters were reviewed. Next, the tight directional couplers, such as parallel-line, branch-line, rat-race, interdigital, tandem, multilayer/broadside, and lumped-element couplers, were compared for usage in the X- and K-band (8 to 40 GHz) and it was decided that the edge-coupled (becoming rather side-coupled when implemented in LIGA) parallel-line configuration would better exemplify the LIGA advantages in RF design and outperform other types of couplers with respect to electrical performance and geometrical dimensions. Specifically, it was solely due to the LIGA capabilities that an edge-coupled parallel-line coupler could prove to be possible for the set goal of a compact coupler with equal division of incident power, or a 3-dB coupler. The next stage was characterization of the LIGA CPW transmission line and coupled-line section in order to relate the geometry of the structures with their electrical characteristics, which was performed with the help of the 3-D electromagnetic simulator HFSS. The characterization was done due to the impossibility of analytical description of the LIGA structures with tall conductors, which was supported by the lack of published analytical techniques to describe conductors whose

height was comparable to other dimensions. Based on the characterization data, a 3-dB coupler was designed and its electrical performance was simulated in HFSS. Then the total structure complete with coupled-line section and half-wavelength transmission lines as well as calibration standards required for measurement were fabricated at FZK, Germany with the participation of the ANKA synchrotron facility using one of their most developed LIGA procedures. The structures were made of nickel supported by alumina substrate. The fabricated structures were then polished to improve the quality of contact between the testing equipment and the conductors as well as conductivity of the top surfaces. The testing of the structures conducted in a custom-made test fixture with the help of a vector network analyzer revealed considerable coupling in the vicinity of the predicted value with good isolation and reflection loss. The found discrepancies between the simulated and measured performance are probably due to some testing issues requiring further consideration. They include improper impedance matching of the coupler at higher frequencies in the test fixture, nonoptimal excitation of the tall LIGA conductors by the air coplanar microprobes designed for planar circuits, and polishing of the conductor top surface that decreased the design height and, therefore, modified the coupler's electrical characteristics.

6.2 Conclusions

This research has proven that application of the LIGA technology is advantageous for fabrication of certain RF devices by demonstrating the feasibility of single metal layer 3-dB edge-coupled couplers. In particular, the influence of HVAR tall conductors on performance of CPW transmission and coupled lines has been studied and the feasibility of building couplers as tight as 3-dB (the couplers with equal power division), in SML has been proven by the example of the LIGA SML 3-dB CPW coupler. The target level of coupling has not been demonstrated by the implemented testing, though approached very closely, due to design, fabrication, and measurement issues. Indeed, the actually measured coupler performance may be masked by its nonoptimal excitation and its testing through LIGA-to-planar transitions may improve the demonstrated results. Nonetheless, the LIGA capabilities routinely allow building yet taller and closer spaced conductors. Therefore, the target 3-dB coupling may be finally approached via either adjustment of the coupler's design or improvement of the testing procedures.

The coupler has also revealed that its output signals are close to the phase quadrature over a wide frequency range, which may lead to creation of wide-bandwidth quadrature phase shifters based on the coupler's topology, which might need some refinement in order to provide more accurate phase quadrature between the output signals in the operating pass-band.

The relations between the geometry and electrical performance, nonexistent in the available literature, have been found for the CPW transmission and coupled lines for the given ranges of dimensions. This data may be used for development of other microwave devices, where introduction of LIGA HVAR transmission and coupled lines will be beneficial with respect to improvement of their electrical performance and dimensions. This would first of all regard coupled-line filters and wide-bandwidth phase shifters.

Reports on other fabricated and tested 3-dB SML couplers have not been found in the available microwave engineering literature. The only available reference on LIGA couplers is [10], where a looser, 6-dB coupler is described. There are reports in the literature on other techniques allowing achievement of tight levels of coupling, with the majority of them relying on multi-metal layer structures, such as [34]. Besides being more complex in fabrication, these couplers exhibit higher losses as the prevailing fraction of their coupled fields is concentrated in the dielectric between the conductors. In addition, they are not as versatile as LIGA and do not provide as many levers to control geometrical and electrical parameters of the structures.

6.3 Future Directions

This project cannot be considered exhaustively explored and the following directions may be noted for its expansion:

1. The materials used were those available in the standard LIGA techniques practiced at IMT. More suitable microwave materials might better exemplify the benefits of LIGA to RF design, especially in the millimetre-wave domain. Specifically, reduction of the effective permittivity by selecting substrate materials with lower relative permittivity may bring about wider operating bandwidth and better dispersive characteristics of the CPW lines. As the simulation results show, the even-mode effective permittivity is more prone to variation versus frequency than its odd-

mode counterpart and the former is usually greater than the latter. The even-mode effective permittivity changes from 3.89 at 1 GHz to 5.492 at 35 GHz, which constitutes a 41.18-% change against the change of the odd-mode effective permittivity from 2.612 at 1 GHz to 2.802 at 35 GHz, which constitutes a 7.27-% change; the values being given for the designed coupler. Simulation of the similar coupler built on a quartz substrate (ε_r=3.8 at 10 GHz) gives the following results: the even-mode effective permittivity varies from 1.934 at 1 GHz to 2.179 at 35 GHz, which is a 12.6-% variation, and the odd-mode effective permittivity varies from 1.512 at 1 GHz to 1.528 at 35 GHz, which is only a 1-% variation. Moreover, this permits a lower difference between the even-mode and the odd-mode permittivity values with a positive effect on the coupler directivity, which suffers from discrepancy between characteristics of the two main propagation modes. Using a substrate with lower relative permittivity will certainly result in higher characteristic impedance values, but this may be offset by building taller conductors, which can be easily done with LIGA. This will further decrease the effective permittivity values. Nickel may also be possibly replaced by a better conductor, such as copper, which will require further development of the fabrication process in order to improve its electroplating yield.

2. Further reduction of the effective permittivity may be reached by distancing the conductors from the substrate and thereby making permittivity almost continuous in the major field concentration regions, which would result in TEM propagation. A method of doing this may be as follows: the substrate is trenched by micro-machining along the axis where the signal trace will lie, the trench is covered with a thin membrane, over which a typical LIGA process is then carried out. With continuous permittivity, the even-mode and odd-mode phase velocities become equal, which results in a better directivity.
3. In order to integrate the LIGA structures into traditional microwave circuits with planar transmission lines, the LIGA-to-planar line transitions must be developed. The transitions should be designed so that a constant characteristic impedance is maintained over the entire length of the transition.

4. Other microwave devices based on coupled lines might benefit from improved performance provided by LIGA. These would first of all include coupled-line filters, which are quite widespread in millimetre-wave systems. The other candidates are broadband DC blocks, baluns, transformers, interdigital capacitors, spiral inductors and transformers. There are also microwave devices that might be significantly influenced by introduction of the LIGA transmission lines. One such example includes ferrimagnetic phase shifters, which are the backbone of the phased-array antennas and are two-port devices providing variable phase shift by changing the bias field of the ferrite. The phase shifter may be built as a bimetallic structure with the conductors electroplated of copper and the core electroplated of the nickel-iron alloy, which is a ferrimagnetic material.
5. Finally, improvement of the microwave systems and subsystems where the coupled-line structures are their integral components may be sought. For instance, the feed networks used in phased-array antennas may potentially be built more compact if using high-performance integrated couplers.

References

[1] E. C. Niehenke, R. A. Pucel, and I. J. Bahl, "Microwave and Millimeter-Wave Integrated Circuits," *IEEE Transactions on Microwave Theory and Techniques*, vol. 50, No. 3, pp. 846–857, March 2002.

[2] B. A. Kopp, M. Borkowski, and G. Jerinic, "Transmit/Receive Modules," *IEEE Transactions on Microwave Theory and Techniques*, vol. 50, No. 3, pp. 827–834, March 2002.

[3] G. I. Haddad and R. J. Trew, "Microwave Solid-State Active Devices," *IEEE Transactions on Microwave Theory and Techniques*, vol. 50, No. 3, pp. 760–779, March 2002.

[4] F. H. Raab et al, "Power Amplifiers and Transmitters for RF and Microwave," *IEEE Transactions on Microwave Theory and Techniques*, vol. 50, No. 3, pp. 814–826, March 2002.

[5] M. J. Madou, *Fundamentals of Microfabrication: The Science of Miniaturization*, CRC Press, 2002.

[6] *Second Workshop on MEMS/Nanotechnology at the Canadian Light Source Synchrotron*, Saskatoon, May 2002.

[7] H. J. De Los Santos, *Introduction to Microelectromechanical (MEM) Microwave Systems*, Artech House, Boston, 1999.

[8] W. Menz, J. Mohr, and O. Paul, *Microsystem Technology*, Wiley-VCH, 2001

[9] T. L. Willke and S.S. Gearhart, "LIGA Micromachined Planar Transmission Lines and Filters," *IEEE Transactions on Microwave Theory and Techniques*, vol. 45, No. 10, pp. 1681-1688, Oct. 1997.

[10] T.L. Willke, E. Onggosanusi, and S.S. Gearhart, "Micromachined Thick-Metal Coplanar Coupled-Line Filters and Couplers," *1998 MTT-S International Microwave Symposium Digest*, vol. I, pp. 115-118, 1998.

[11] K. Y. Park et al, "A New Three-Dimensional 30 GHz Bandpass Filter Using the LIGA Micromachined Process," Microwave and Optical Technology Letters, vol. 30, No. 3, pp. 199-201, Aug. 2001.

[12] R. Mongia, I. Bahl, P. Bhartia, *RF and Microwave Coupled-Line Circuits*, Artech House, Boston, 1999.

[13] D. M. Pozar, *Microwave Engineering*, Addison-Wesley Publishing Company, 1990.

[14] W. Heinrich, "Quasi-TEM Description of MMIC Coplanar Lines Including Conductor-Loss Effects," *IEEE Trans. Microwave Theory Tech.*, vol. MTT-41, pp. 45-52, Jan. 1993.

[15] I. D. Robertson and S. Lucyszyn, *RFIC and MMIC Design and Technology*, The Institution of Electrical Engineers, London, 2001.

[16] M. Ozgur, V. Milanov, C. Zincke, M. Gaitan, and M. E. Zaghloul, "Quasi-TEM Characteristic Impedance of Micromachined CMOS Coplanar Waveguides," *IEEE Trans. Microwave Theory Tech.*, vol. MTT-48, pp. 852-854, May 2000.

[17] C. P. Wen, "Coplanar Waveguide: A Surface Strip Transmission Line Suitable for Nonreciprocal Gyromagnetic Device Applications," *IEEE Trans. Microwave Theory Tech.,* vol. MTT-17, pp. 1087-1090, Dec. 1969.

[18] S. S. Bedair and I. Wolff, "Fast, Accurate and Simple Approximate Analytic Formulas for Calculating the Parameters of Supported Coplanar Waveguides for (M)MIC's," *IEEE Trans. Microwave Theory Tech*., vol. MTT-40, pp. 41-48, Jan. 1992.

[19] G. Ghione and C. U. Naldi, "Coplanar Waveguides for MMIC Applications: Effect of Upper Shielding, Conductor Backing, Finite-Extent Ground Planes, and Line-to-Line Coupling," *IEEE Trans. Microwave Theory Tech*., vol. MTT-35, pp. 260-267, Mar. 1987.

[20] M. E. Davis, E. W. Williams, and A. C. Celestini, "Finite-Boundary Corrections to the Coplanar Waveguide Analysis," *IEEE Trans. Microwave Theory Tech*. (Short Papers), vol. MTT-21, pp. 594-596, Sept. 1973.

[21] J. B. Knorr and K. D. Kuchler, "Analysis of Coupled Slots and Coplanar Strips on Dielectric Substrate," *IEEE Trans. Microwave Theory Tech*., vol. MTT-23, pp. 541–548, July 1975.

[22] E. Chen and S.Y. Chou, "Characteristics of Coplanar Transmission Lines on Multilayer Substrates: Modeling and Experiments," *IEEE Trans. Microwave Theory Tech*., vol. MTT-45, pp. 939-945, Jun. 1997.

[23] G. Ghione, M. Goano, G. L. Madonna, G. Omegna, M. Pirola, S. Bosso, D. Frassati, and A. Perasso, "Microwave Modeling and Characterization of Thick Coplanar Waveguides on Oxide-Coated Lithium Niobate Substrates for Electrooptical Applications," *IEEE Trans. Microwave Theory Tech*., vol. MTT-47, pp. 2287-2293, Dec. 1999.

[24] G. Ghione, M. Goano, and M. Pirola, "Exact, Conformal-Mapping Models for the High-Frequency Losses of Coplanar Waveguides with Thick Electrodes of Rectangular or Trapezoidal Cross Section," *1999 MTT-S International Microwave Symposium Digest*, vol. III, pp. 1311-1314, Mar. 1999.

[25] C. Veyres and V. Fouad Hanna, "Extension of the Application of Conformal Mapping Techniques to Coplanar Lines with Finite Dimensions," *International Journal of Electronics*, vol. 48, pp. 47-56, Jan. 1980.

[26] L. M. Magid, *Electromagnetic Fields, Energy, and Waves*, John Wiley and Sons, 1972.

[27] M. Goano, F. Bertazzi, P. Caravelli, G. Ghione, and T. A. Driscoll, "A General Conformal Mapping Approach to the Optimum Electrode Design of Coplanar Waveguides With Arbitrary Cross Section," *IEEE Trans. Microwave Theory Tech.,* vol. MTT-49, pp. 1573-1580, Sep. 2001.

[28] C. P. Wen, "Coplanar-Waveguide Directional Couplers," *IEEE Trans. Microwave Theory Tech.,* vol. MTT-18, pp. 318-322, June 1970.

[29] T. Kitazawa and R. Mittra, "Quasi-Static Characteristics of Asymmetrical and Coupled Coplanar-Type Transmission Lines," *IEEE Trans. Microwave Theory Tech.,* vol. MTT-33, pp. 771-778, Sep. 1985.

[30] T. Itoh, *Numerical Techniques for Microwave and Millimeter-Wave Passive Structures*, John Wiley and Sons, 1989.

[31] K. J. Binns and P. J. Lawrenson, *Analysis and Computation of Electric and Magnetic Field Problems*, Pergamon Press, Oxford, 1973.

[32] Ansoft's Online Technical Support, http://www.ansoft.com/ots/
[33] *In-Fixture Measurements Using Vector Network Analyzers. Agilent AN 1287-9 Application Note*, Agilent Technologies, 2000
[34] T. Gokdemir, I. D. Robertson, Q. H. Wang, and A. A. Rezadeh, "K/Ka-Band Coplanar Waveguide Directional Couplers Using a Three-Metal-Level MMIC Process," *IEEE Microwave Guided Wave Letters*, vol. 6, pp. 76–78, Feb. 1996.